NATIONAL ADVISORY COMMITTEE FOR AERONAUTICS

TECHNICAL NOTE 4177

WIND-TUNNEL INVESTIGATION OF THE STATIC LONGITUDINAL STABILITY AND TRIM CHARACTERISTICS OF A SWEPTBACK-WING JET-TRANSPORT MODEL EQUIPPED WITH AN EXTERNAL-FLOW JET-AUGMENTED FLAP

By Joseph L. Johnson, Jr.

Langley Aeronautical Laboratory
Langley Field, Va.

Washington
January 1958

1K

NATIONAL ADVISORY COMMITTEE FOR AERONAUTICS

TECHNICAL NOTE 4177

WIND-TUNNEL INVESTIGATION OF THE STATIC LONGITUDINAL STABILITY AND TRIM CHARACTERISTICS OF A SWEPTBACK-WING JET-TRANSPORT MODEL EQUIPPED WITH AN EXTERNAL-FLOW JET-AUGMENTED FLAP

By Joseph L. Johnson, Jr.

SUMMARY

A wind-tunnel investigation has been carried out to determine the static longitudinal stability and trim characteristics of a sweptback-wing jet-transport model equipped with an external-flow jet-augmented flap. The investigation included tests of the model to determine the effects of wing position, vertical position of the horizontal tail, and size of the horizontal tail.

The results of the investigation indicated that static longitudinal stability and trim could be achieved up to a lift coefficient of about 6 with a horizontal tail having an area of about 25 percent of the wing area. In order to achieve this result, it was necessary to locate the horizontal tail well above the chord plane of the wing and to incorporate both variable incidence and an elevator. For the flap-down, power-off condition, the downwash factor was found to be relatively large (0.8 to 0.9). The downwash factor decreased with increasing momentum coefficient, the greatest reduction occurring for the low tail position. In order to obtain a given amount of stability, larger tail areas were therefore required for the low tail position than for the high tail position. Results of calculations comparing the relative merits of various trim devices for use on airplanes equipped with jet-augmented flaps indicated that a fixed canard surface utilizing jet augmentation would provide longitudinal trim and stability at a given lift coefficient for less overall jet thrust than a conventional tail, a free-floating canard surface, or a trim-jet arrangement.

INTRODUCTION

In connection with a study to establish the configuration of a free-flying model incorporating a jet-augmented flap (ref. 1), some information was obtained on the longitudinal stability and trim characteristics of a sweptback-wing jet-transport model equipped with an external-flow jet-augmented flap. Most of the stability and trim data obtained were omitted from reference 1, however, in order to expedite publication of some of the results. Since the unpublished portion of the data also appears to be of general interest, the complete results of the study on longitudinal stability and trim, together with a limited amount of analysis, are presented herein.

The investigation consisted of force tests of a sweptback-wing jet-transport model in a low- and high-wing configuration. Each of these configurations was tested with two horizontal tails of different size and with two different vertical locations. Calculations were made to determine the trim requirements of several airplane configurations equipped with jet-augmented flaps. The configurations studied included a conventional horizontal-tail arrangement, fixed and free-floating canard arrangements, and trim-jet arrangements.

In addition to the longitudinal stability and trim problem which is covered in the present investigation, the external-flow jet-augmented flap introduces other problems that are beyond the scope of this investigation. For example, the problem of obtaining structural integrity at the high temperatures and noise levels involved and the weight problem associated with the high flap loads and the impingement of the jet exhaust on the flap must be solved before successful application of such a flap arrangement can be made.

SYMBOLS

The data are referred to the stability system of axes originating at a center of gravity located at 0.40 mean aerodynamic chord and on the fuselage reference line.

S	wing area, sq ft
$\bar{c}$	mean aerodynamic chord, ft
V	velocity, ft/sec
q	dynamic pressure, $\frac{1}{2}\rho V^2$, lb/sq ft

ρ air density, slugs/cu ft

T thrust at the nozzles, lb

α angle of attack, deg

S_t horizontal-tail area, sq ft

i_t incidence of horizontal tail, deg

δ jet-deflection angle, measured in a plane perpendicular to flap hinge line, deg

ϵ angle of downwash, deg

$1 - \frac{d\epsilon}{d\alpha}$ downwash factor $\left(\text{determined from } \frac{C_{m_{\alpha,t}}}{C_{m_{i_t}}}\right)$

l tail length, ft

h distance from center of gravity to neutral point, ft

n distance from aerodynamic center of wing-fuselage combination to neutral point, ft

x distance from aerodynamic center of wing-fuselage combination to flap center of pressure, ft

M_Y pitching moment, ft-lb

C_L lift coefficient, $\frac{\text{Lift}}{qS}$

C_μ momentum coefficient based on thrust measured at nozzle, $\frac{T}{qS}$

C_D drag coefficient, $\frac{\text{Drag}}{qS}$

C_m pitching-moment coefficient, $\frac{M_Y}{qS\bar{c}}$

$C_{m_\alpha} = \frac{\partial C_m}{\partial \alpha}$ per deg

$C_{L_\alpha} = \frac{\partial C_L}{\partial \alpha}$ per deg

$C_{m_{i_t}} = \frac{\partial C_m}{\partial i_t}$ per deg

$\frac{\partial C_m}{\partial C_L}$ static margin, $\frac{h}{c}$, chords

Subscripts:

t horizontal tail (tail coefficients based on tail area)

wf wing-fuselage combination

f jet-augmented flap

nj nose jet

tj tail jet

APPARATUS AND MODEL

The investigation was conducted in the Langley full-scale tunnel. All tests were made with a vertical-strut support system and strain-gage balances. The test setup was located in the forward portion of the test section near the lower lip of the entrance cone.

A drawing of the sweptback-wing jet-transport model used in the investigation is presented in figure 1(a) for the high-wing configuration and in figure 1(b) for the low-wing configuration. Dimensional characteristics of the model are presented in table I. The wing of the model had 30° sweep of the quarter-chord, an aspect ratio of 6.60, and a taper ratio of 0.367. The airfoil section was NACA 65_1-414 at the root and NACA 65_1-410 at the tip. Pod-mounted engines were simulated by two nacelles attached to the wing on pylons. Compressed air was supplied to each nacelle through flexible hoses which passed internally through the model. These cold-air jets were used to simulate the jet-engine exhaust.

A detailed drawing of the jet-flap arrangement used on the model is shown in figure 2. For take-off and landing, the jets from the pod-mounted engines are spread out into a horizontal sheet by retractable deflectors and directed toward the base of a slotted flap which then turns the flattened jet sheet downward. The full-span slotted flap was hinged on the bottom surface of the wing in such a way that a smooth fairing was obtained between the upper surface of the slot and the lower surface of the wing for a flap deflection of 60°.

TESTS

The tests for longitudinal stability and trim were made over an angle-of-attack range from -8° to 12° for the model in the high-wing configuration and low-wing configuration shown in figures 1(a) and 1(b), respectively. The geometric flap angle was set at 60° for all tests but the measured jet-deflection angle was found to vary slightly with C_μ and model configuration. Average values of the measured jet-deflection angle were found to be 60° for the high-wing configuration and 55° for the low-wing configuration. Each of these configurations was tested with two horizontal tails of different sizes $\left(S_t/S = 0.17 \text{ and } 0.34\right)$ and for two different locations on the vertical tail. One location was at the base of the vertical tail (designated low tail position) and the other at the top of the vertical tail (designated high tail position). For some tests, the horizontal tail was equipped with leading-edge and trailing-edge flaps. All of these tests were made over a momentum-coefficient range from 0 to 3.8.

All of the tests in this investigation were made at a dynamic pressure of about 1.6 pounds per square foot which corresponds to a velocity of about 37 feet per second and a Reynolds number of about 170,000 based on the mean aerodynamic chord of the wing.

REDUCTION OF DATA

No wind-tunnel corrections have been applied to the data since the model was relatively small compared with the size of the tunnel test section.

The coefficient C_μ used in this report is defined as T/qS where T is the thrust at the nozzle and is determined from force tests. This coefficient is approximately equivalent to the momentum coefficient C_μ which has been used in boundary-layer-control investigations and in the jet-augmented-flap investigations reported in references 2, 3, and 4. In order to determine thrust losses in spreading and deflecting the jet, values of thrust were obtained from force measurements made during static calibrations of the cruising configuration (flaps and deflectors retracted) and of the landing configuration (flaps and deflectors extended). Comparison of the calibration data for these two conditions indicated that the thrust losses caused by spreading and deflecting the jet were about 25 percent for the 60° flap deflection.

RESULTS AND DISCUSSION

Presentation of Data

The results of the investigation are presented in the form of basic data and summary data. The following table shows the order in which the data are presented:

Basic data.-

	Figure
C_L, C_D, and C_m against α; tail off:	
Low wing	3(a)
High wing	3(b)
Flap c.p., $\left(C_{L_\alpha}\right)_{wf}$, and wing-fuselage a.c. against C_μ	3(c)
C_L, C_D, and C_m against α; low wing:	
Low tail	4, 5
High tail	6
C_L, C_D, and C_m against α; high wing:	
Low tail	7, 8
High tail	9, 10
C_L against α; isolated horizontal tails	11
C_L, C_D, and C_m against α; high wing:	
Low tail with flaps	12, 13
High tail with flaps	14, 15

Summary data.-

$C_{m,t}$ against α; low wing:	
Low tail	16(a)
High tail	16(b)
$C_{m,t}$ against α; high wing; low and high tail	17

Figure

$C_{m,t}$ against α, high wing:
Low tail with flaps 18
High tail with flaps 19

$C_{m_{\alpha,t}}$ and $C_{m,t}$ against S_t/S; low wing:
Low tail . . . . . 20(a)
High tail . . . . . 20(b)

$C_{m_{\alpha,t}}$ and $C_{m,t}$ against S_t/S; high wing; low and high tail . . . 21

$C_{m_{\alpha,t}}$ and $C_{m,t}$ against S_t/S; high wing:
Low tail with flaps . . . . . 22(a)
High tail with flaps . . . . . 22(b)

$\frac{\partial C_m}{\partial C_L}$ against S_t/S; low wing; low and high tail 23

$\frac{\partial C_m}{\partial C_L}$ against S_t/S; high wing; low and high tail 24

$\frac{\partial C_m}{\partial C_L}$ against S_t/S; high wing; low and high tail with flaps . . . 25

S_t/S for 5-percent static margin against C_μ 26

S_t/S for trim and 5-percent static margin against tail height . 27

$C_{m,t}$ against i_t; low wing; low and high tail 28

$C_{m,t}$ against i_t; high wing; low and high tail with flaps 29

ϵ against C_μ 30

ϵ against tail height 31

$C_{m_{\alpha,t}}$ and $C_{m_{i_t}}$ against C_μ 32

Figure

$1 - \frac{d\epsilon}{d\alpha}$ against C_μ 33

$1 - \frac{d\epsilon}{d\alpha}$ against tail height 34

$C_{L,t}$ and total C_μ for trim and 10-percent static margin against S_t/S 35

Longitudinal Stability and Trim

The results of the tests on longitudinal stability and trim are presented in figures 3 to 15 and summarized in figures 16 to 35. The data for the low- and high-wing configurations are presented for jet-deflection angles of 55° and 60°, respectively. These angles were used for the stability and trim study since the range of jet-deflection angles required for steady-state flight in the landing condition is somewhere near these values for existing jet transport airplanes. The landing condition was chosen for this study because the longitudinal stability and trim problems appear to be more serious for this condition than for the take-off condition. All of the pitching-moment data are referred to a center-of-gravity location of 40 percent mean aerodynamic chord since analysis indicated that this location would permit a reasonable relationship between stability and trim and horizontal-tail area.

Low-wing configuration.- The data for the low-wing configuration are presented in figures 3(a) and 4 to 6. For the tail-off configuration (fig. 3(a)), the negative pitching moments increased and the static instability decreased with increasing C_μ. These variations in pitching-moment characteristics are similar to those shown in previous investigations on jet flaps. The large diving moments are a result of the rearward location of the very large flap loads. The pitch-up at positive angles of attack is characteristic of swept wings having high aspect ratios with flap centers of pressure located inboard on the wing. The decrease in instability with increasing C_μ as measured by the value of $\partial C_m/\partial C_L$ is attributed partly to the fact that there is an increase in lift-curve slope $\left(\text{theoretically } C_{L_\alpha} = \left(C_{L_\alpha}\right)_{C_\mu=0} + \frac{C_\mu \cos(\delta + \alpha)}{57.3}\right)$ without a corresponding increase in the slope of the pitching-moment curve C_{m_α}. The variations of lift-curve slope, flap center of pressure, and aerodynamic center with C_μ are shown in figure 3(c).

The data for the low-wing configuration with the small and large tails in the low position (figs. 4 and 5) show that the values of negative pitching moment and instability noted for the tail-off configuration were so large that even the large horizontal tail (fig. 5) did not provide both trim and stability at the higher values of C_μ. These data show that at an angle of incidence of 0° the large horizontal tail provided trim but it was stalled and therefore provided little or no increment of stability. At the higher angles of incidence, these tails provided some stability but not enough positive pitching moment to provide trim.

In an effort to increase the longitudinal stability by placing the tail in a more favorable downwash field, the horizontal tail was moved to the top of the vertical tail. The data for this configuration (fig. 6) show, in general, an increase in stability for a given tail size when the tail is moved from the low to the high position. For 0° incidence, the large horizontal tail provided trim and stability up to a lift coefficient of about 4.

High-wing configuration.- The longitudinal stability and trim characteristics of the high-wing configuration were found to be generally similar to those of the low-wing configuration. Over the range of C_μ investigated, however, the high-wing configuration gave considerably higher lift coefficients for given values of C_μ than the low-wing configuration. (See figs. 3(a) and (b).) The results of preliminary tests in this investigation of the model in the high- and low-wing configuration with various flap deflections indicated that the lower values of C_L for the low-wing configuration can be attributed partly to wing-fuselage interference effects and partly to the lower jet deflection for this configuration (55° compared with 60° for the high-wing configuration).

The data in figures 7 to 10 show that when the tail is moved from the low to the high position a slight gain in stability was generally realized for a given configuration, but stability and trim of the model could not be obtained at the higher lift coefficients even with the large tail.

High-lift devices on tail.- An analysis of the data in figures 3 to 10 indicated that the low trimming power of the horizontal tail could be attributed to a relatively low maximum lift coefficient of the tail which resulted from the low scale of the tests. The results of force tests of the isolated tail surfaces (presented in fig. 11) indicated that the maximum lift coefficient of these tails was only about 0.7. The data of figure 11 show that the addition of a leading-edge flap increased the maximum lift coefficient of these tails to about 1.0 and 1.2. It is believed that the maximum lift coefficient of the tails

with leading-edge flaps in these low-scale tests would be approximately the same as that obtained at full scale without leading-edge flaps. The addition of leading-edge and trailing-edge flaps increased the maximum lift coefficient of these tails up to about 1.4 and 1.5. The lower maximum lift coefficient for the large tail is attributed to the poor airfoil section for this particular tail. (The large tail was formed by the use of a crudely shaped metal glove which fitted over the small tail.)

The data obtained for the high-wing configuration with the leading- and trailing-edge flaps on the horizontal tail are presented in figures 12 to 15. In the low position neither the small tail nor the large tail was adequate for stability and trim in the higher lift-coefficient range. In the high position the large tail was more than adequate for stability and trim up to the highest lift coefficients but the small tail was still inadequate.

Horizontal-tail area required.- In order to indicate the horizontal-tail area required for longitudinal stability and trim over the lift-coefficient range investigated, the incremental pitching moments of the horizontal tails were determined from figures 3 to 15 and plotted against angle of attack in figures 16 to 19. The slopes of these incremental-pitching-moment curves (which represent the tail contribution to stability) and the increments of pitching moment at an angle of attack of 0° (which represent the tail contribution to trim) are presented against S_t/S in figures 20 to 22. The data for the model without the high-lift devices on the tail (figs. 20 and 21) show clearly that both stability and trim were not possible within the range of tail sizes investigated. The data of figure 22 generally indicate, however, that in the unstalled range a horizontal-tail area of about 20 to 25 percent of the wing area provided stability and trim when the horizontal tail was located in a position well above the chord plane of the wing and was equipped with leading-edge and trailing-edge flaps. The tail arrangement in this case simulates an all-movable horizontal tail equipped with an elevator.

Effect of tail height on tail area required.- In order to afford a direct comparison of the longitudinal stability of the various configurations tested, the slopes at $\alpha = 0^\circ$ of the pitching-moment curves of figures 4 to 10 and 12 to 15 are plotted against tail areas in figures 23 to 25. The horizontal-tail areas required for a static margin of 5 percent at angles of incidence for which the horizontal tail was unstalled were obtained from these figures and plotted against C_μ in figure 26. (In order to keep the horizontal tail unstalled, it was necessary to increase the angle of incidence as C_μ increased.) These data show that an increase in tail area is required to maintain a constant value of stability as C_μ is increased and that the effect appears to be more pronounced for the low tail position than for the high tail position.

This increase in tail area required for stability is attributed to a decrease in the downwash factor $1 - \frac{d\epsilon}{d\alpha}$ as C_μ is increased. A detailed discussion of the downwash characteristics determined in this investigation is presented in the following section of this report.

In order to obtain a better indication of the effect of tail height on tail-area requirements, the data of figures 22 and 25 were used to determine the tail area required to provide both trim and a static margin of 5 percent. The results are plotted in figure 27 and illustrate the increase in tail area required for the low tail position over that for the high tail position for a given value of C_μ.

Downwash Characteristics

Downwash angle.- The angle of downwash ϵ was determined from plots of the variation of the pitching moment of the tail with i_t at an angle of attack of 0° (presented in figs. 28 and 29) by assuming ϵ to be equal to the angle of incidence of the tail for zero pitching moment corrected for the angle of attack for zero lift of the isolated tail determined from figure 11. For the high-wing configuration with leading- and trailing-edge flaps on the tail (fig. 29), the tail pitching moments were generally positive for all values of C_μ, and the curves were extrapolated to determine the tail incidence for zero pitching moment. Values of ϵ determined in this manner are plotted in figure 30. These data show large variations of ϵ with C_μ, particularly for the low tail position. The data show a difference in the downwash angle for the small and large tails, apparently because of a nonuniform flow field over the tails. A cross plot of figure 30 to determine the variation of ϵ with tail height (presented in fig. 31) shows the data to be somewhat erratic, but an average line drawn through the symbols indicates a large overall increase in ϵ when the tail is moved from the high to the low position, particularly for a value of C_μ of 3.80. Also presented in figure 31 are some downwash data from figure 13(a) of reference 4 which were measured behind an unswept wing equipped with an internal-flow jet-augmented flap. The data of reference 4 show similar variations in ϵ with tail height and with changes in C_μ.

Downwash factor $1 - \frac{d\epsilon}{d\alpha}$.- Estimates of the downwash factor $1 - \frac{d\epsilon}{d\alpha}$ were determined from the ratio of $C_{m_{\alpha,t}}$ to $C_{m_{i_t}}$ for the various configurations tested. Values of $C_{m_{\alpha,t}}$ determined from figures 20 to 22,

along with values of $C_{m_{i_t}}$ determined from figures 28 and 29, are presented in figure 32. These data were obtained at angles of incidence for which the horizontal tail was unstalled; and, as pointed out previously, the angle of incidence had to be increased as C_μ increased in order to keep the tail unstalled. The data of figure 32 show a decrease in $C_{m_{\alpha,t}}$ as C_μ increased, whereas $C_{m_{i_t}}$ was assumed to be constant over the C_μ range.

Values of $1 - \frac{d\epsilon}{d\alpha}$ determined from the data of figure 32 are presented in figure 33. The data of this figure show considerable scatter but an average curve drawn through the measured values indicates a decrease in $1 - \frac{d\epsilon}{d\alpha}$ with increasing C_μ, the greatest reduction occurring for the low tail position. A cross plot of this figure (presented in fig. 34) shows relatively large values of the downwash factor (0.8 to 0.9) for $C_\mu = 0$ and a slight decrease in the downwash factor with decreasing tail height. For values of C_μ of 2.2 and 3.8, however, the downwash factor decreased rapidly with decreasing tail height and very low values of $1 - \frac{d\epsilon}{d\alpha}$ were obtained for the low tail position. The low values of $1 - \frac{d\epsilon}{d\alpha}$ for the low tail position explain the pronounced increase in tail area required for stability for this tail position discussed previously. Also presented in figure 34 are values of $1 - \frac{d\epsilon}{d\alpha}$ estimated from the data of reference 4 for an unswept-wing conventional model with a full-span internal-flow jet-augmented flap. The data of reference 4 are in fairly good agreement with the data of the present investigation at $C_L = 6$ or 7 and show the decrease in $1 - \frac{d\epsilon}{d\alpha}$ with increasing C_μ noted in the data of the present investigation.

Calculation of Longitudinal-Trim Requirements of Several Airplane Configurations Equipped With Jet-Augmented Flaps

From the results of stability and trim tests discussed in preceding sections of this report, it is apparent that one of the problems requiring careful consideration in the application of a jet-augmented flap to an airplane is the provision of adequate means for trimming the large nose-down pitching moment produced by the flap. In order to obtain some

indication of the relative merits of several means of trimming, calculations have been made of the trim requirements of several airplane configurations equipped with jet-augmented flaps.

In these calculations the various methods considered for trim of a sweptback-wing configuration equipped with a jet-augmented flap included a conventional horizontal-tail arrangement, a fixed canard surface, a free-floating canard surface, a nose jet, and a tail jet. For these calculations, trim lift coefficients of 5 and 10 (including the tail lift for trim) were considered. The aerodynamic center of the wing-fuselage combination was assumed to be 0.30 mean aerodynamic chord forward of the flap center of pressure, and the center of gravity was positioned to give a static margin of 0.1 mean aerodynamic chord for the conditions investigated. The tail length (distance from center of gravity to tail surface or trim jet) was assumed to be 3 wing chords. For the conventional configuration, the downwash factor $1 - \frac{d\epsilon}{d\alpha}$ was assumed to be 0.5, but for the canard configuration the effect of tail downwash on the wing was assumed to be negligible $\left(\text{that is, } 1 - \frac{d\epsilon}{d\alpha} \text{ was assumed to be } 1.0\right)$. The ratio of the lift-curve slope of the tail to that of the wing was taken as 0.75. The maximum tail lift coefficient without jet augmentation was considered to be 1.4. In cases for which lift coefficients greater than 1.4 were required for trim, the tail surfaces were assumed to be equipped with jet-augmented flaps. Experimental data of figure 3(b) were used in estimating values of C_μ required on surfaces equipped with jet-augmented flaps. The results of these calculations are presented in figure 35. The equations used in the calculations are presented in the appendix.

The data of the upper portion of figure 35 show the variation in tail lift coefficient required for trim and stability plotted against tail area for several airplane configurations. These data show that, for low values of S_t/S, jet augmentation is required to achieve the high values of lift coefficient necessary for trim and stability in all of the arrangements considered. An increase in tail area reduces the tail lift coefficient required but jet augmentation must be used on the fixed canard surface at trim lift coefficients of 5 and 10 for the range of tail areas investigated. The free-floating canard surface requires jet augmentation for tail areas smaller than about 40 percent of the wing area at a trim lift coefficient of 5 and must be equipped with jet augmentation for even larger tail areas at a trim lift coefficient of 10. In the case of the conventional tail surface, jet augmentation must be used for values of S_t/S smaller than about 0.22 and 0.27 for trim lift coefficients of 5 and 10, respectively. The lift coefficients required for trim and stability for the nose-jet and tail-jet arrangements are

listed rather than plotted in the upper portion of figure 35 since these values are based on wing area and are therefore not directly comparable with the other data.

One significant point illustrated by these data is that the lift of the canard surfaces acts upward and therefore adds to the lift of the wing, whereas the lift on the conventional tail acts downward (except for values of S_t/S larger than about 0.37) and therefore subtracts from the lift of the wing. The reason for the change in sign of the lift load on the conventional tail is that an increase in tail area shifts the neutral point rearward so that at a value of S_t/S of about 0.37 the neutral point falls directly on the flap center of pressure and at higher values of S_t/S moves rearward of this point. It is this variation in neutral point with tail area in the conventional design that permits moving the center of gravity back closer to the flap center of pressure to reduce the flap diving moment and thereby permits a horizontal tail of reasonable size to be used to trim to a moderately high lift coefficient without resorting to jet augmentation. In the fixed canard arrangement, the opposite effect occurs; that is, the neutral point moves forward with an increase in tail area and causes an increase in flap diving moment since the center of gravity must be moved forward to maintain stability. The free-floating canard surface and the nose and tail jets at large deflection angles do not affect the stability of the airplane; therefore, the trim requirements for these arrangements are somewhere between those for the conventional tail and the fixed canard arrangements.

The data of the lower portion of figure 35 show the variation of the total momentum coefficient required for trim and stability plotted against tail area. These values of total C_μ are the summation of C_μ of the tail or trim jet and C_μ of the wing to give trim lift coefficients of 5 and 10. These data show that the fixed canard surface provides trim and stability for less total C_μ (and therefore less total thrust) than any other arrangement considered except at very small values of S_t/S where the free-floating canard surface shows a slight advantage. The fixed canard arrangement offers this advantage in C_μ over the other arrangements because, in a canard design, the relatively large up load on the tail required for trim results in a lower lift coefficient on the wing to achieve a given trim lift coefficient of the airplane. This reduction in the wing lift permits operation in a more efficient range of the curve of C_L against C_μ where the ratio of the circulation lift to the jet reaction is higher. A similar effect occurs for the free-floating canard arrangement but in this case the wing carries a larger portion of the lift load. The free-floating canard surface appears to offer an advantage over the conventional tail,

nose-jet, and tail-jet arrangements but requires a very large area for trim without jet augmentation. The nose-jet arrangement provides trim at lower values of C_μ than the conventional tail up to values of S_t/S of 0.30 or 0.40. The tail-jet arrangement, however, requires a larger total C_μ for trim at a given lift coefficient than any other arrangement considered.

SUMMARY OF RESULTS

A wind-tunnel investigation was made to determine the static longitudinal stability and trim characteristics of a sweptback-wing jet-transport model equipped with an external-flow jet-augmented flap. The results may be summarized as follows:

1. Static longitudinal stability and trim could be achieved up to a lift coefficient of about 6 with a horizontal tail having an area of about 25 percent of the wing area. In order to achieve this result, it was necessary to locate the horizontal tail in a position well above the chord plane of the wing and to incorporate both variable incidence and an elevator.

2. For the flap-down, power-off condition, the downwash factor was found to be relatively large (0.8 to 0.9). The value of downwash factor decreased with increasing momentum coefficient, the greatest reduction occurring for the low tail position. In order to obtain a given amount of stability, larger tail areas were therefore required for the low tail position than for the high tail position.

3. Results of calculations comparing the relative merits of various trim devices for use on airplanes equipped with jet-augmented flaps indicated that a fixed canard surface utilizing jet augmentation would provide longitudinal trim and stability at a given lift coefficient for less overall jet thrust than a conventional tail, a free-floating canard surface, or a trim-jet arrangement.

Langley Aeronautical Laboratory,
National Advisory Committee for Aeronautics,
Langley Field, Va., September 16, 1957.

APPENDIX

DERIVATION OF EXPRESSIONS FOR CALCULATING LONGITUDINAL-TRIM REQUIREMENTS OF SEVERAL AIRPLANE CONFIGURATIONS EQUIPPED WITH JET-AUGMENTED FLAPS

The equations in this appendix were obtained by considering the relation between the lift produced by a jet-augmented flap on a wing-fuselage combination and the lift produced by various trim devices. The equations for stability and trim were determined by setting the moments equal to zero about the neutral point and the center of gravity, respectively. The equation for lift was determined by the summation of the lift forces on the wing and tail with a positive sign representing an upward direction. The configurations examined in this investigation are illustrated in the following sketches:

Conventional Configuration

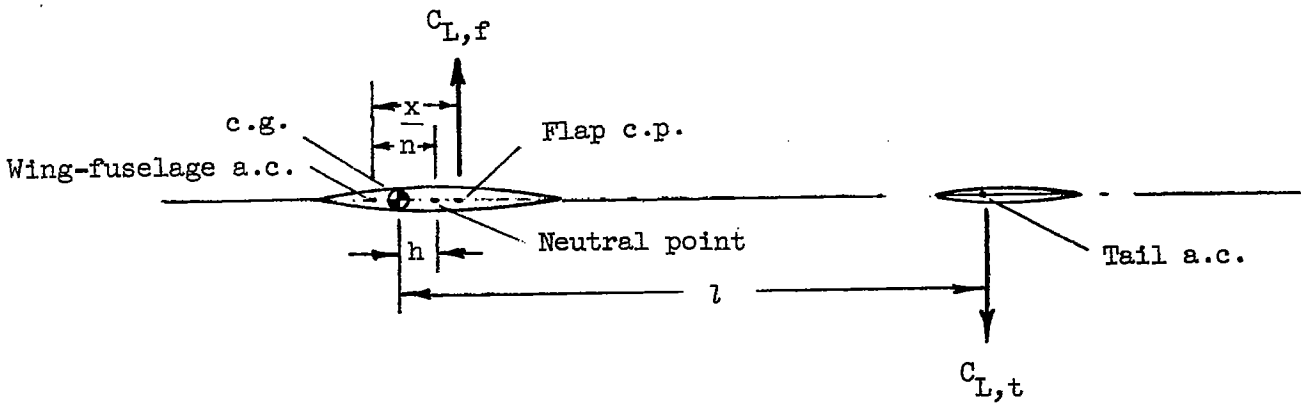

Stability equation:

$$C_{L_{\alpha,t}} \frac{S_t}{S} \left(\frac{l}{\bar{c}} - \frac{h}{\bar{c}}\right) \left(1 - \frac{d\epsilon}{d\alpha}\right) = \left(C_{L_\alpha}\right)_{wf} \frac{n}{\bar{c}} \tag{1}$$

Trim equation:

$$C_{L,t} \frac{l}{\bar{c}} \frac{S_t}{S} = C_{L,f} \left(\frac{x}{\bar{c}} - \frac{n}{\bar{c}} + \frac{h}{\bar{c}}\right) \tag{2}$$

Lift equation:

$$C_{L,trim} = C_{L,f} - C_{L,t}\frac{S_t}{S} \tag{3}$$

By combining equations (1) to (3) to eliminate n, it is possible to obtain an expression for determining $C_{L,t}$ or S_t/S for any given trim lift coefficient of a conventional configuration.

Fixed Canard Configuration

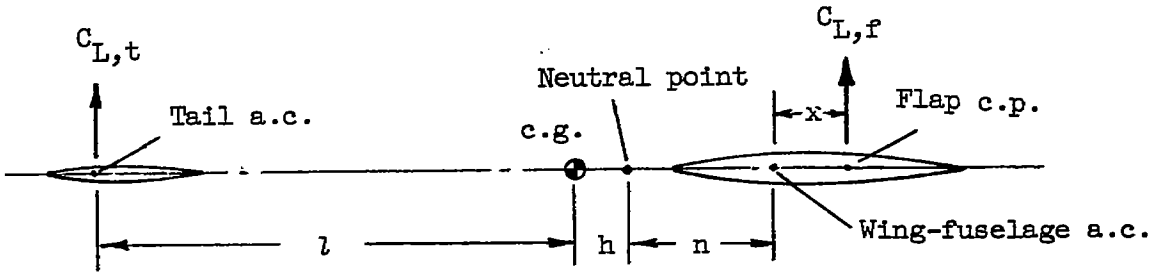

Stability equation:

$$C_{L_{\alpha,t}}\frac{S_t}{S}\left(\frac{l}{\bar{c}} + \frac{h}{\bar{c}}\right) = \left(C_{L_\alpha}\right)_{wf}\frac{n}{\bar{c}} \tag{4}$$

Trim equation:

$$C_{L,t}\frac{l}{\bar{c}}\frac{S_t}{S} = C_{L,f}\left(\frac{x}{\bar{c}} + \frac{n}{\bar{c}} + \frac{h}{\bar{c}}\right) \tag{5}$$

Lift equation:

$$C_{L,trim} = C_{L,f} + C_{L,t}\frac{S_t}{S} \tag{6}$$

Free-Floating Canard Configuration

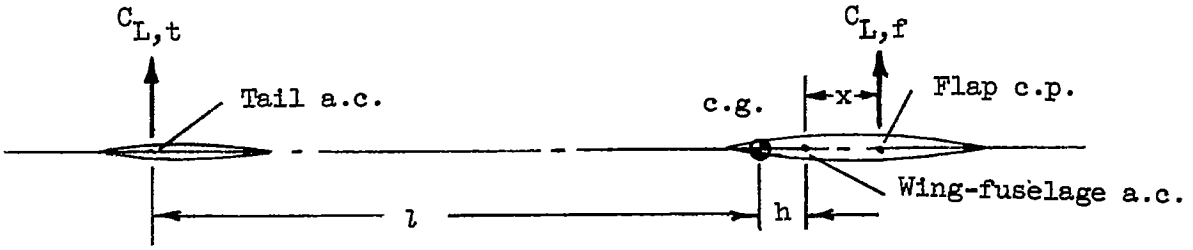

In the configuration with the free-floating canard surface the horizontal tail does not contribute to the stability of the configuration since $C_{L_{\alpha,t}}$ is zero. The stability of this configuration is determined by the distance of the center of gravity forward of the aerodynamic center of the wing-fuselage combination.

Trim equation:

$$C_{L,t} \frac{l}{c} \frac{S_t}{S} = C_{L,f} \left(\frac{x}{c} + \frac{h}{c} \right) \tag{7}$$

Lift equation:

$$C_{L,trim} = C_{L,f} + C_{L,t} \frac{S_t}{S} \tag{8}$$

Nose-Jet Configuration

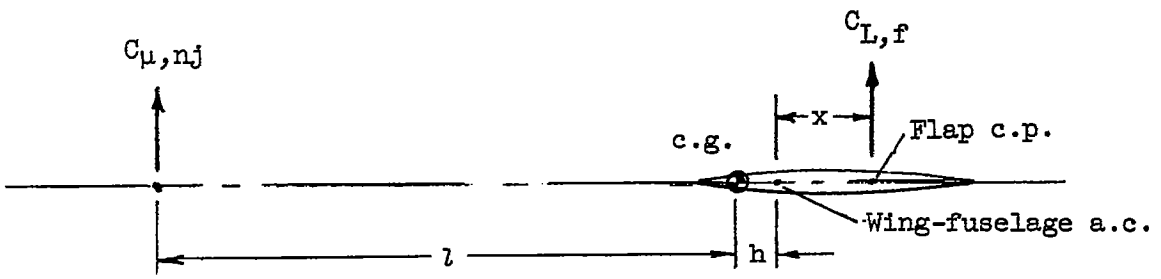

For the nose- and tail-jet configurations the stability is determined by the distance of the center of gravity forward of the aerodynamic center of the wing-fuselage combination. In cases for which the nose or tail jet is tilted other than 90° to provide trim in drag as well as in pitch, there is a possibility that these trim devices might have some

effect on stability. This effect would be small, however, since C_μ of the trim jet is relatively small compared with that of the wing.

Trim equation:

$$C_{\mu,nj}\,\frac{l}{c} = C_{L,f}\left(\frac{x}{c} + \frac{h}{c}\right) \tag{9}$$

Lift equation:

$$C_{L,trim} = C_{L,f} + C_{\mu,nj} \tag{10}$$

Tail-Jet Configuration

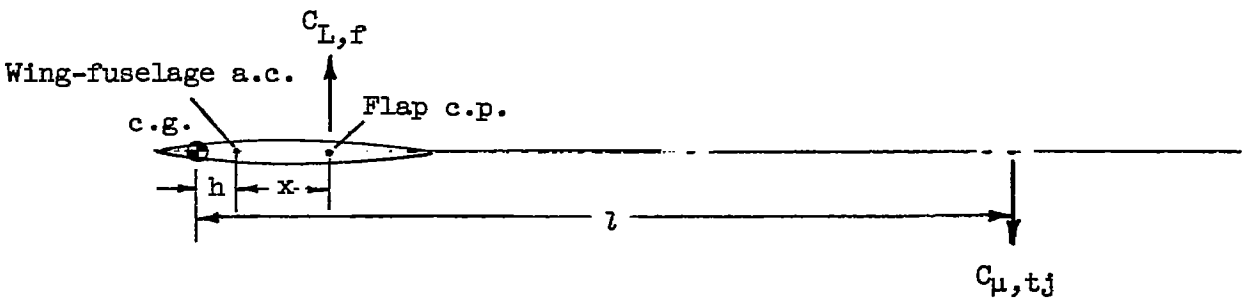

Trim equation:

$$C_{\mu,tj}\,\frac{l}{c} = C_{L,f}\left(\frac{x}{c} + \frac{h}{c}\right) \tag{11}$$

Lift equation:

$$C_{L,trim} = C_{L,f} - C_{\mu,tj} \tag{12}$$

REFERENCES

1. Campbell, John P., and Johnson, Joseph L., Jr.: Wind-Tunnel Investigation of an External-Flow Jet-Augmented Slotted Flap Suitable for Application to Airplanes With Pod-Mounted Jet Engines. NACA TN 3898, 1956.

2. Lockwood, Vernard E., Turner, Thomas R., and Riebe, John M.: Wind-Tunnel Investigations of Jet-Augmented Flaps on a Rectangular Wing to High Momentum Coefficients. NACA TN 3865, 1956.

3. Lowry, John G., and Vogler, Raymond D.: Wind-Tunnel Investigation at Low Speeds To Determine the Effect of Aspect Ratio and End Plates on a Rectangular Wing With Jet Flaps Deflected 85°. NACA TN 3863, 1956.

4. Vogler, Raymond D., and Turner, Thomas R.: Wind-Tunnel Investigation at Low Speeds To Determine Flow-Field Characteristics and Ground Influence on a Model With Jet-Augmented Flaps. NACA TN 4116, 1957.

TABLE I.- DIMENSIONAL CHARACTERISTICS OF THE MODEL

Wing:	
Area, sq ft	3.07
Aspect ratio	6.60
Mean aerodynamic chord, ft	0.732
Airfoil section, root	NACA 65_1-414
Airfoil section, tip	NACA 65_1-410
Flap chord, wing chords	0.25
Flap span, wing spans	1.00
Root chord, ft	1.00
Tip chord, ft	0.367
Span, ft	4.50
Taper ratio	0.367
Sweep of quarter-chord, deg	30
Horizontal tail (small):	
Area (total), sq ft	0.53
Length (distance from 0.40$\bar{c}$ of wing to 0.25$\bar{c}$ of tail):	
Low position, wing chords	2.52
High position, wing chords	2.75
Span, ft	1.58
Root chord, ft	0.52
Tip chord, ft	0.15
Mean aerodynamic chord, ft	0.38
Aspect ratio	4.71
Sweep of leading edge, deg	38
Taper ratio	0.289
Airfoil section	NACA 65-009
Horizontal tail (large):	
Total area, sq ft	1.06
Length (distance from 0.40$\bar{c}$ of wing to 0.25$\bar{c}$ of tail):	
Low position, wing chords	2.68
High position, wing chords	2.91
Span, ft	2.33
Root chord, ft	0.62
Tip chord, ft	0.29
Mean aerodynamic chord, ft	0.473
Aspect ratio	5.12
Sweep of leading edge, deg	32
Taper ratio	0.47
Airfoil section	NACA 65-009
Vertical tail:	
Exposed area, sq ft	0.44
Exposed span, ft	0.96
Root chord at fuselage intersection, ft	0.750
Tip chord, ft	0.17
Sweep of leading edge, deg	42
Airfoil section	NACA 65-009

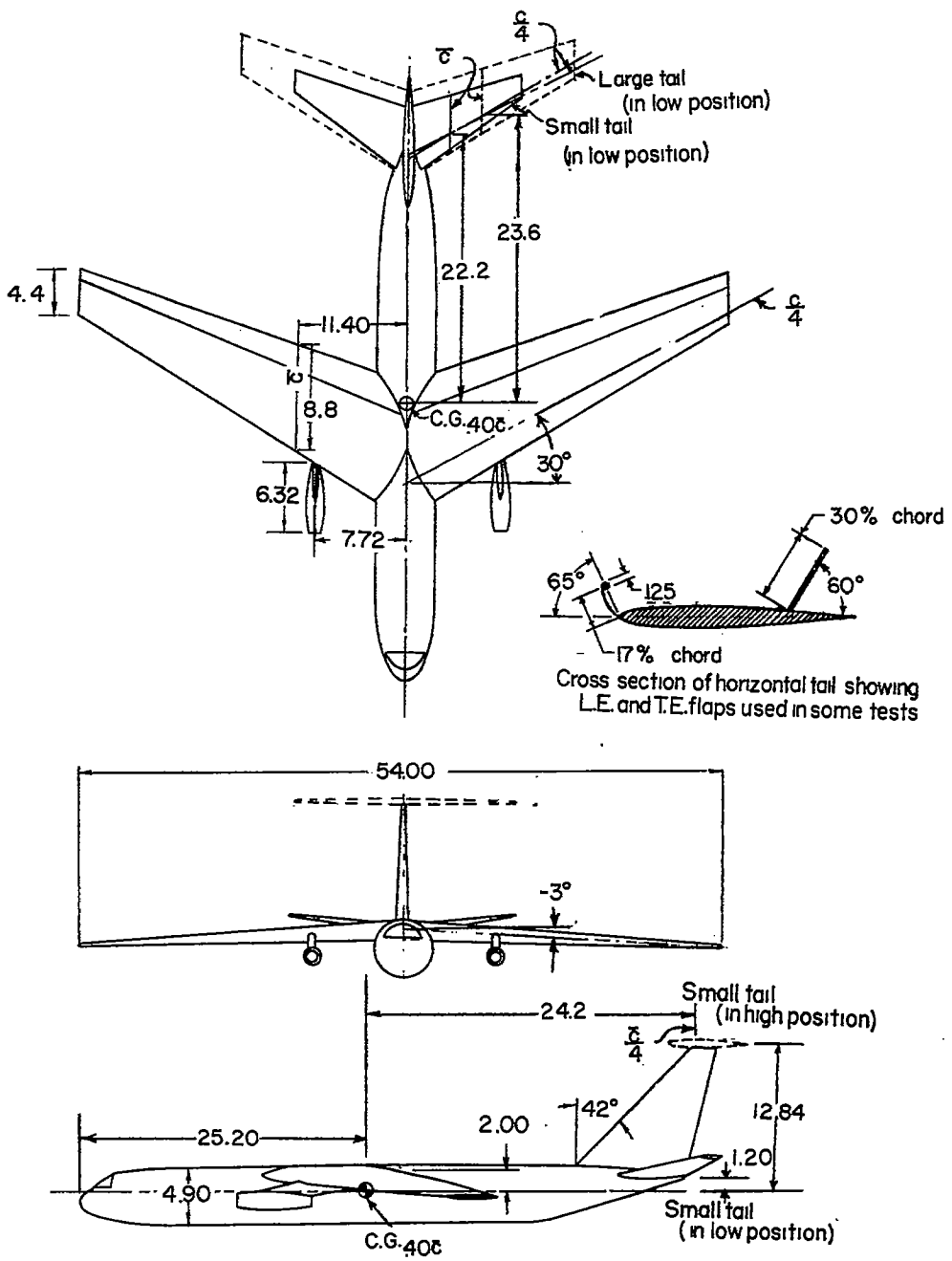

(a) High-wing configuration.

Figure 1.- Swept-wing jet-transport model used in the investigation. All dimensions are in inches unless otherwise noted.

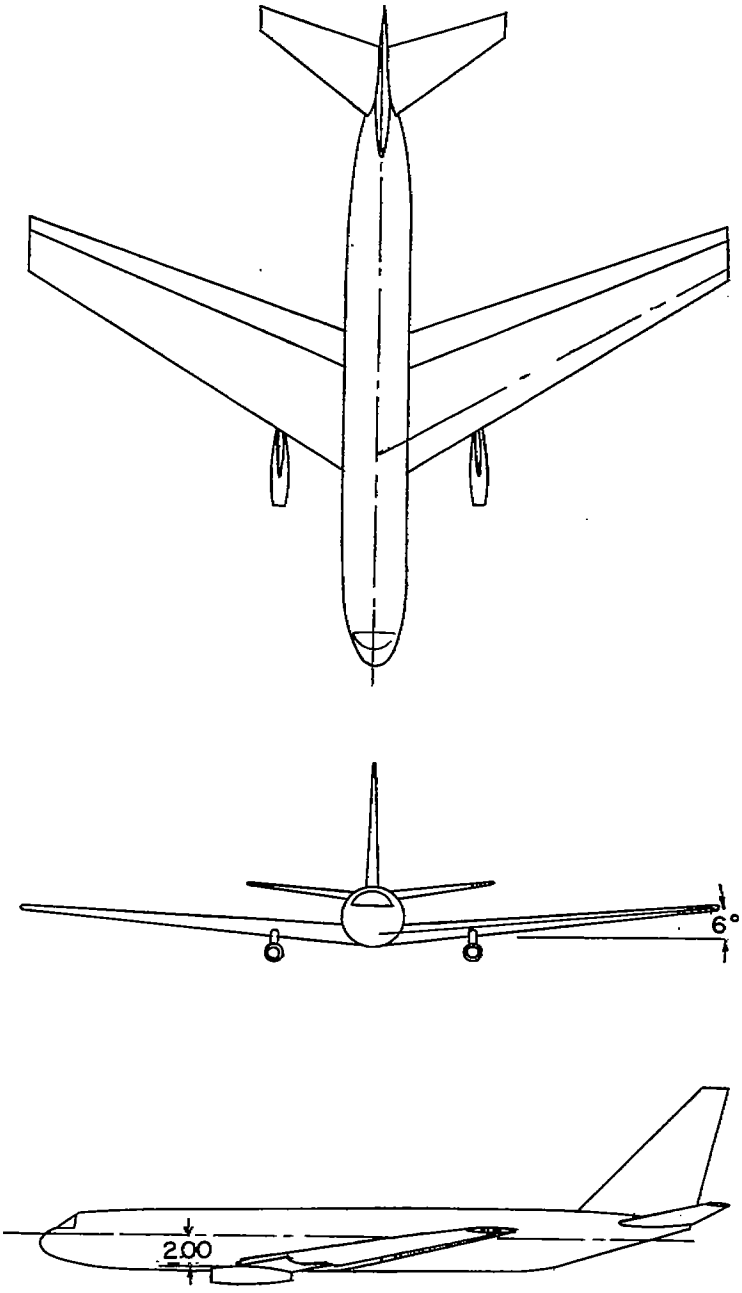

(b) Low-wing configuration. Geometric characteristics of model are the same as those shown in figure 1(a) except as noted.

Figure 1.- Concluded.

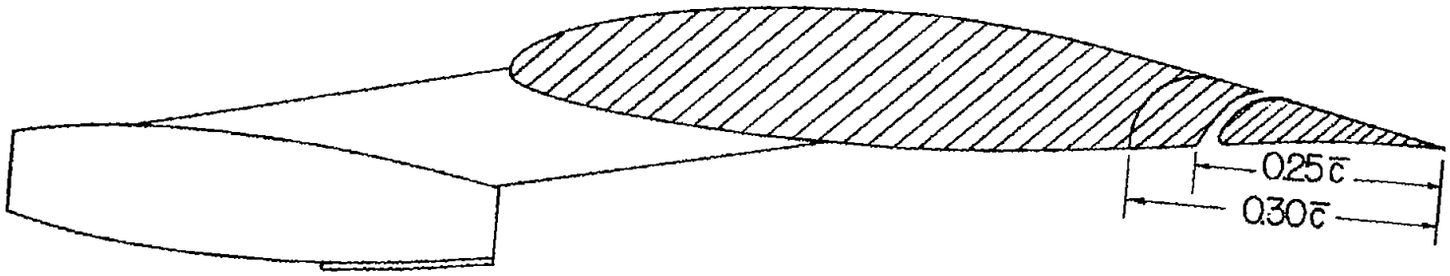

(a) Cross section of wing for cruising-flight condition.

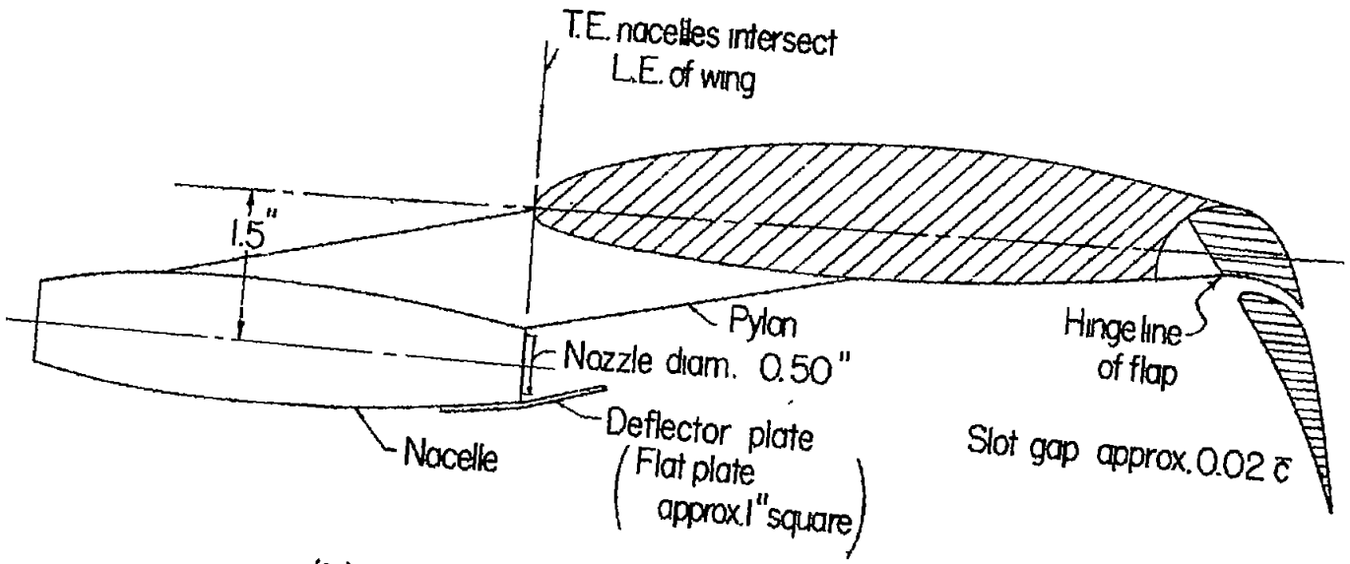

(b) Cross section of wing for landing condition.

Figure 2.- Arrangement of external-flow jet-augmented slotted flap used on the model.

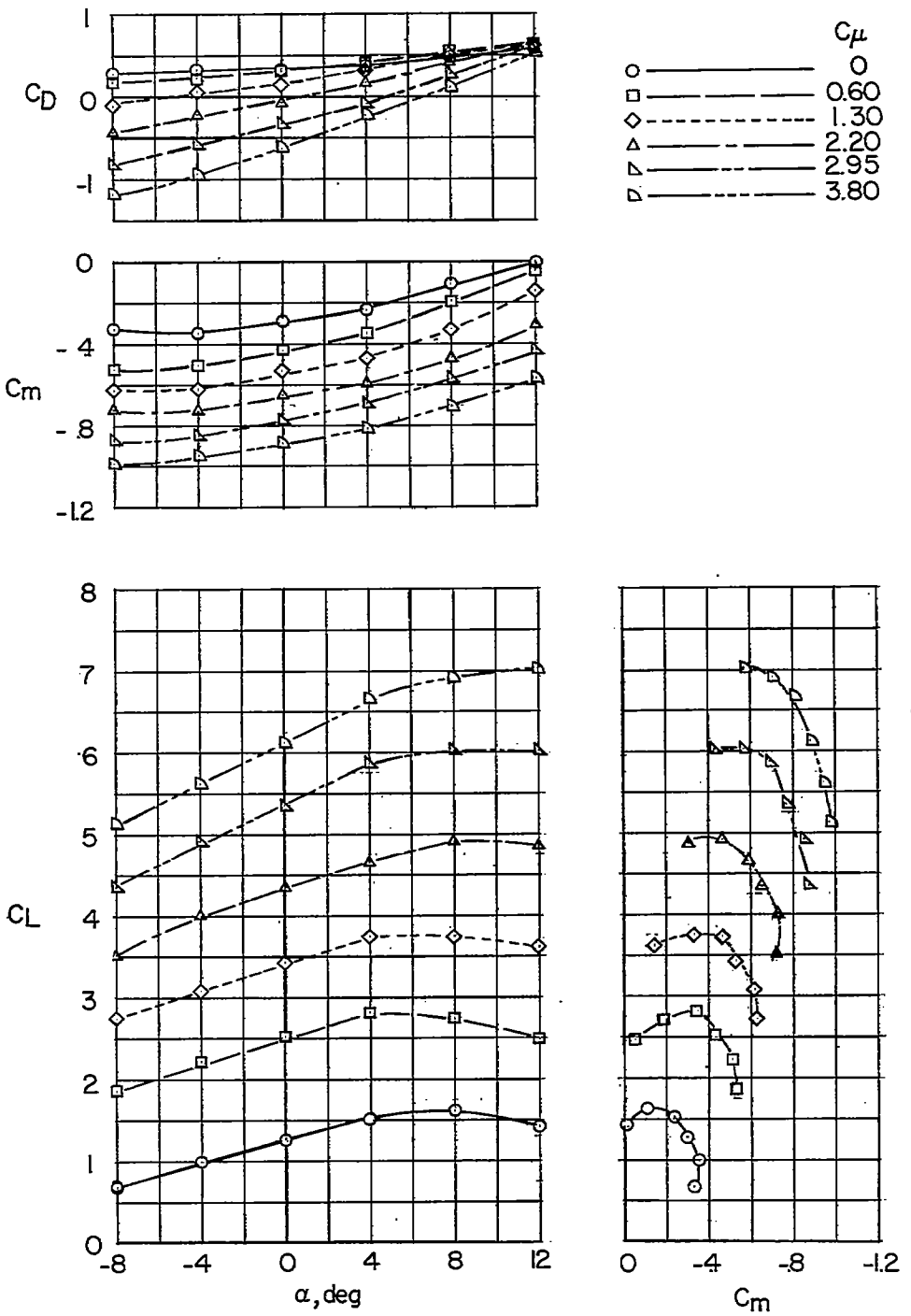

(a) Low-wing configuration. $\delta = 55^\circ$.

Figure 3.- Longitudinal stability and trim characteristics of the model. Horizontal tail off.

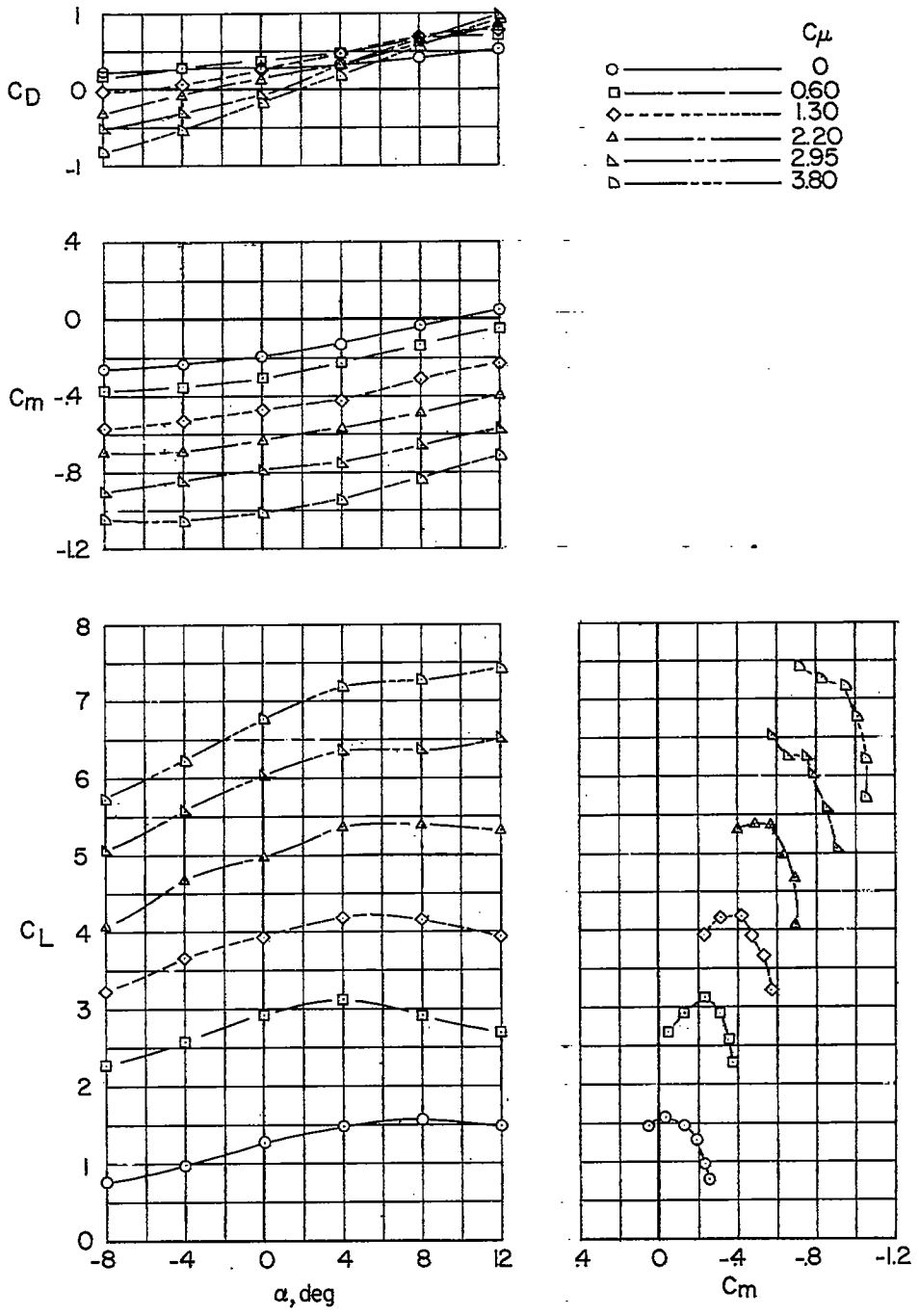

(b) High-wing configuration. $\delta = 60^\circ$.

Figure 3.- Continued.

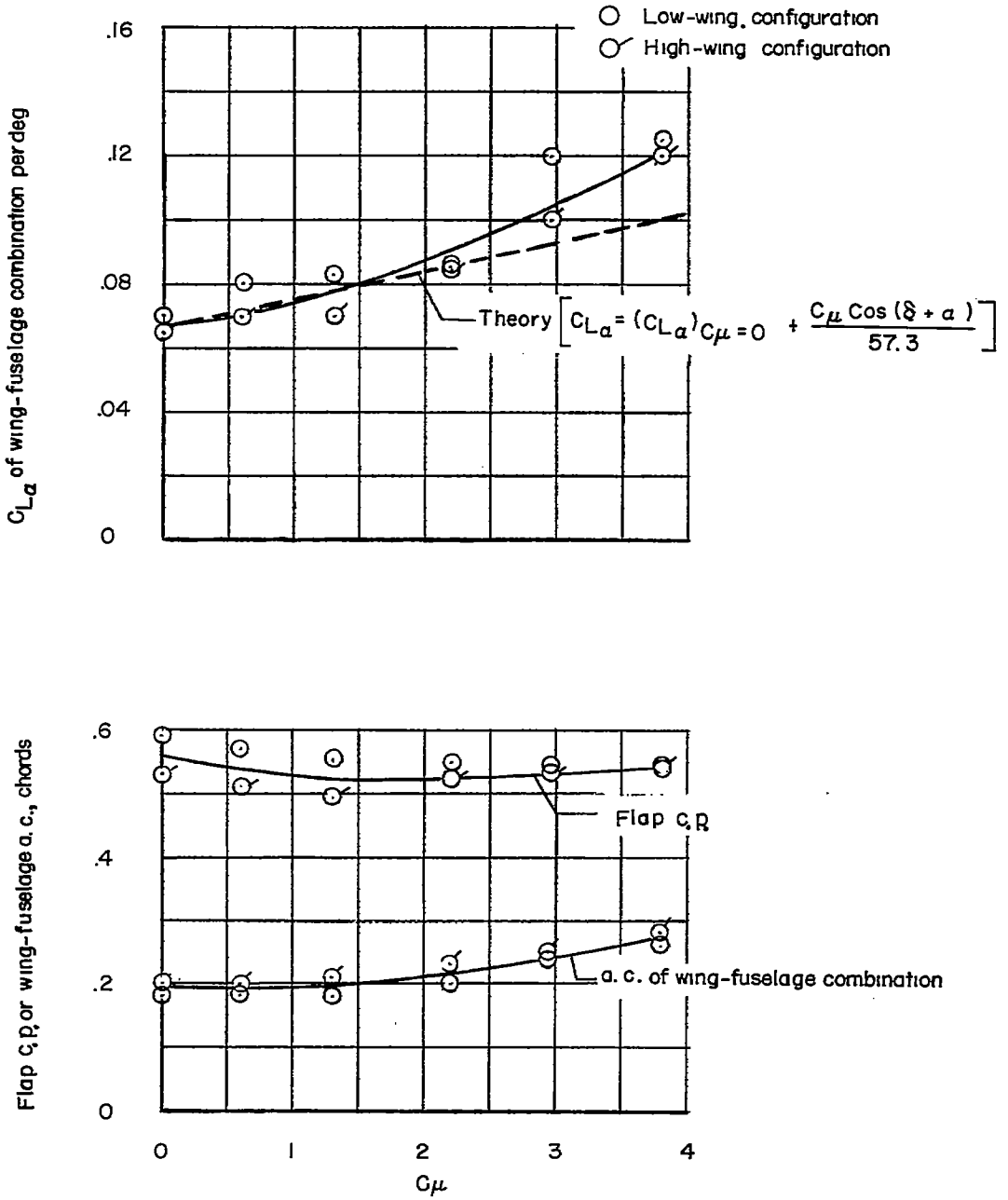

(c) Flap center of pressure, C_{L_α}, and aerodynamic center of wing-fuselage combination.

Figure 3.- Concluded.

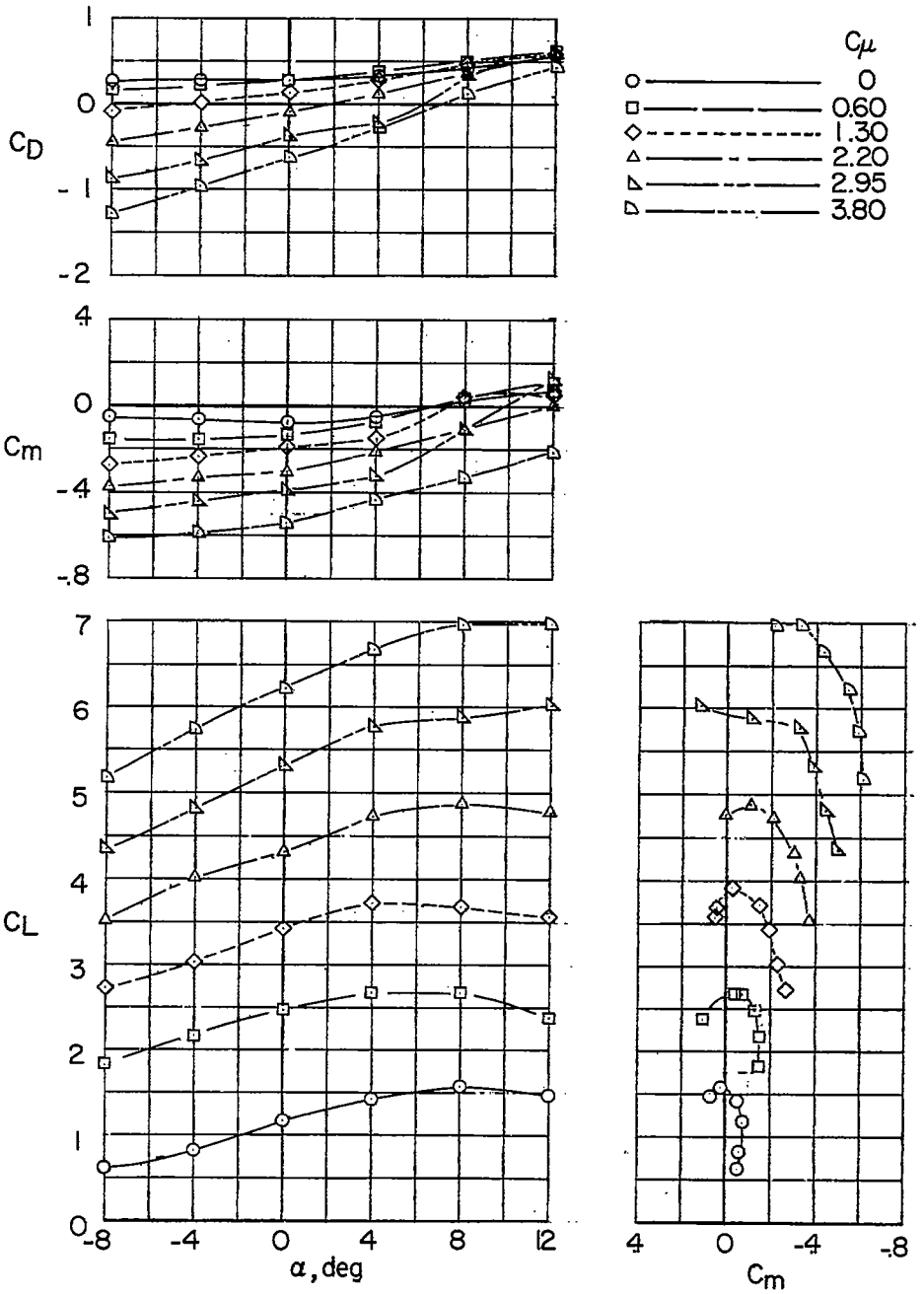

(a) $i_t = 0°$.

Figure 4.- Longitudinal stability and trim characteristics of the low-wing configuration. Low tail position; $\delta = 55°$; $S_t/S = 0.17$.

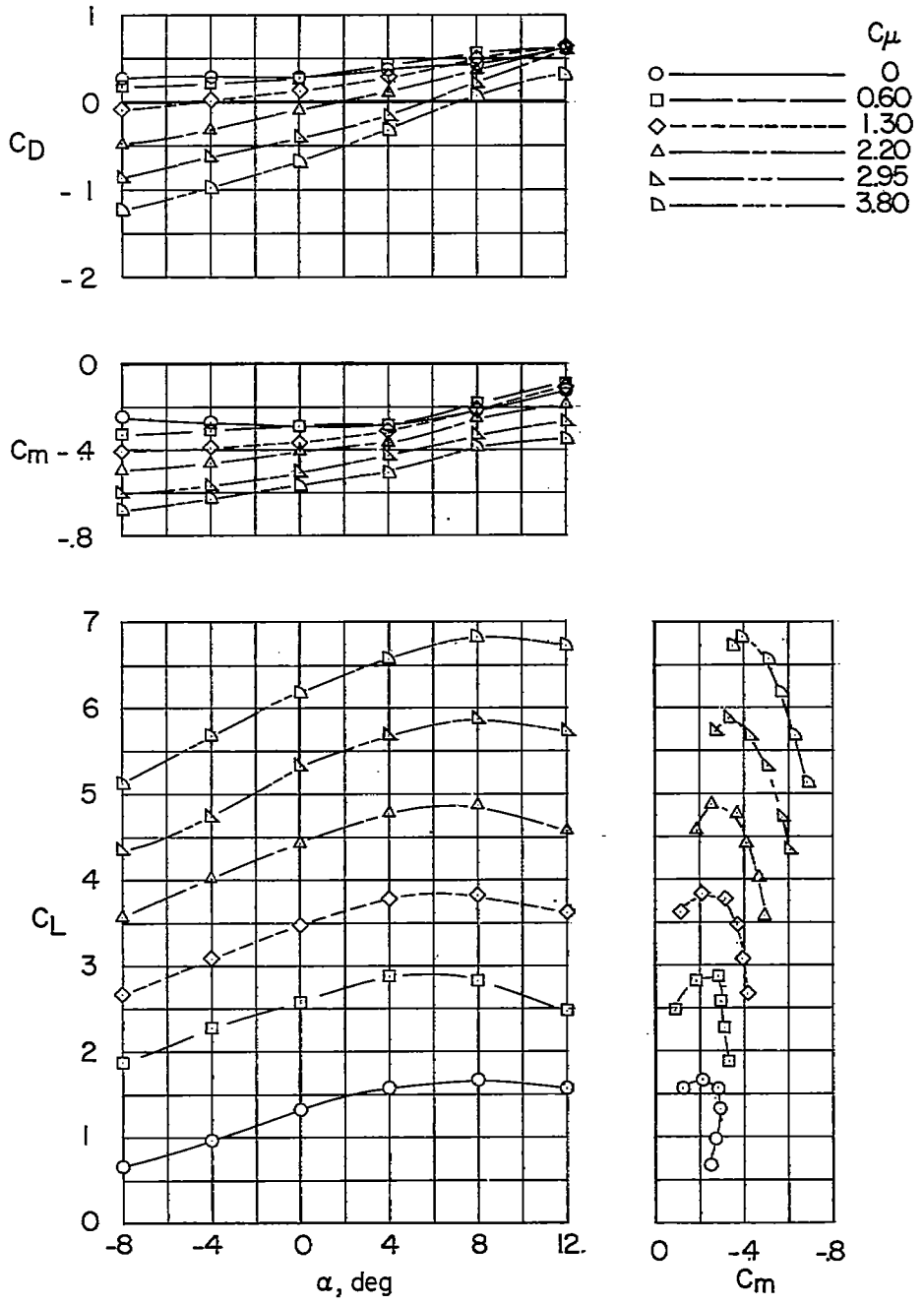

(b) $i_t = 10°$.

Figure 4.- Continued.

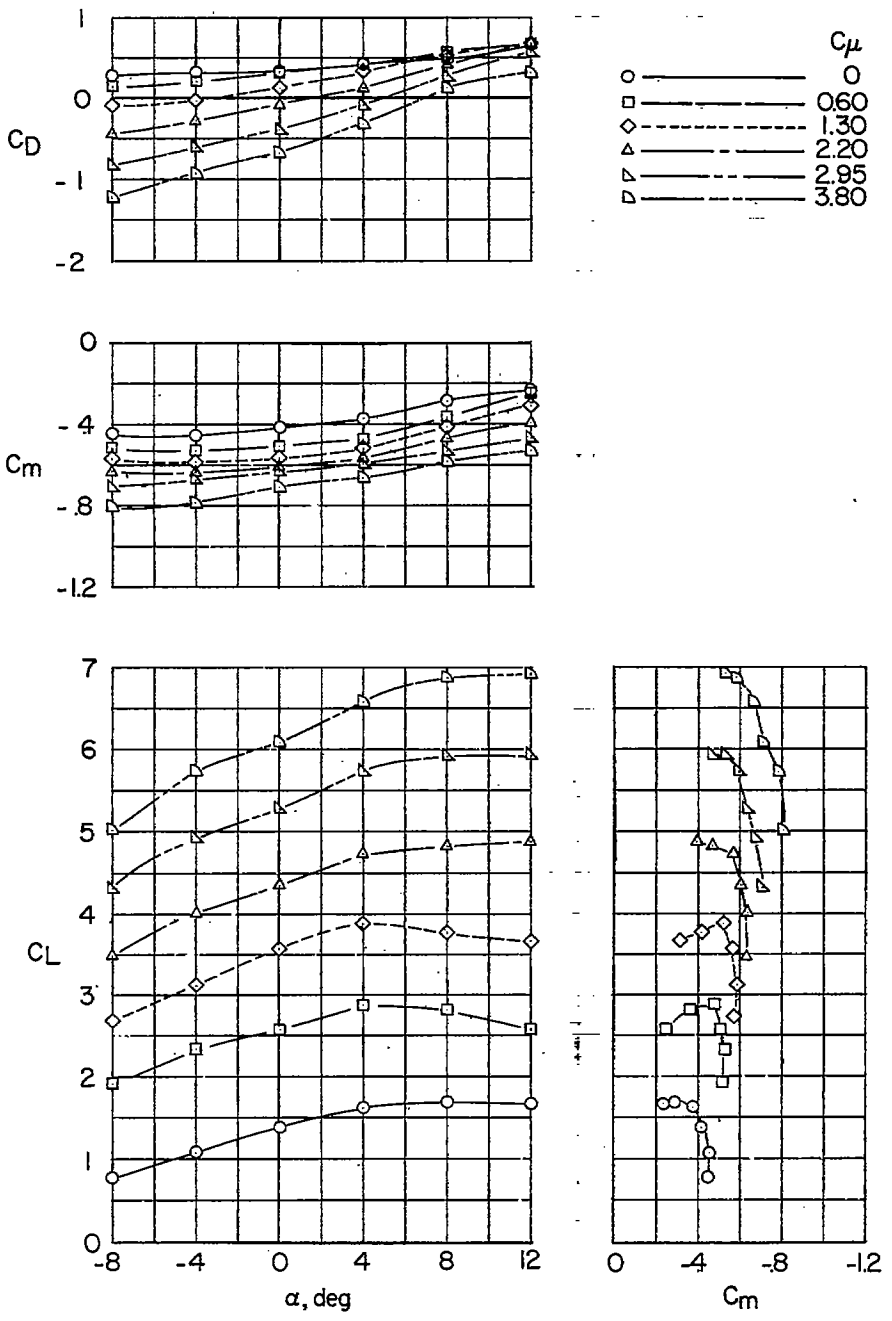

(c) $i_t = 20°$.

Figure 4.- Continued.

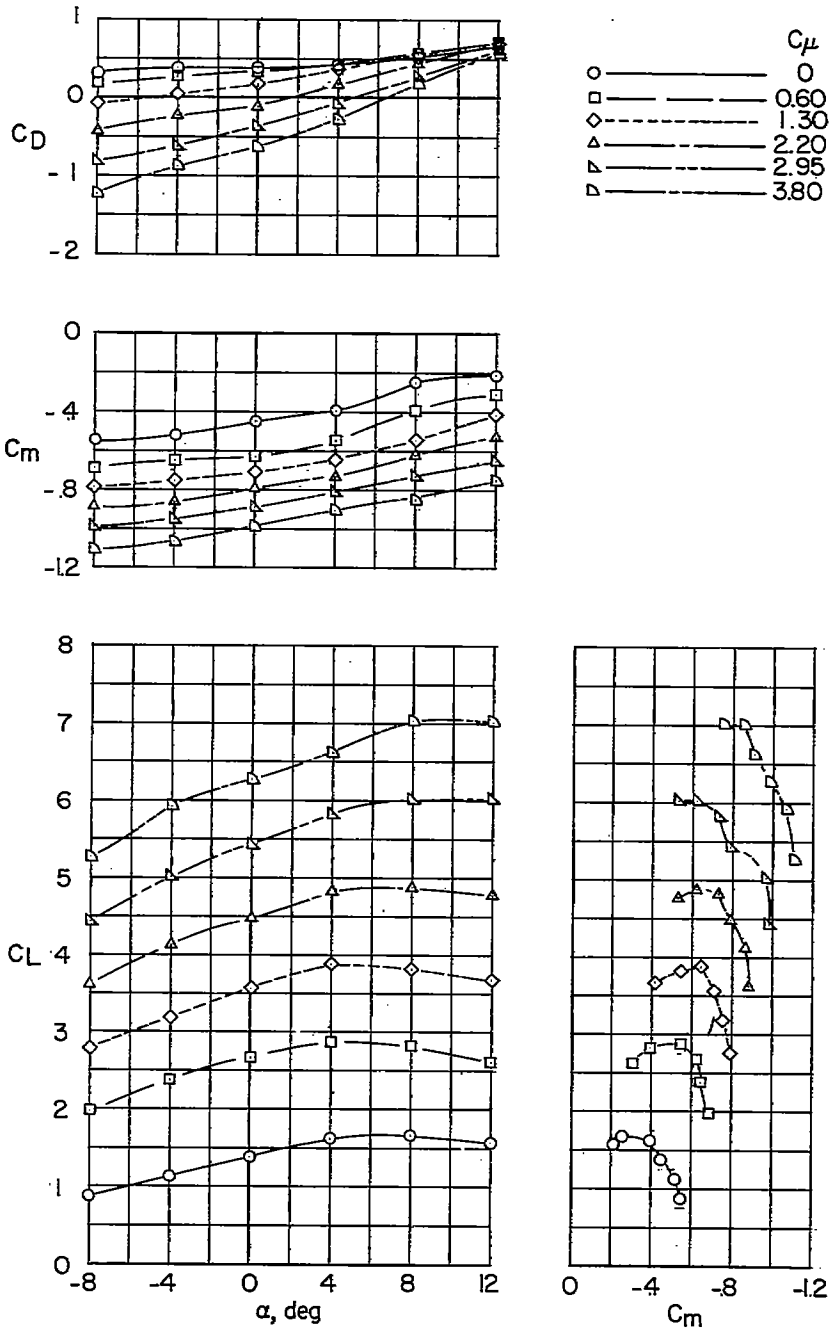

(d) $i_t = 30°$.

Figure 4.- Concluded.

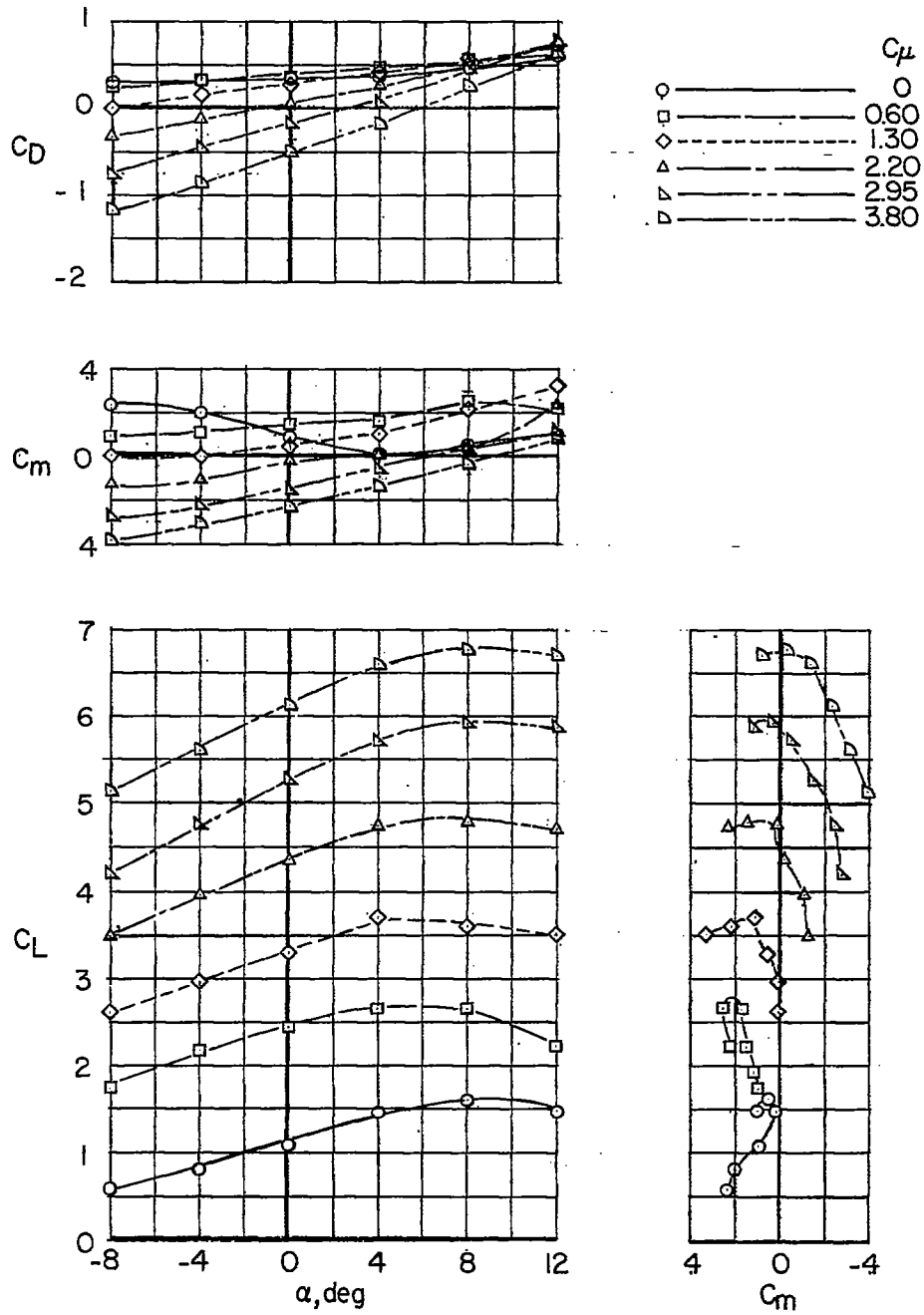

(a) $i_t = 0°$.

Figure 5.- Longitudinal stability and trim characteristics of the low-wing configuration. Low tail position; $\delta = 55°$; $S_t/S = 0.34$.

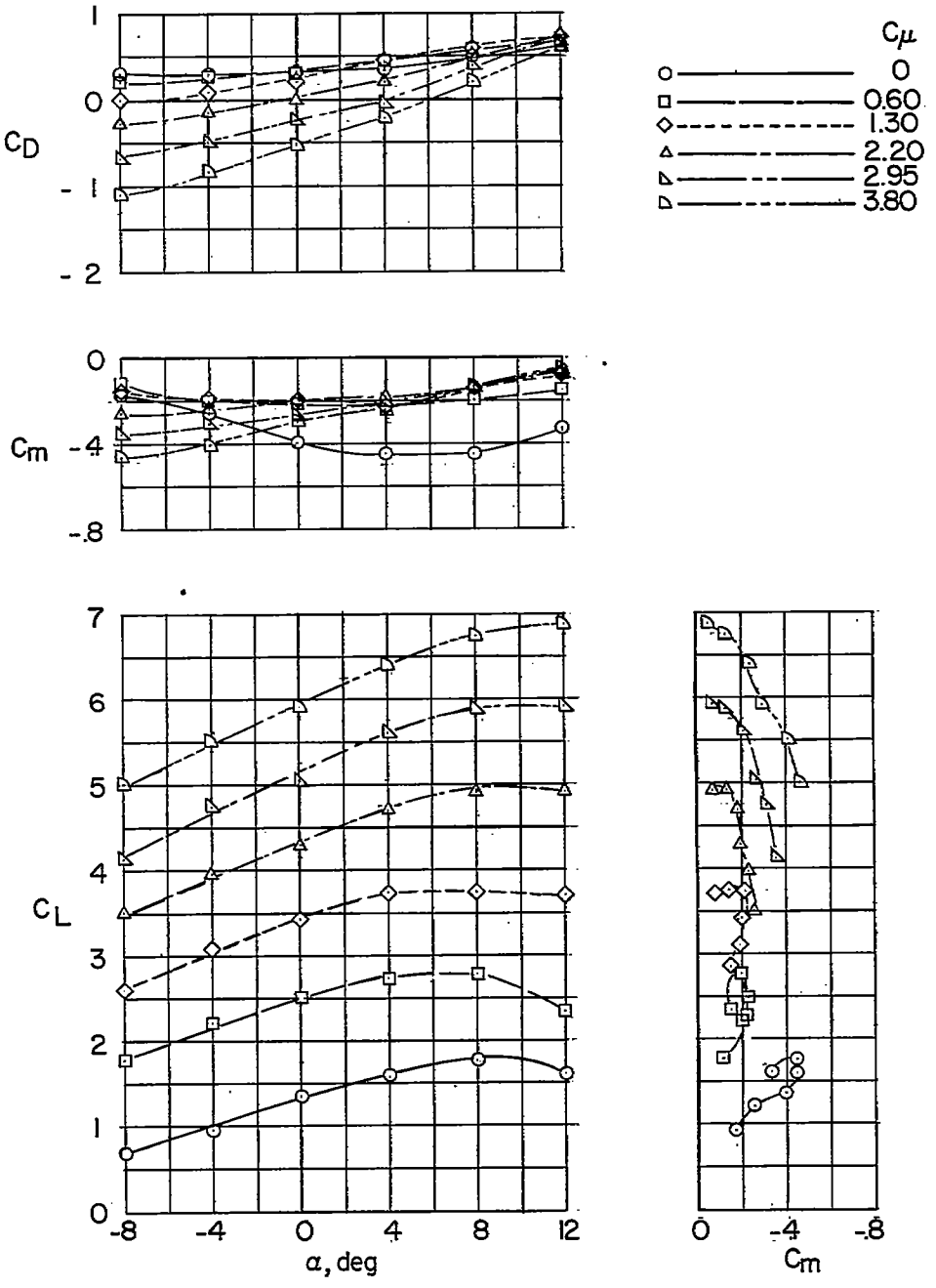

(b) $i_t = 10^\circ$.

Figure 5.- Continued.

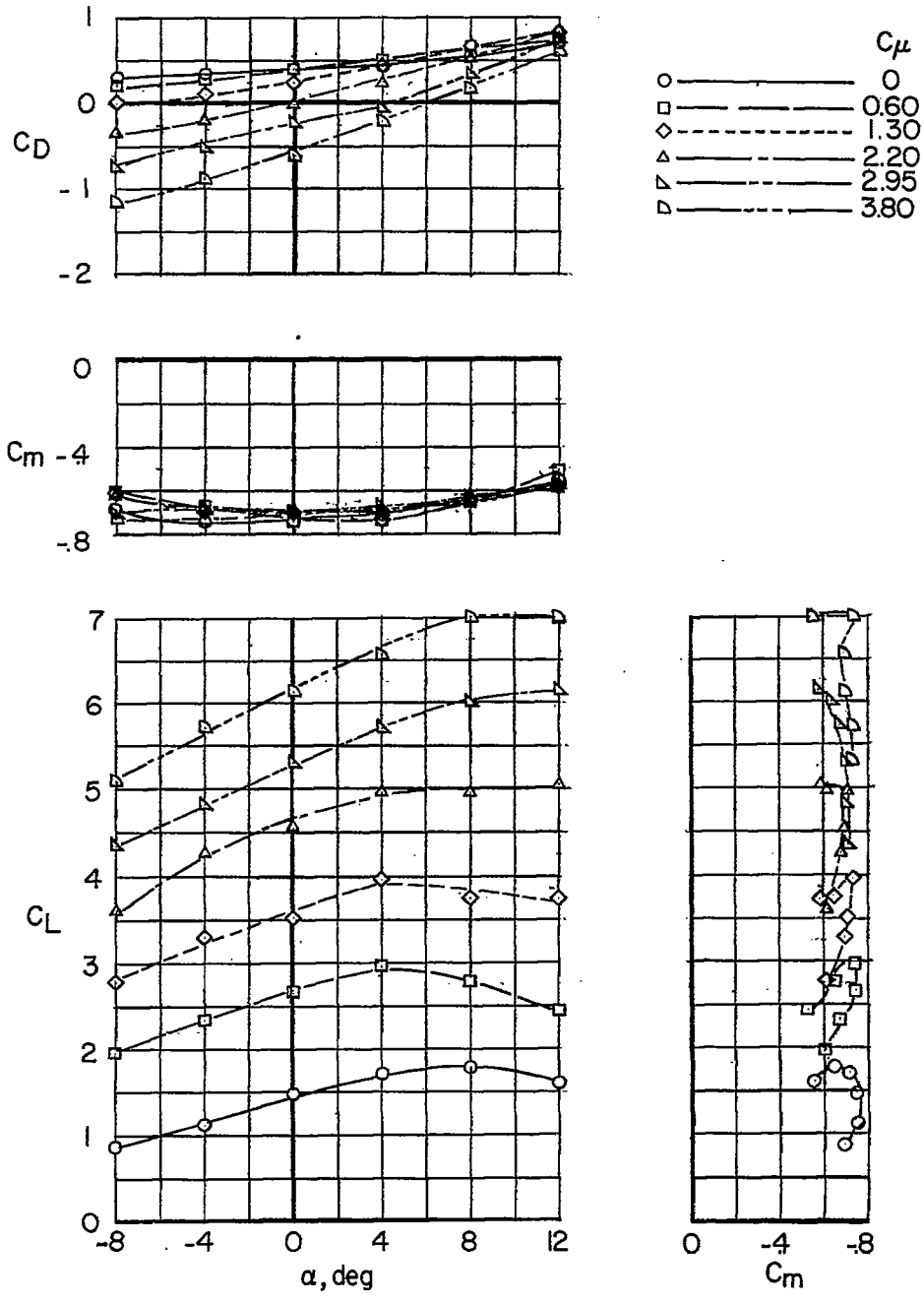

(c) $i_t = 20^\circ$.

Figure 5.- Continued.

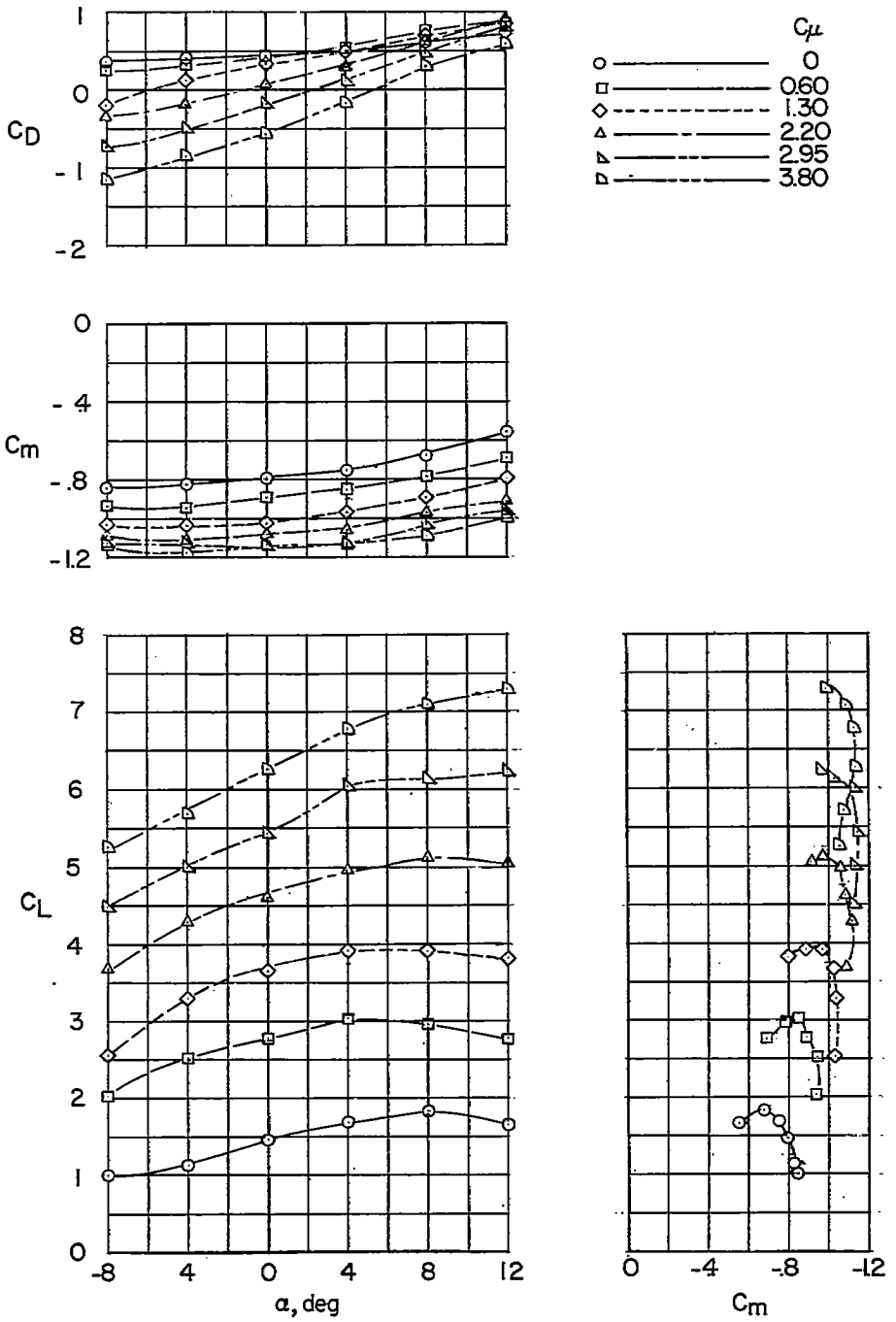

(d) $i_t = 30°$.

Figure 5.- Concluded.

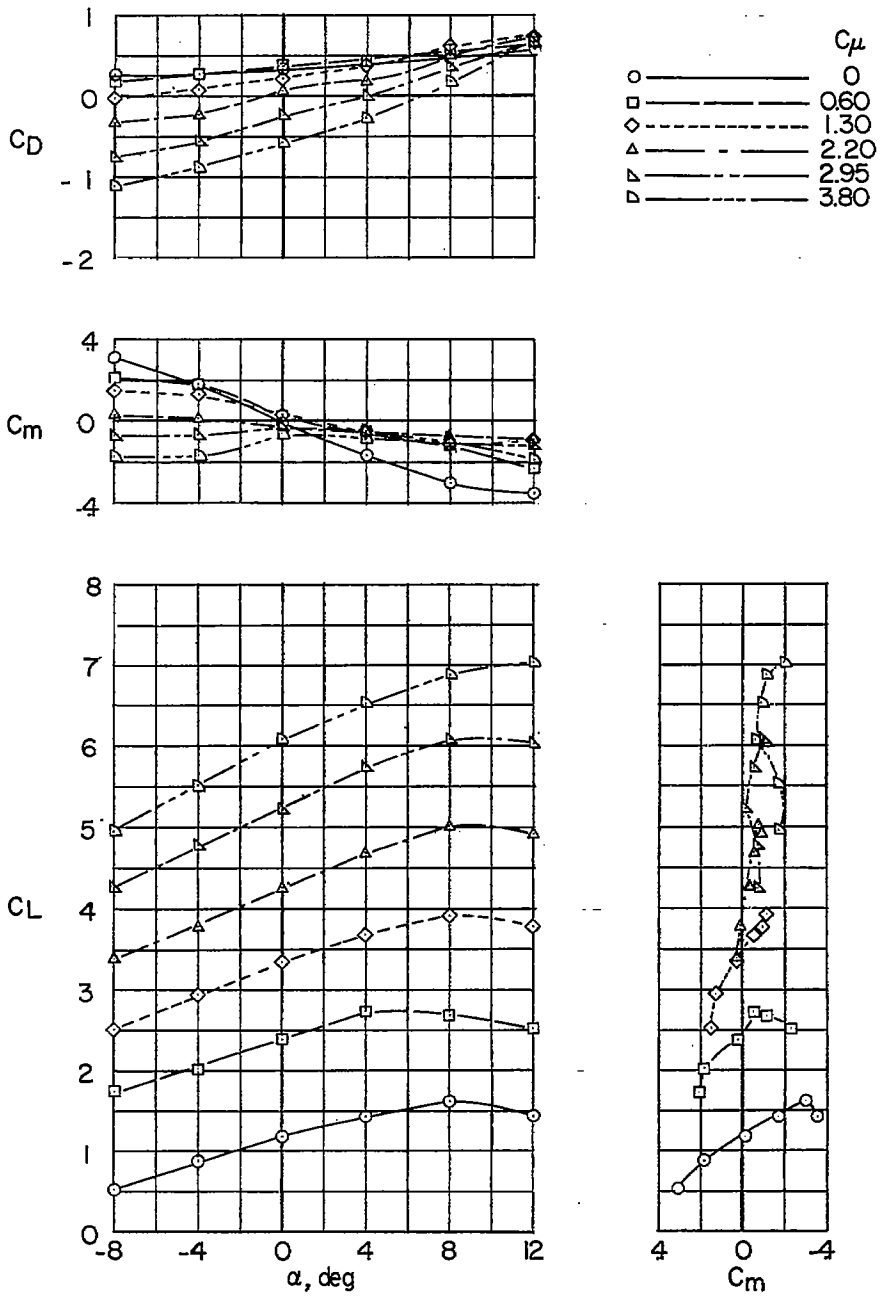

(a) $i_t = 0°$.

Figure 6.- Longitudinal stability and trim characteristics of the low-wing configuration. High tail position; $\delta = 55°$; $S_t/S = 0.34$.

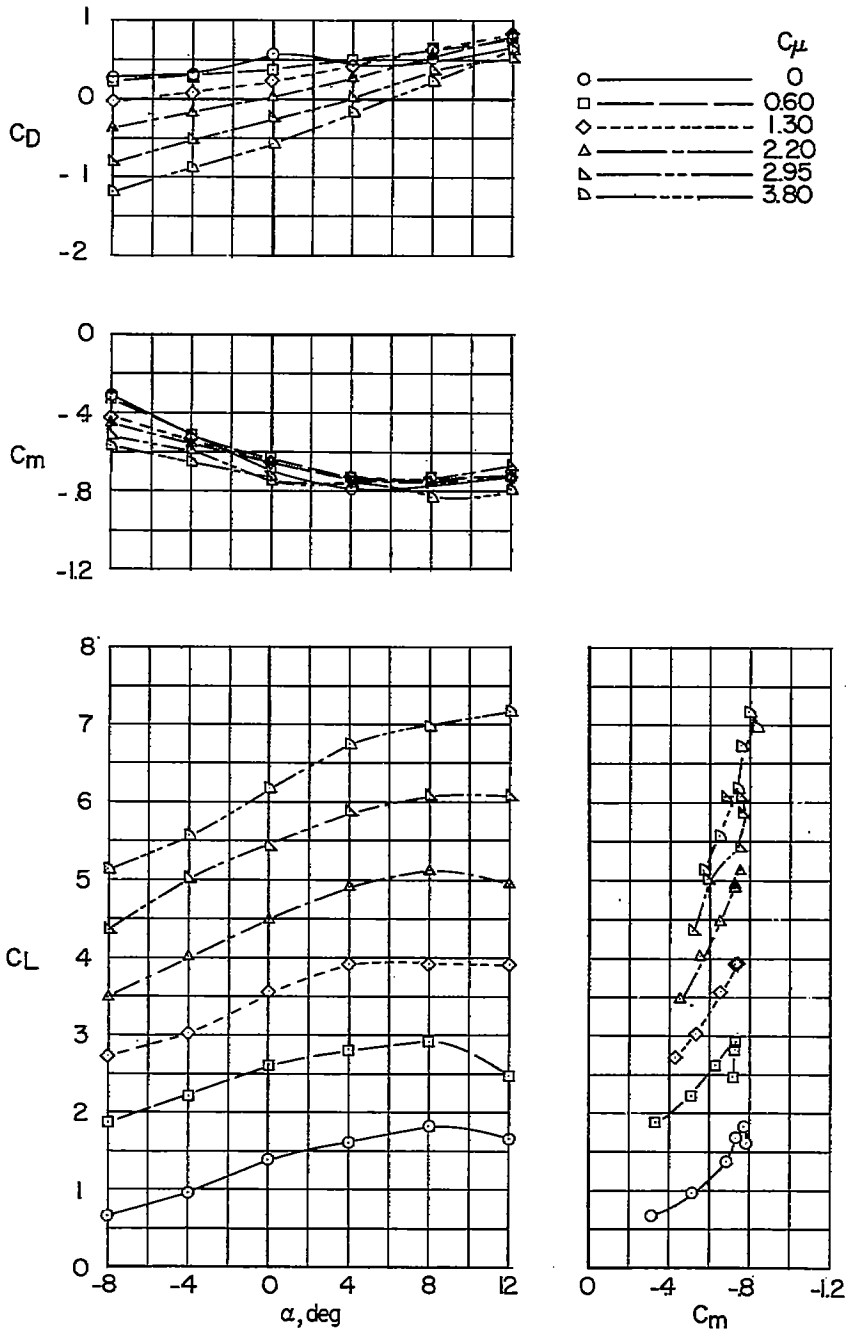

(b) $i_t = 10°$.

Figure 6.- Continued.

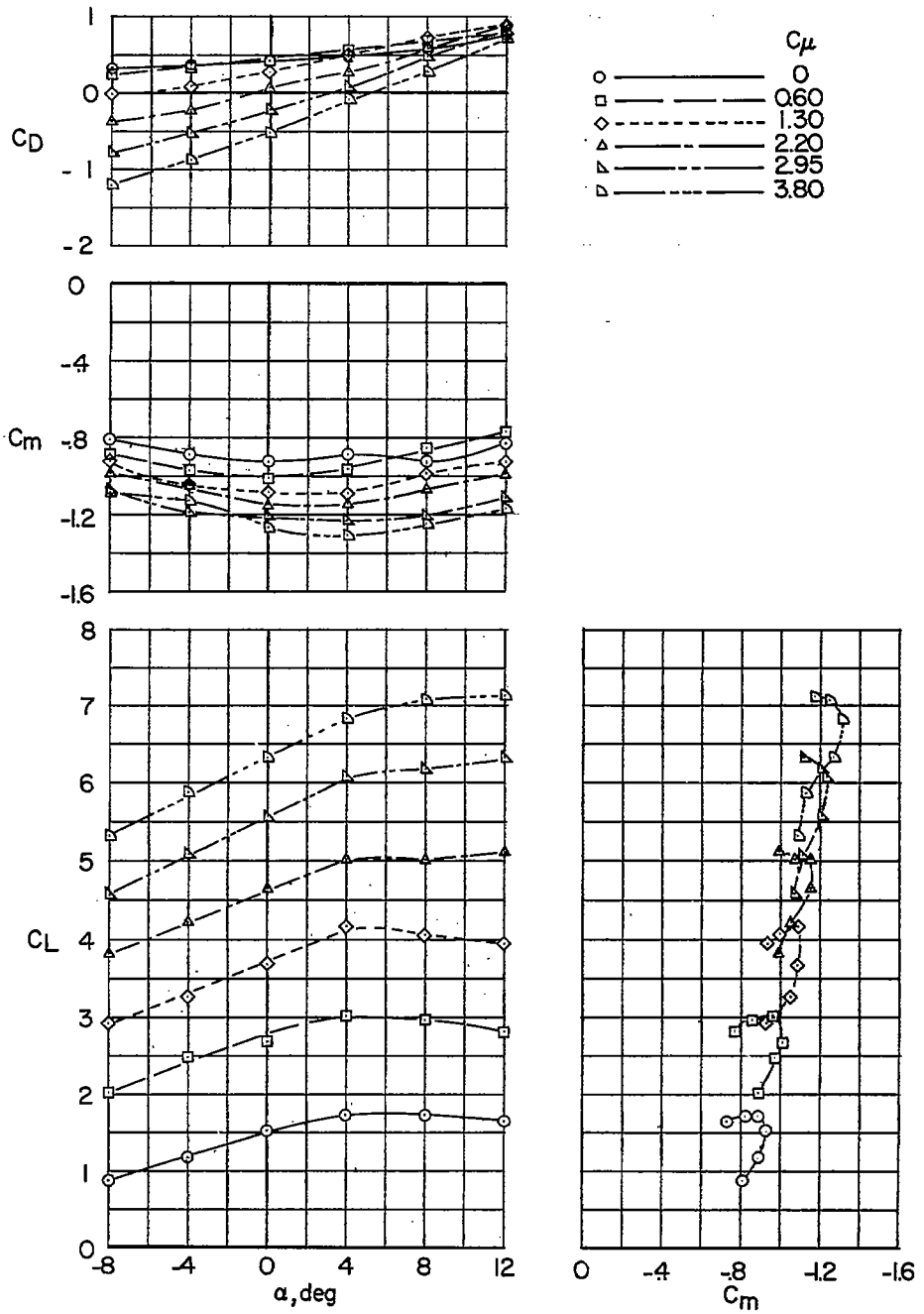

(c) $i_t = 20°$.

Figure 6.- Continued.

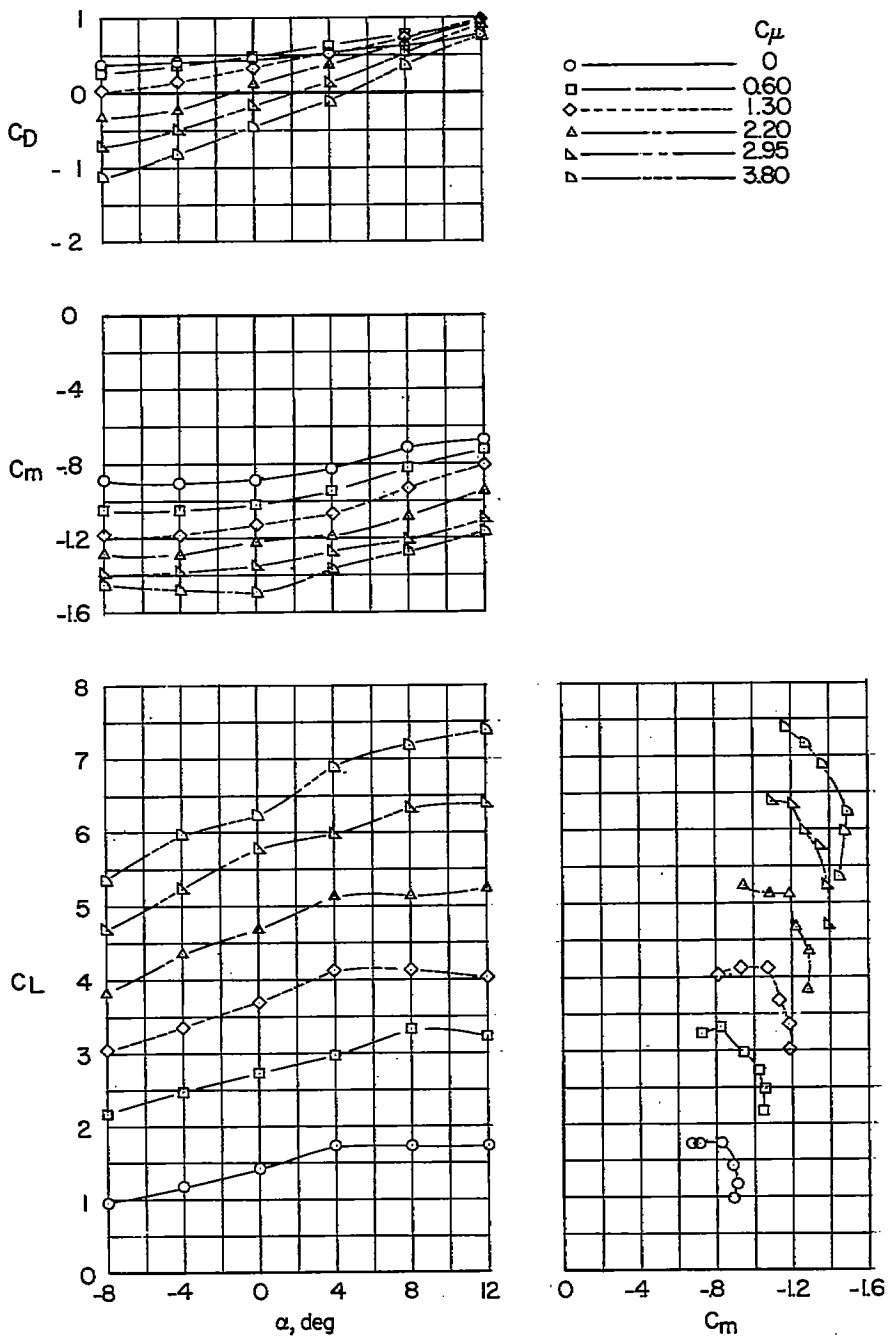

(d) $i_t = 30^\circ$.

Figure 6.- Concluded.

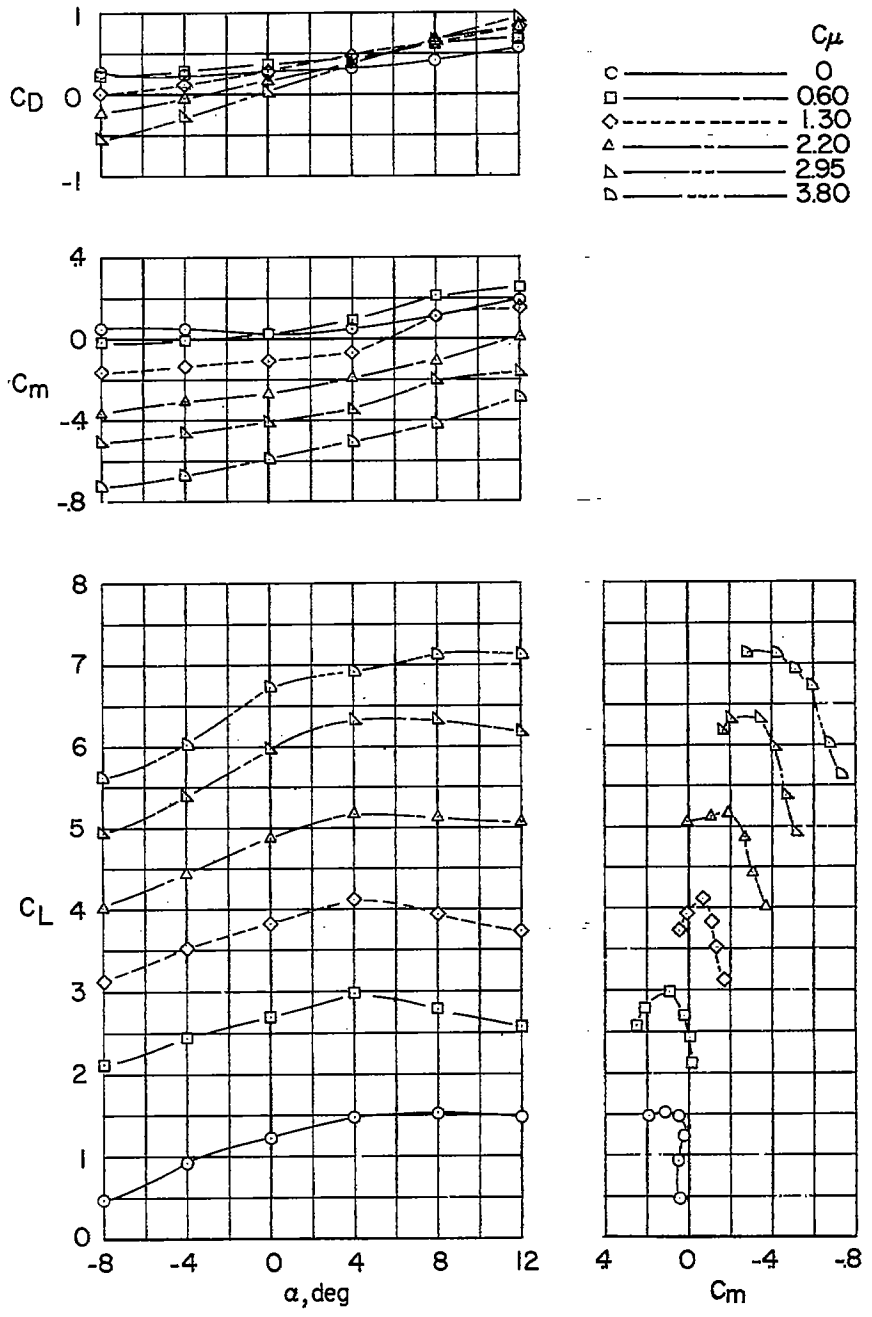

(a) $i_t = 0°$.

Figure 7.- Longitudinal stability and trim characteristics of the high-wing configuration. Low tail position; $\delta = 60°$; $S_t/S = 0.17$.

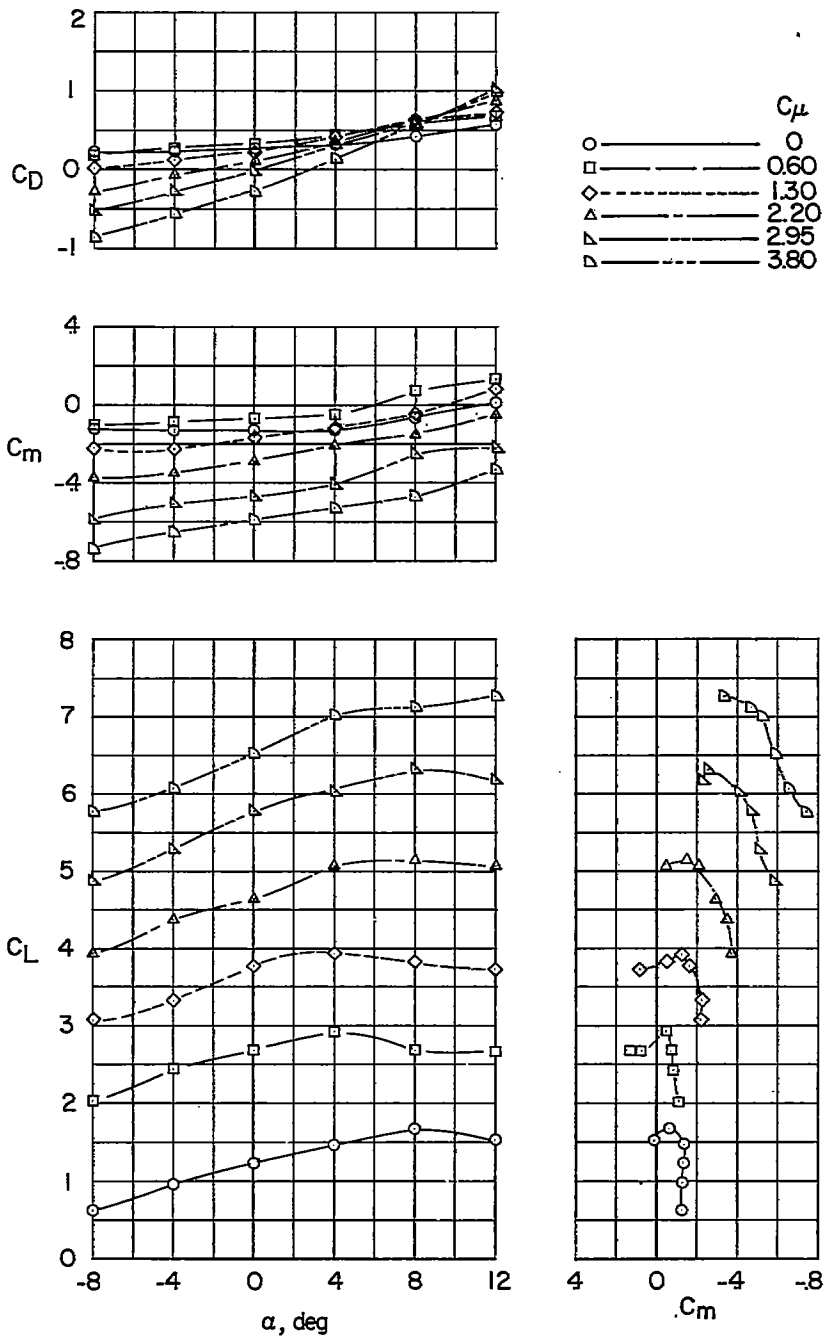

(b) $i_t = 10°$.

Figure 7.- Concluded.

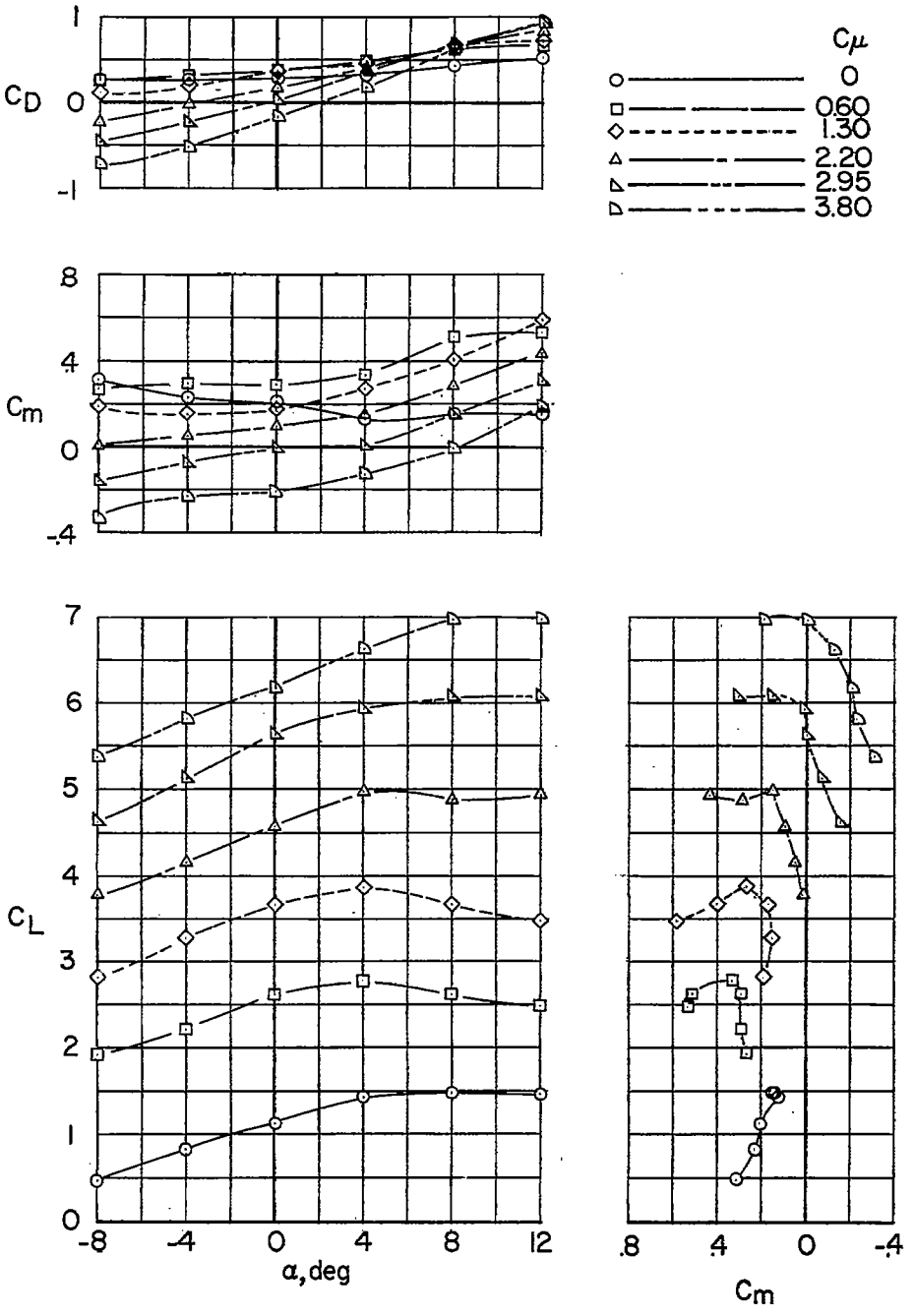

(a) $i_t = 0°$.

Figure 8.- Longitudinal stability and trim characteristics of the high-wing configuration. Low tail position; $\delta = 60°$; $S_t/S = 0.34$.

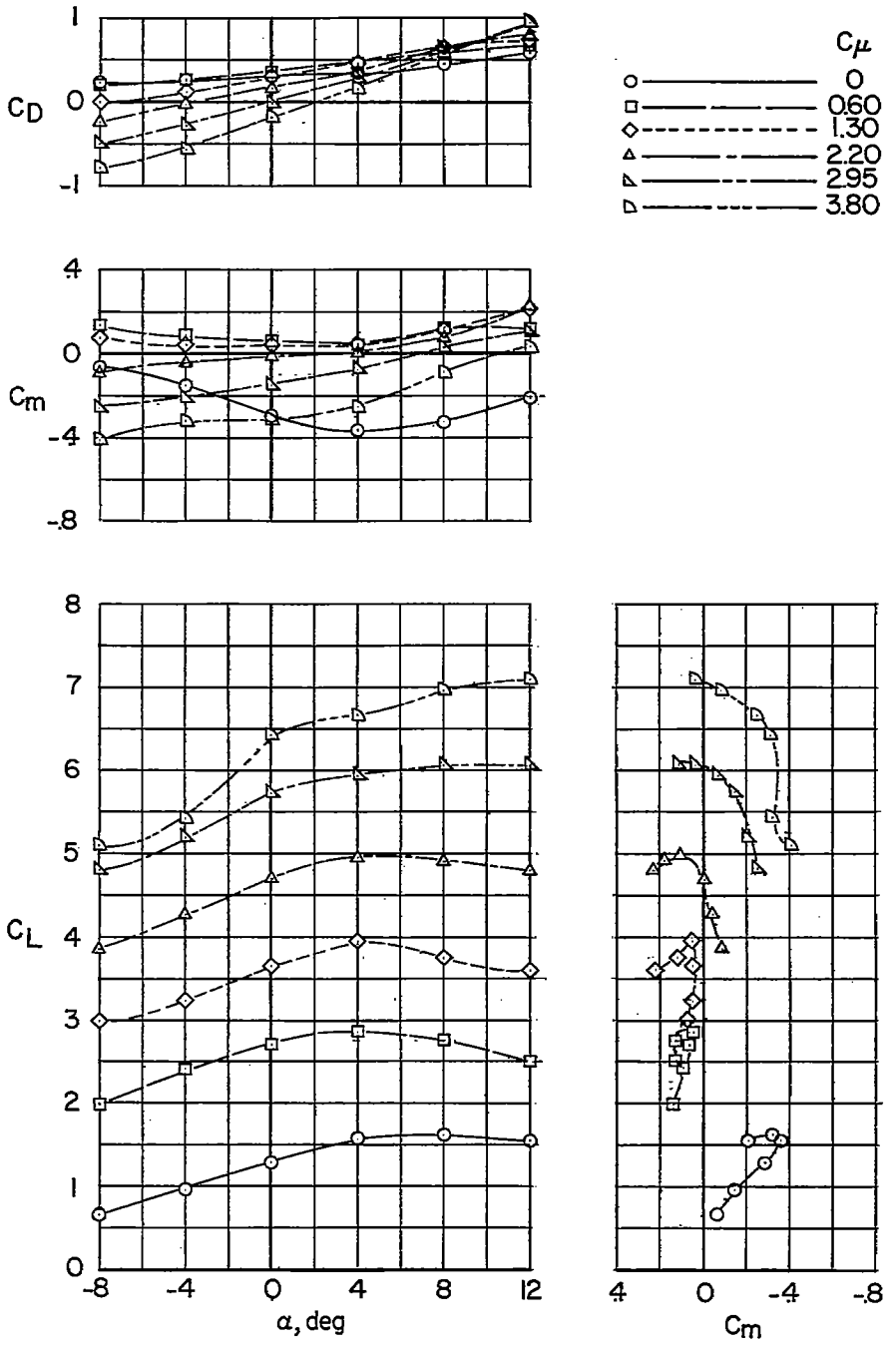

(b) $i_t = 10^\circ$.

Figure 8.- Concluded.

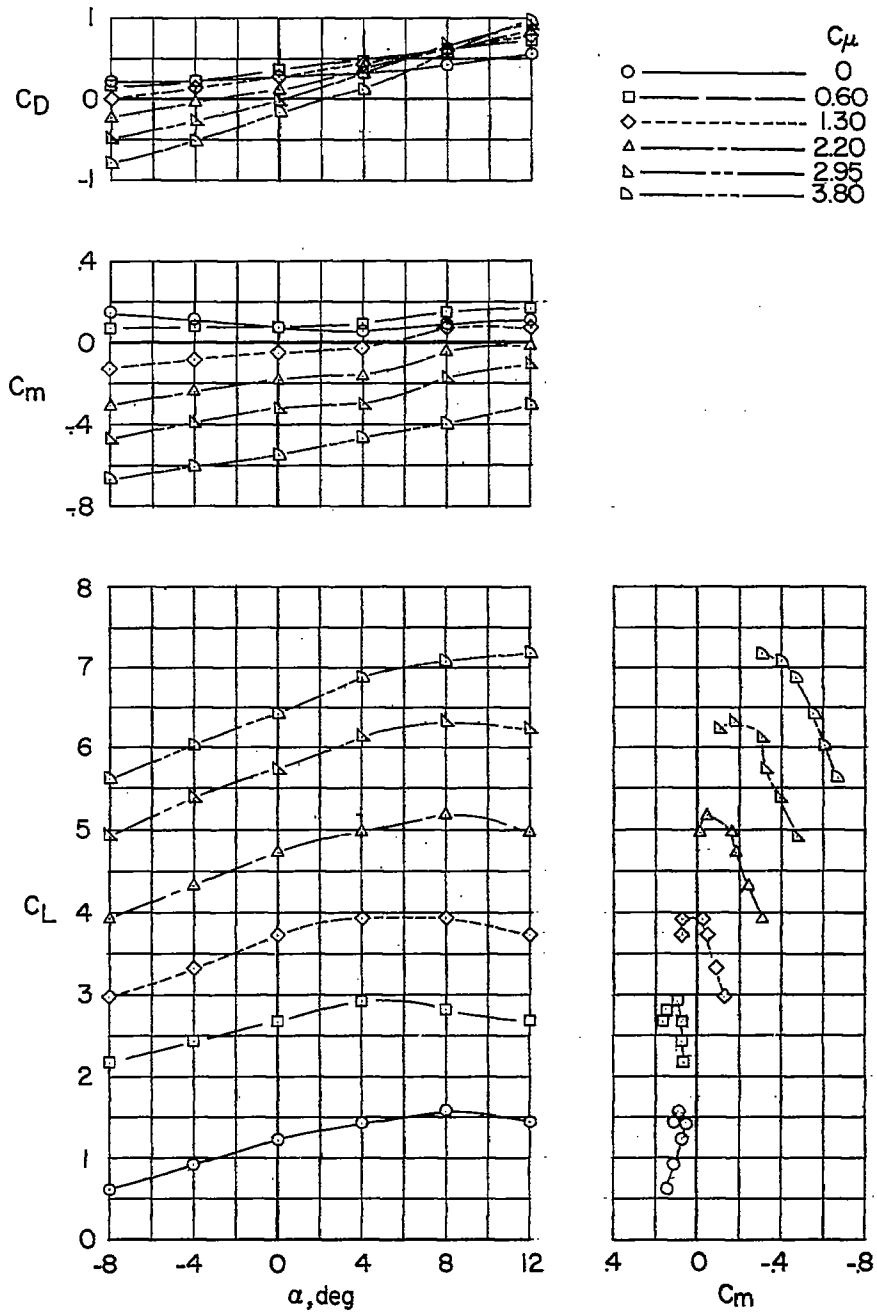

(a) $i_t = 0°$.

Figure 9.- Longitudinal stability and trim characteristics of the high-wing configuration. High tail position; $\delta = 60°$; $S_t/S = 0.17$.

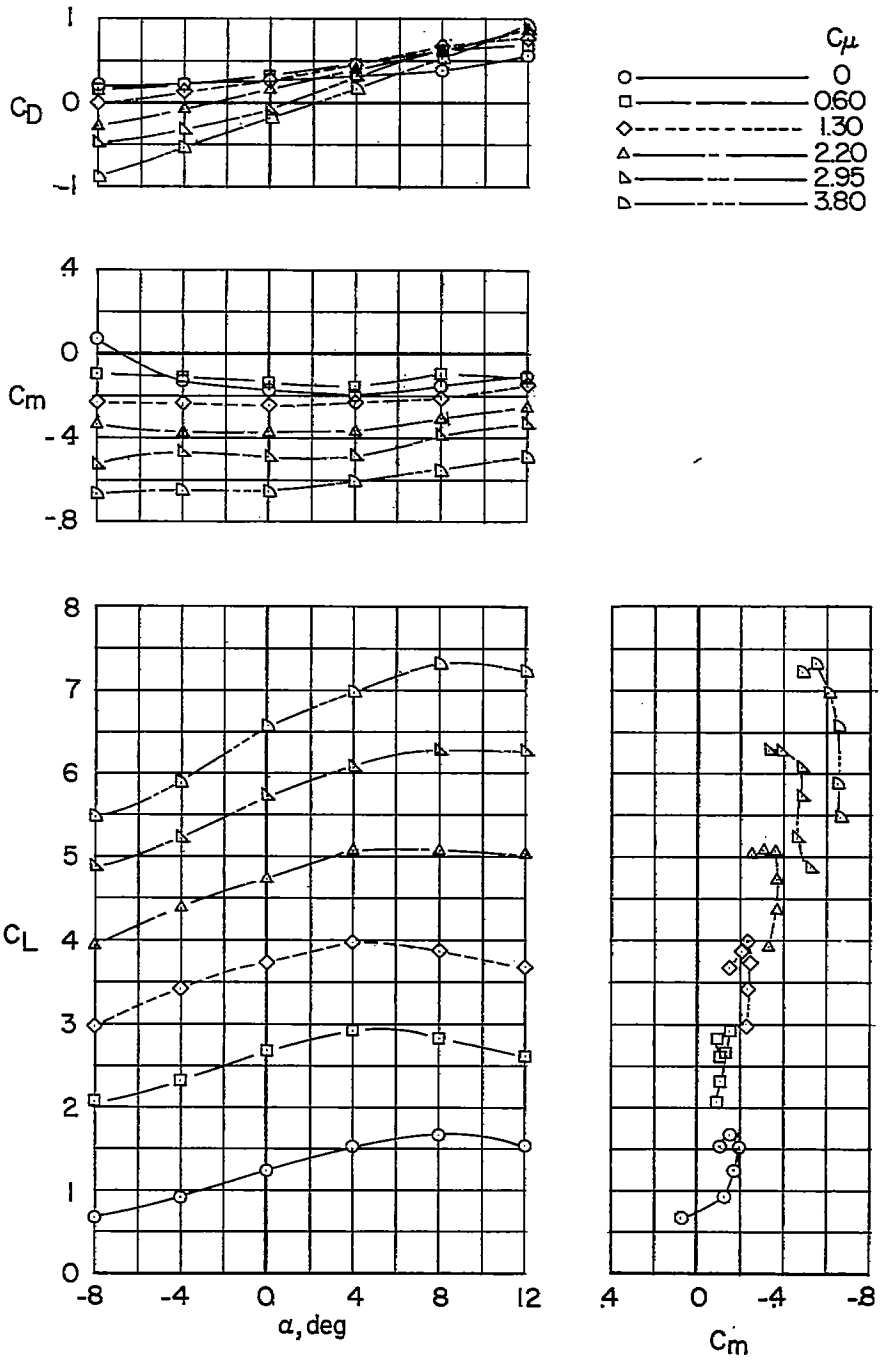

(b) $i_t = 10°$.

Figure 9.- Concluded.

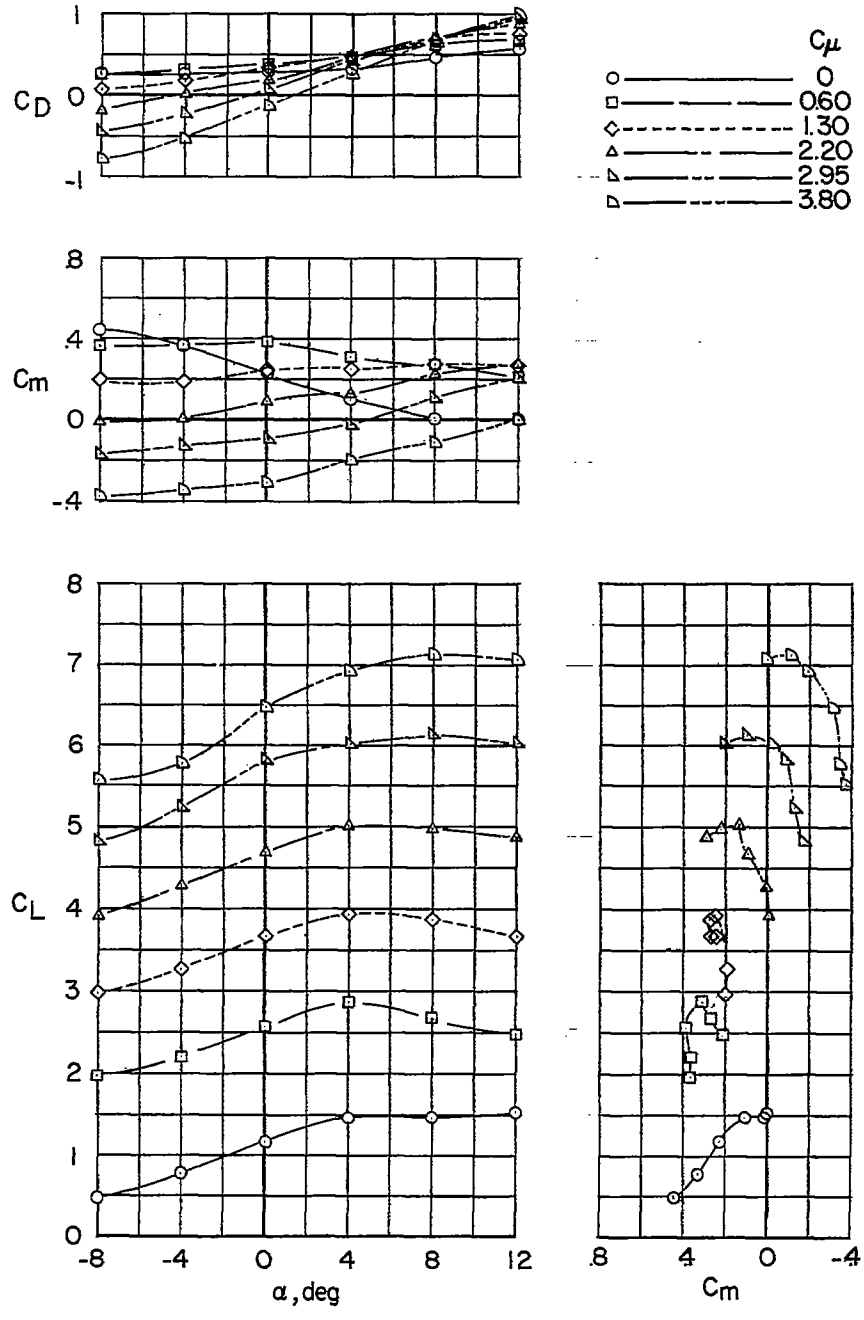

(a) $i_t = 0°$.

Figure 10.- Longitudinal stability and trim characteristics of the high-wing configuration. High tail position; $\delta = 60°$; $S_t/S = 0.34$.

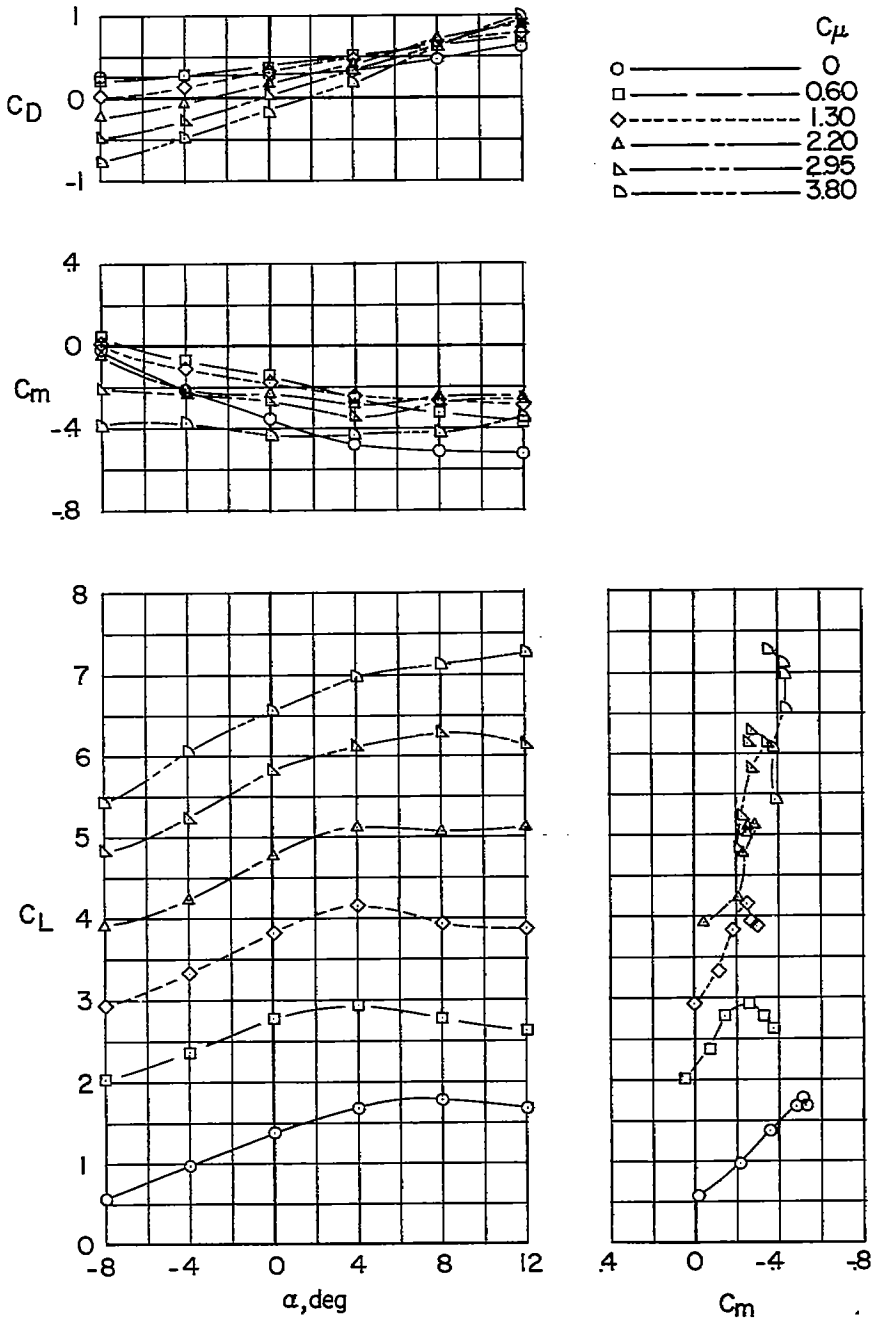

(b) $i_t = 10^\circ$.

Figure 10.- Concluded.

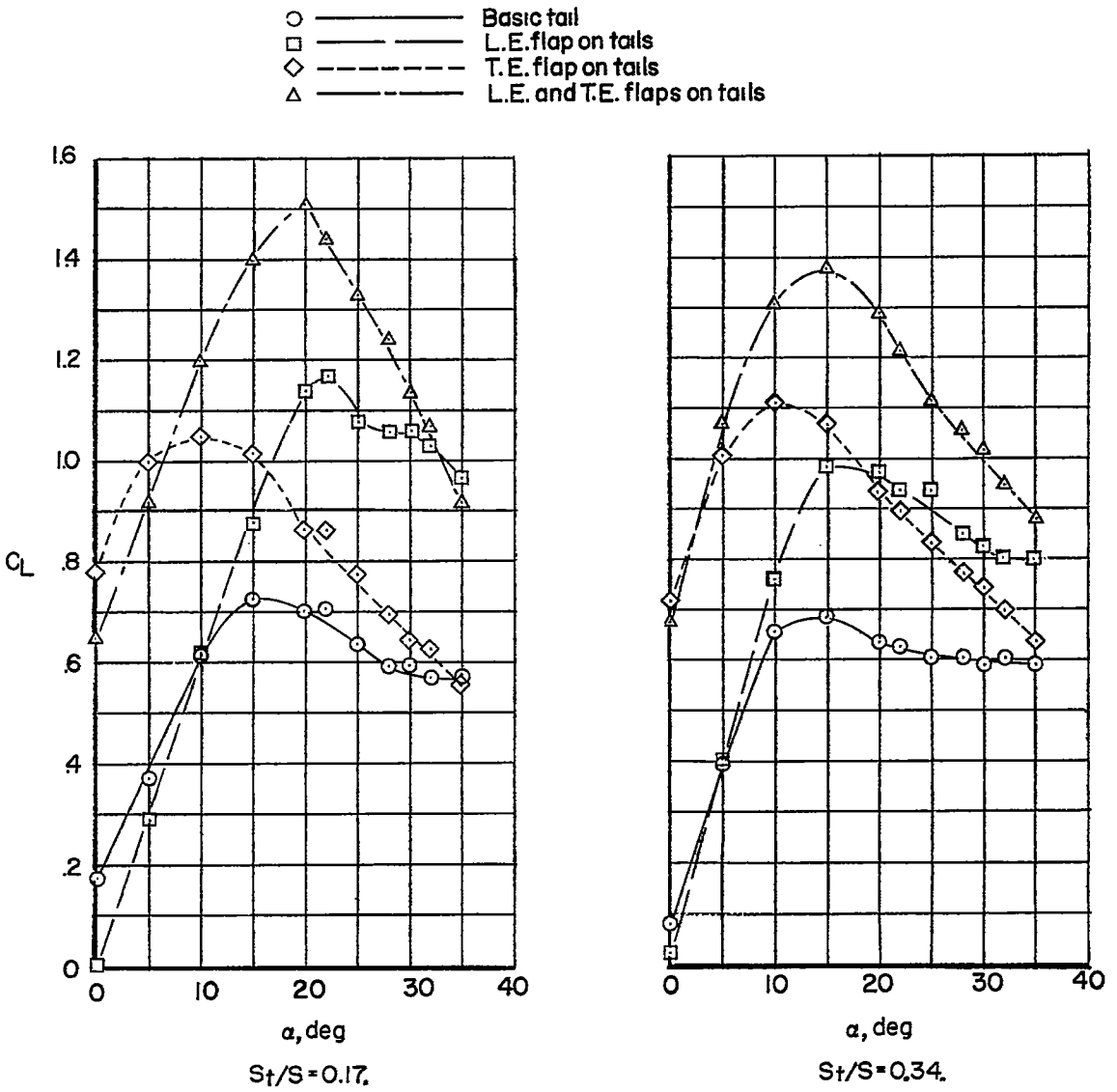

Figure 11.- Aerodynamic characteristics of the horizontal-tail surfaces used on the model.

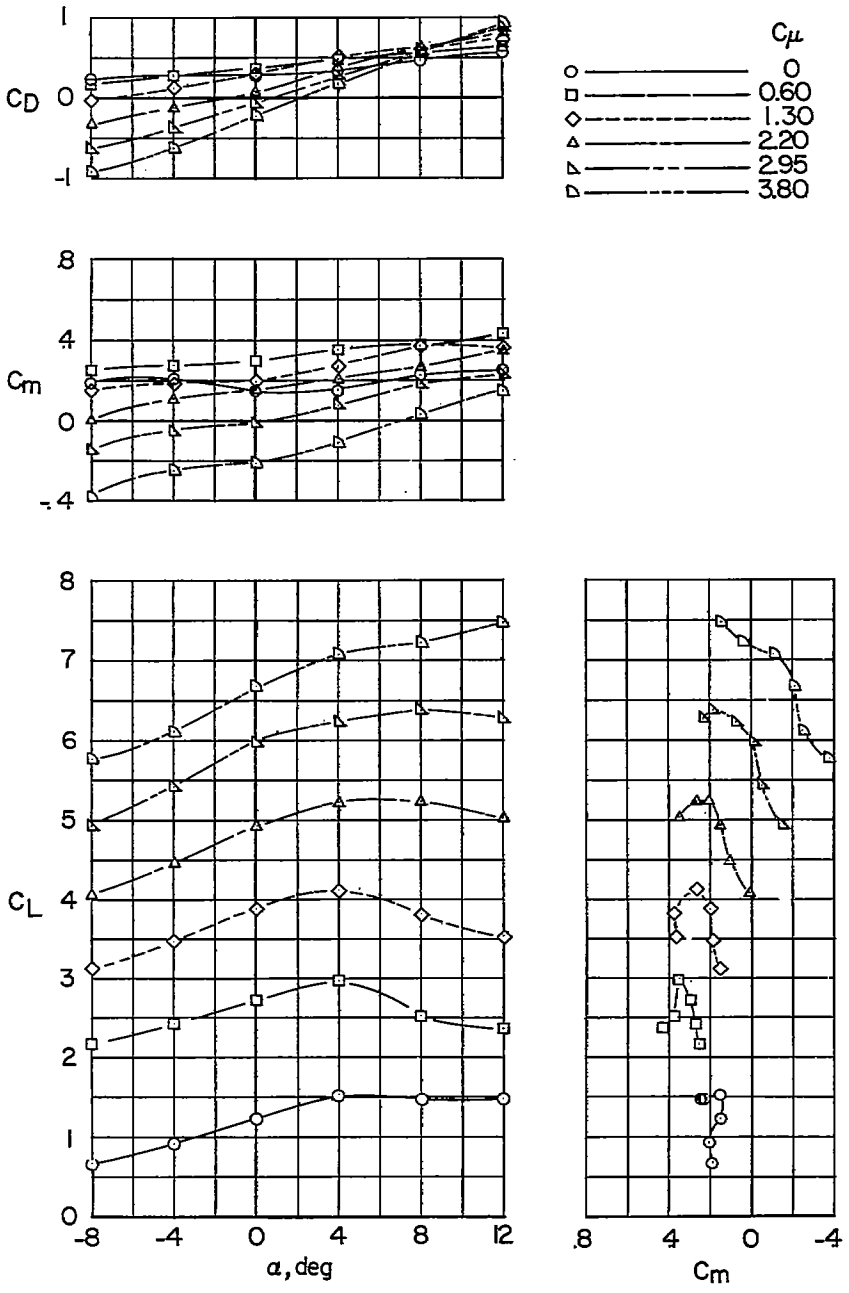

(a) $i_t = 10°$.

Figure 12.- Longitudinal stability and trim characteristics of the high-wing configuration. Low tail position; leading- and trailing-edge flaps on the horizontal tail; $\delta = 60°$; $S_t/S = 0.17$.

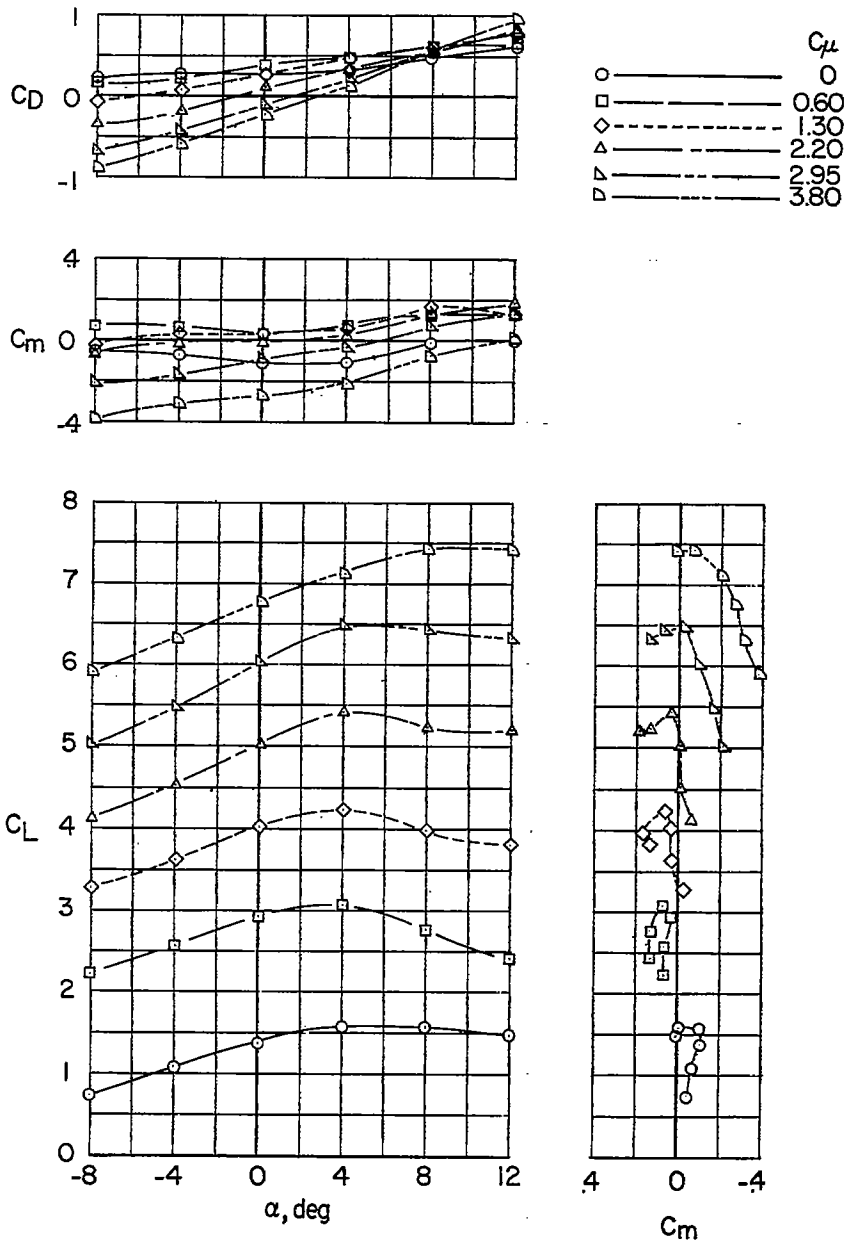

(b) $i_t = 20°$.

Figure 12.- Continued.

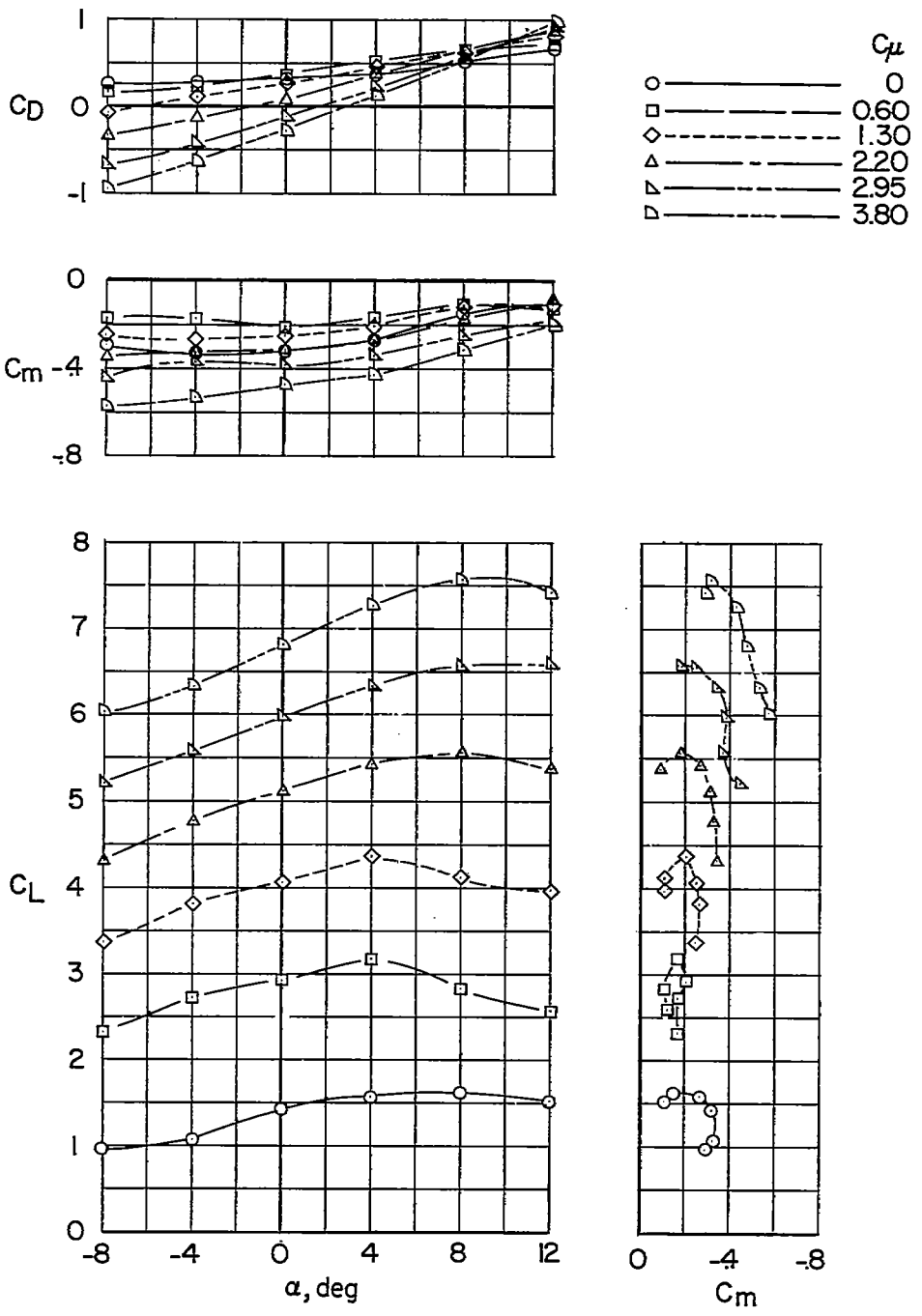

(c) $i_t = 30°$.

Figure 12.- Concluded.

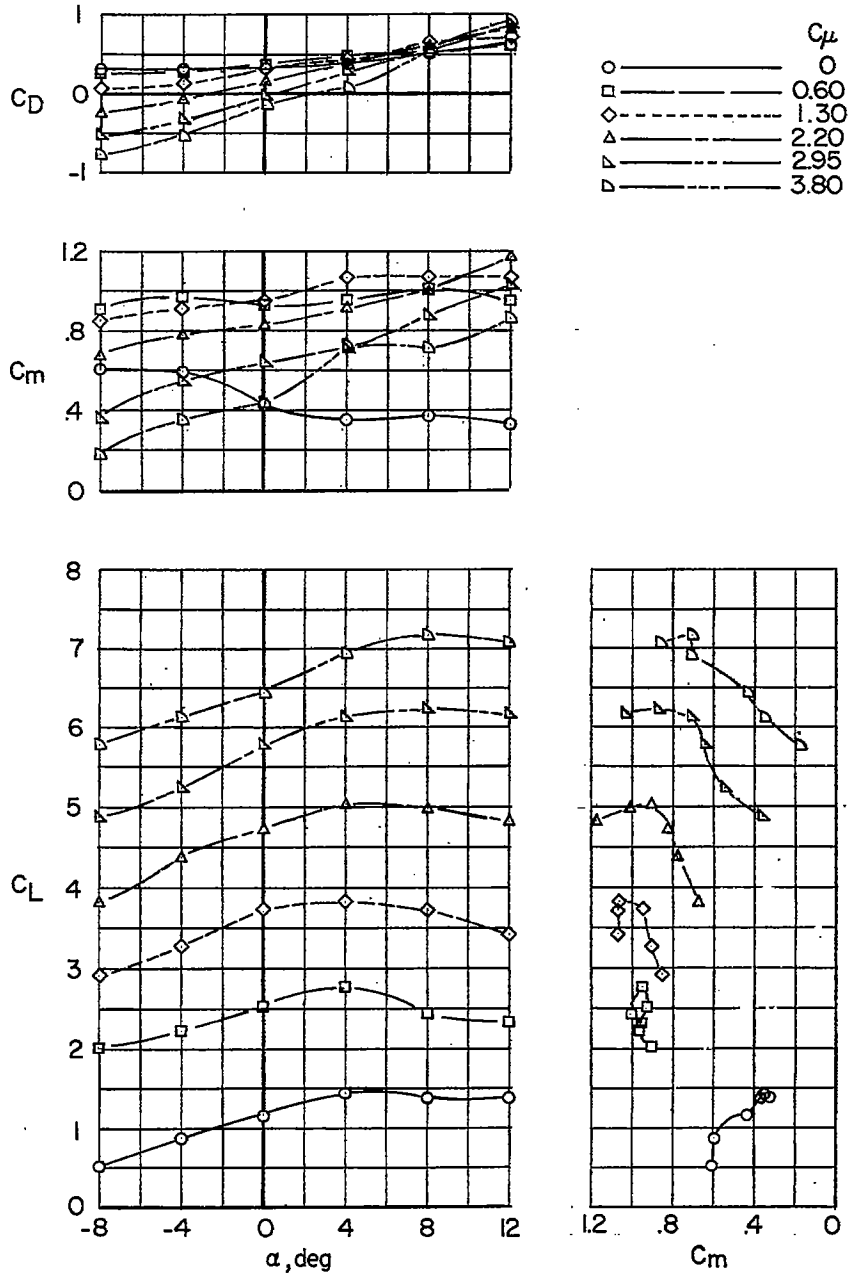

(a) $i_t = 10^\circ$.

Figure 13.- Longitudinal stability and trim characteristics of the high-wing configuration. Low tail position; leading- and trailing-edge flaps on the horizontal tail; $\delta = 60^\circ$; $S_t/S = 0.34$.

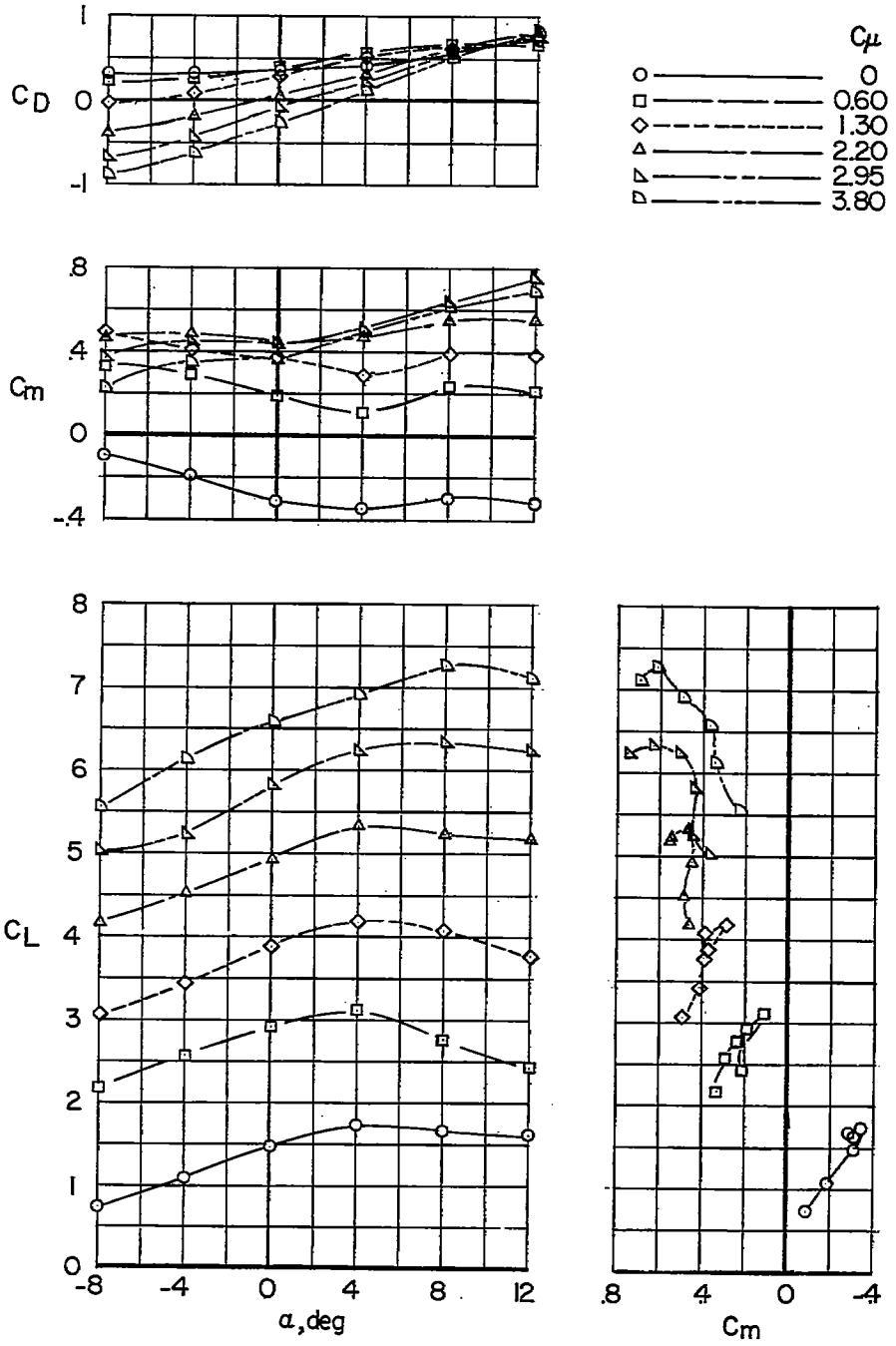

(b) $i_t = 20°$.

Figure 13.- Continued.

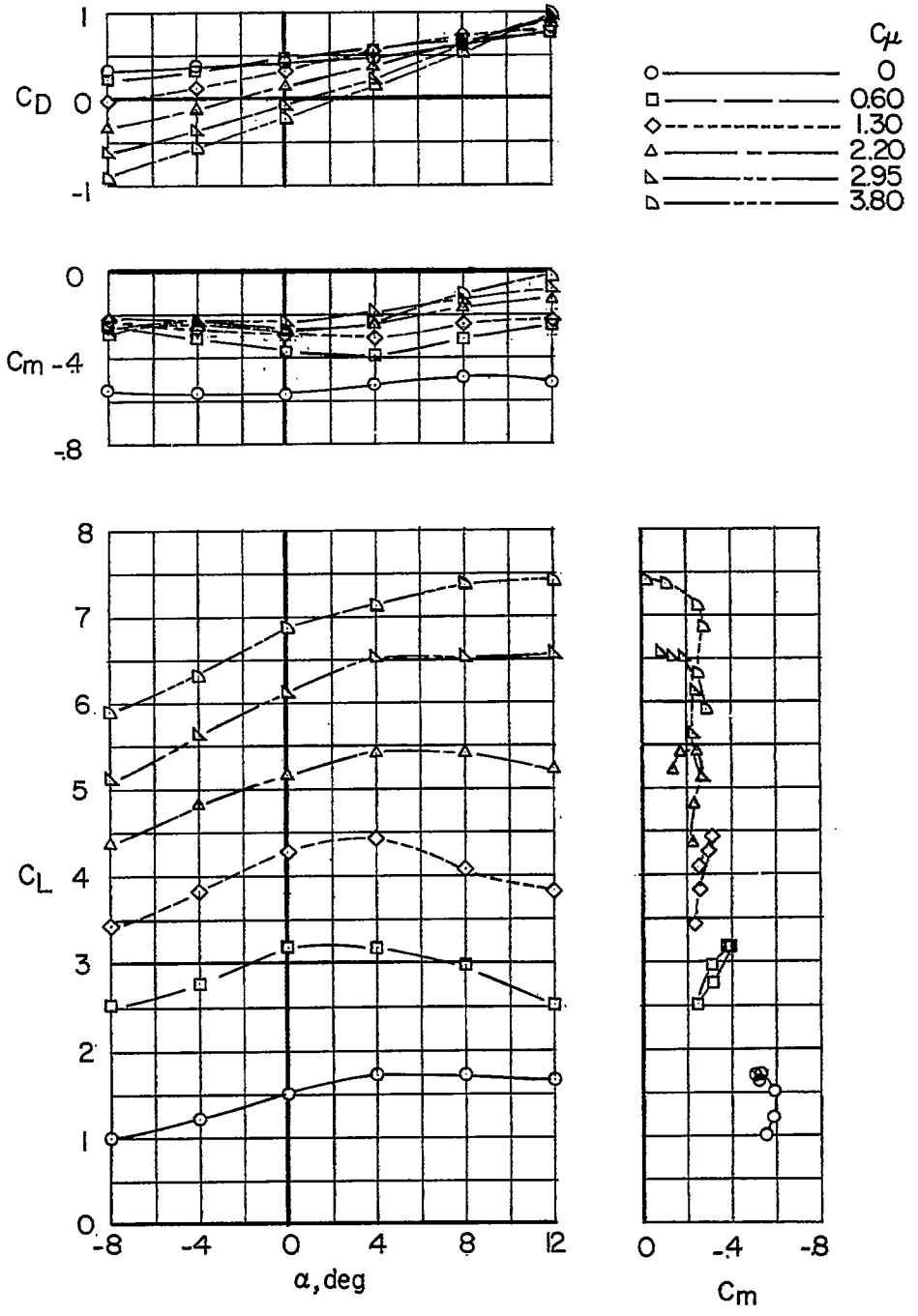

(c) $i_t = 30°$.

Figure 13.- Concluded.

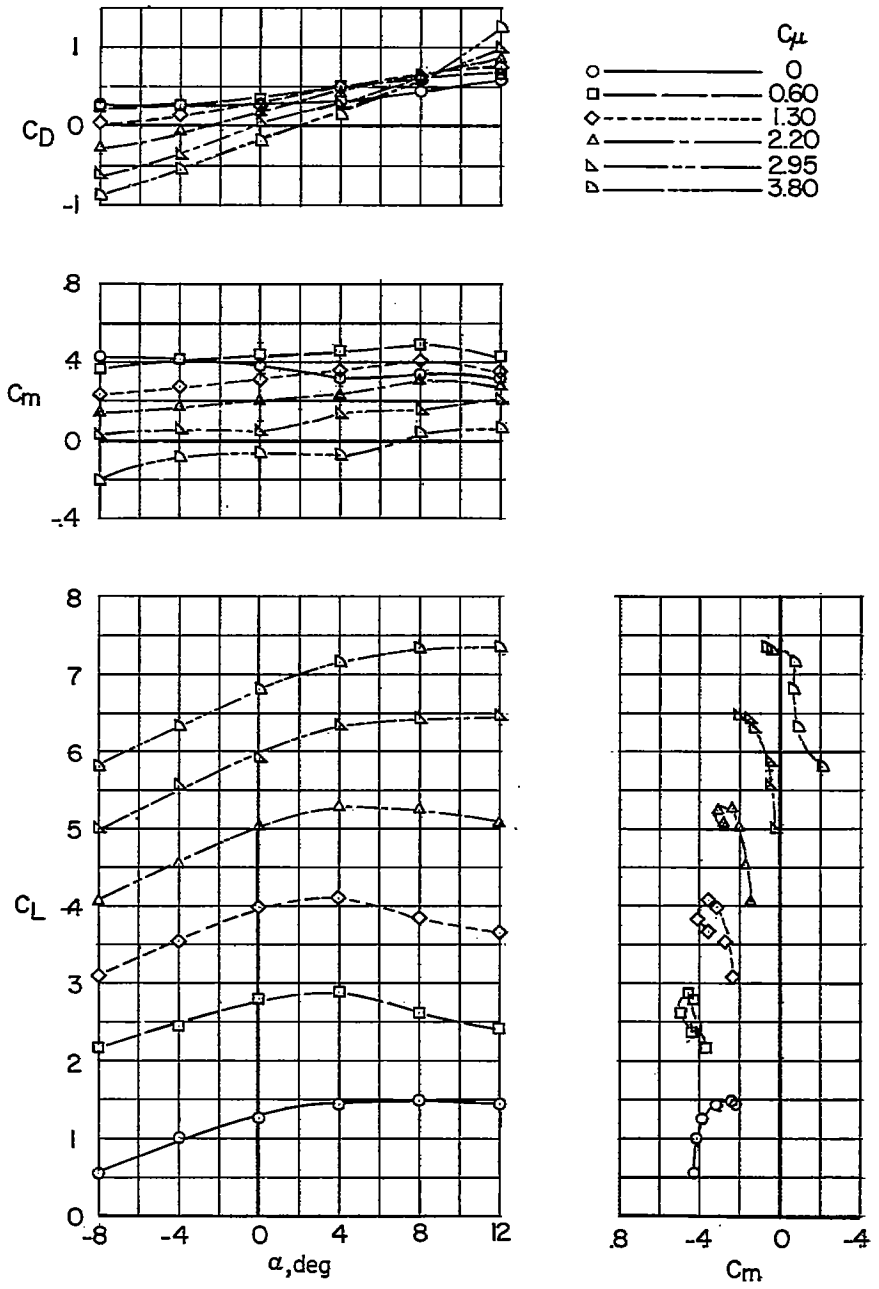

(a) $i_t = 0°$.

Figure 14.- Longitudinal stability and trim characteristics of the high-wing configuration. High tail position; leading- and trailing-edge flaps on the horizontal tail. $\delta = 60°$; $S_t/S = 0.17$.

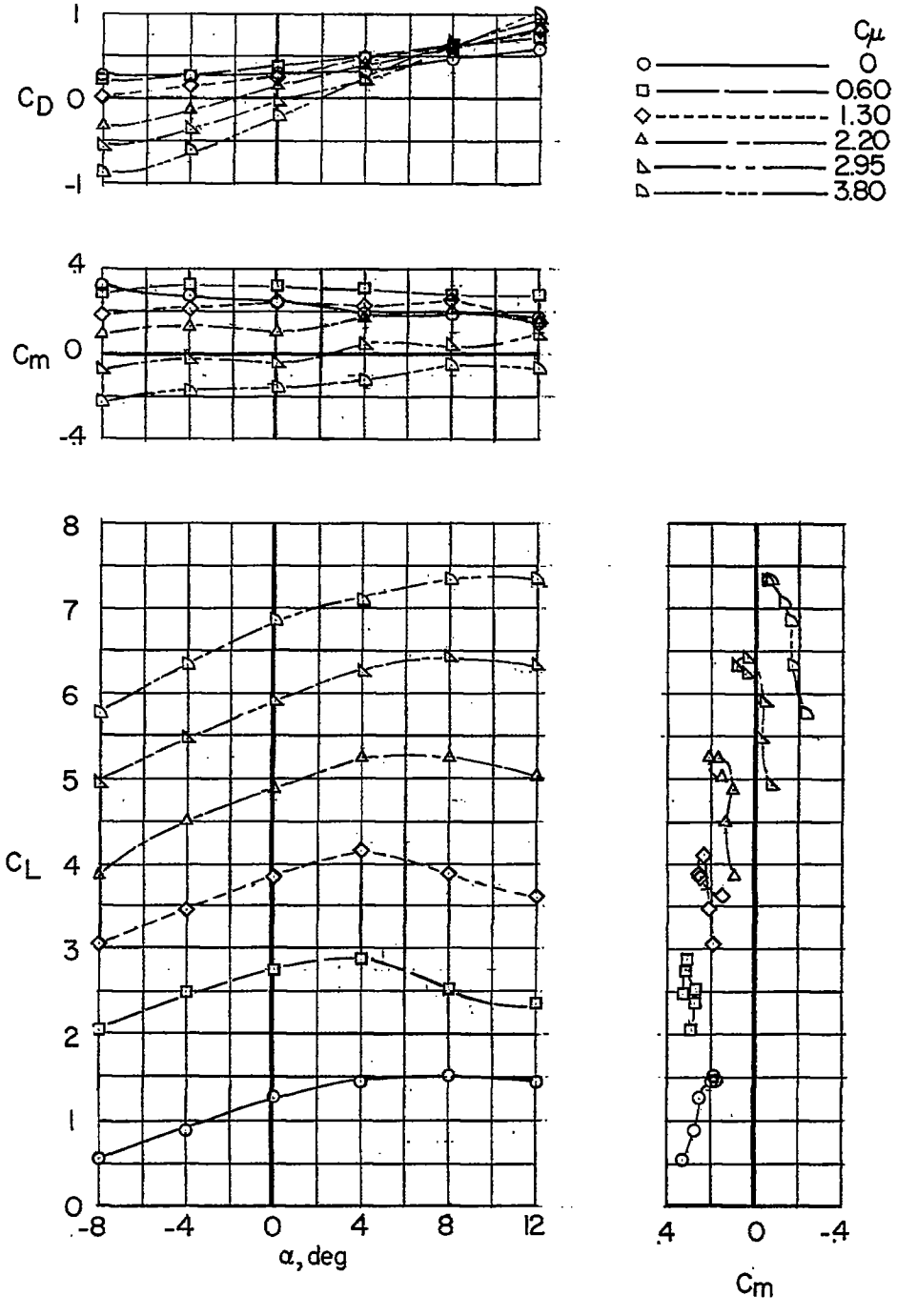

(b) $i_t = 5°$.

Figure 14.- Continued.

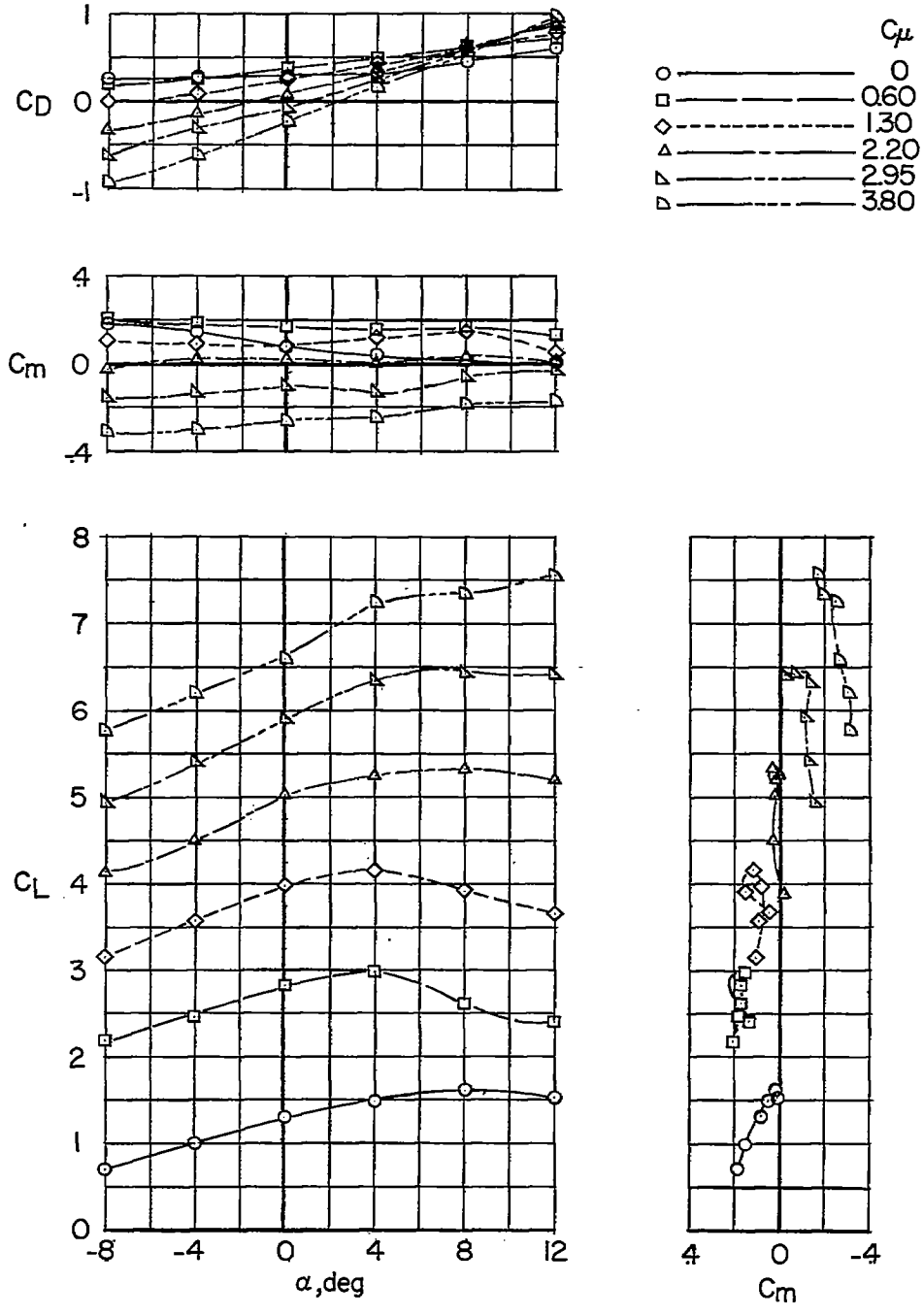

(c) $i_t = 10°$.

Figure 14.- Continued.

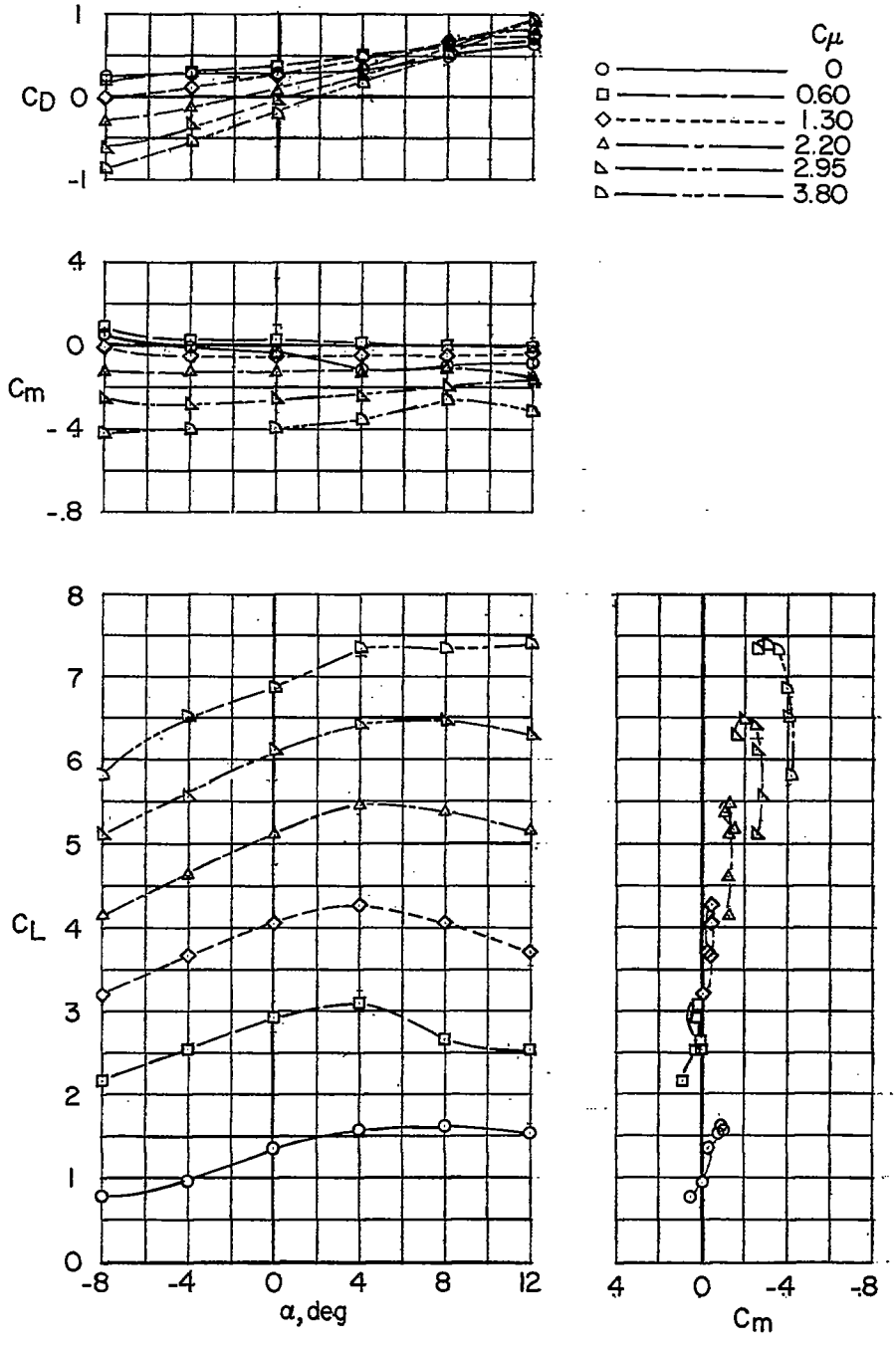

(d) $i_t = 15°$.

Figure 14.- Continued.

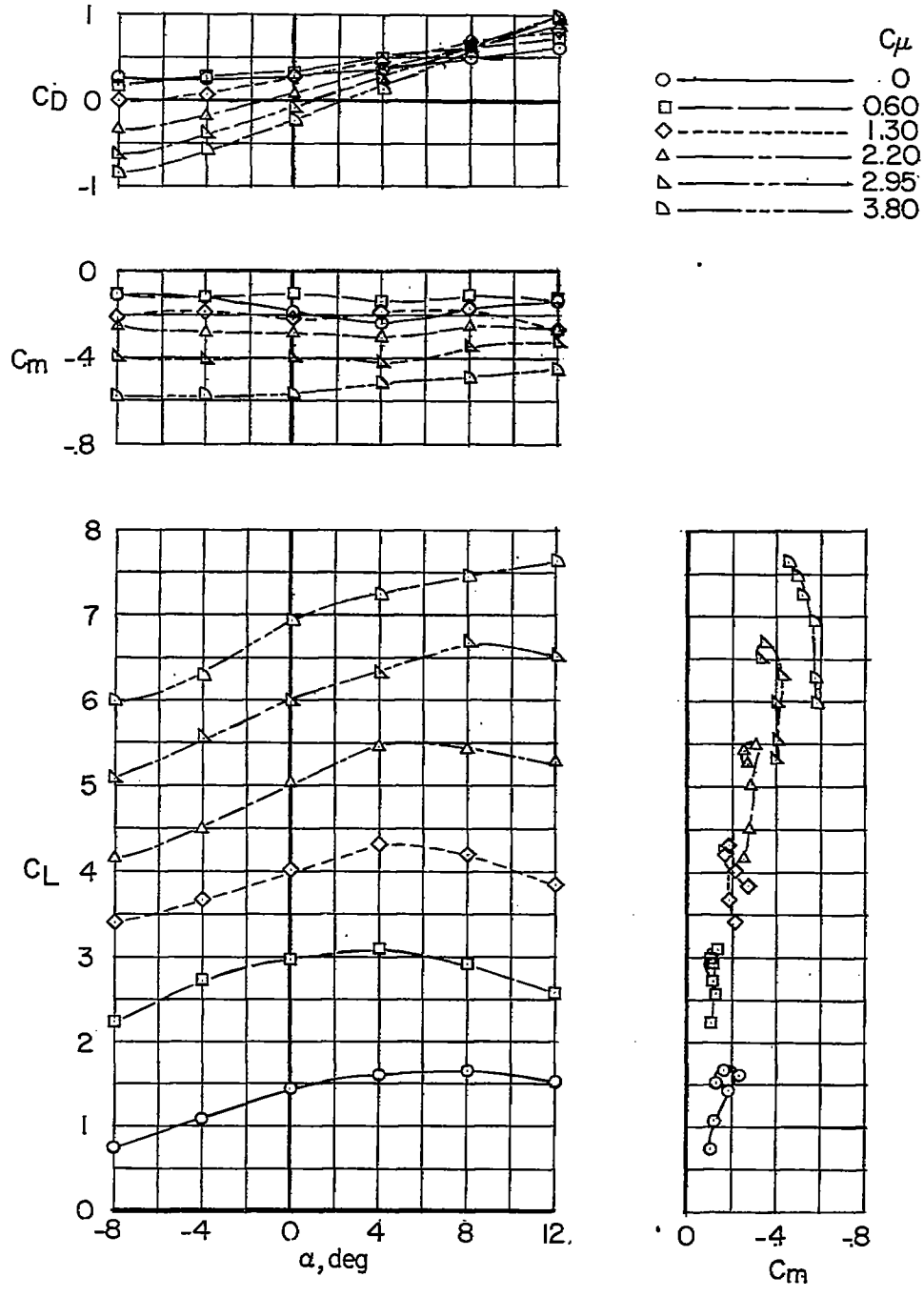

(e) $i_t = 20°$.

Figure 14.- Concluded.

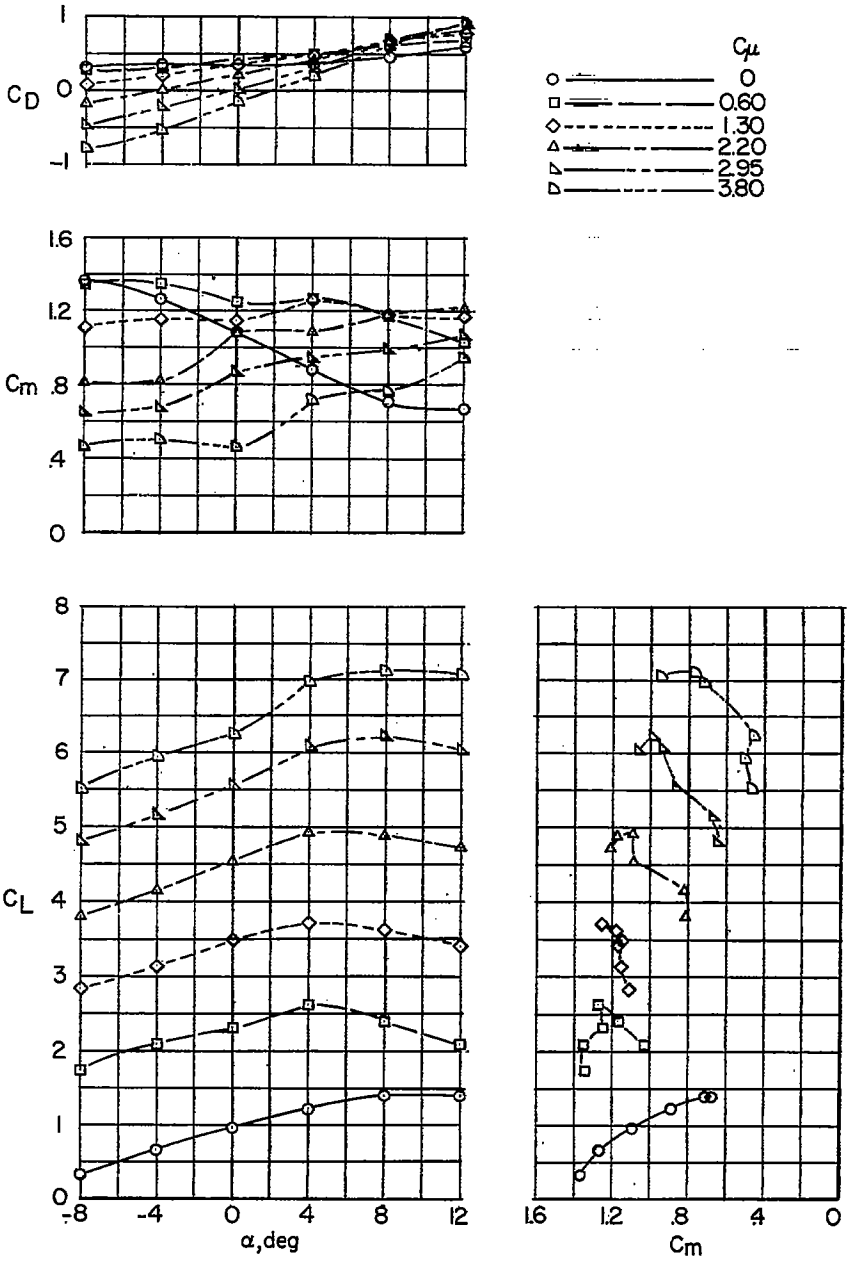

(a) $i_t = 0^\circ$.

Figure 15.- Longitudinal stability and trim characteristics of the high-wing configuration. High tail position; leading- and trailing-edge flaps on the horizontal tail; $\delta = 60^\circ$; $S_t/S = 0.34$.

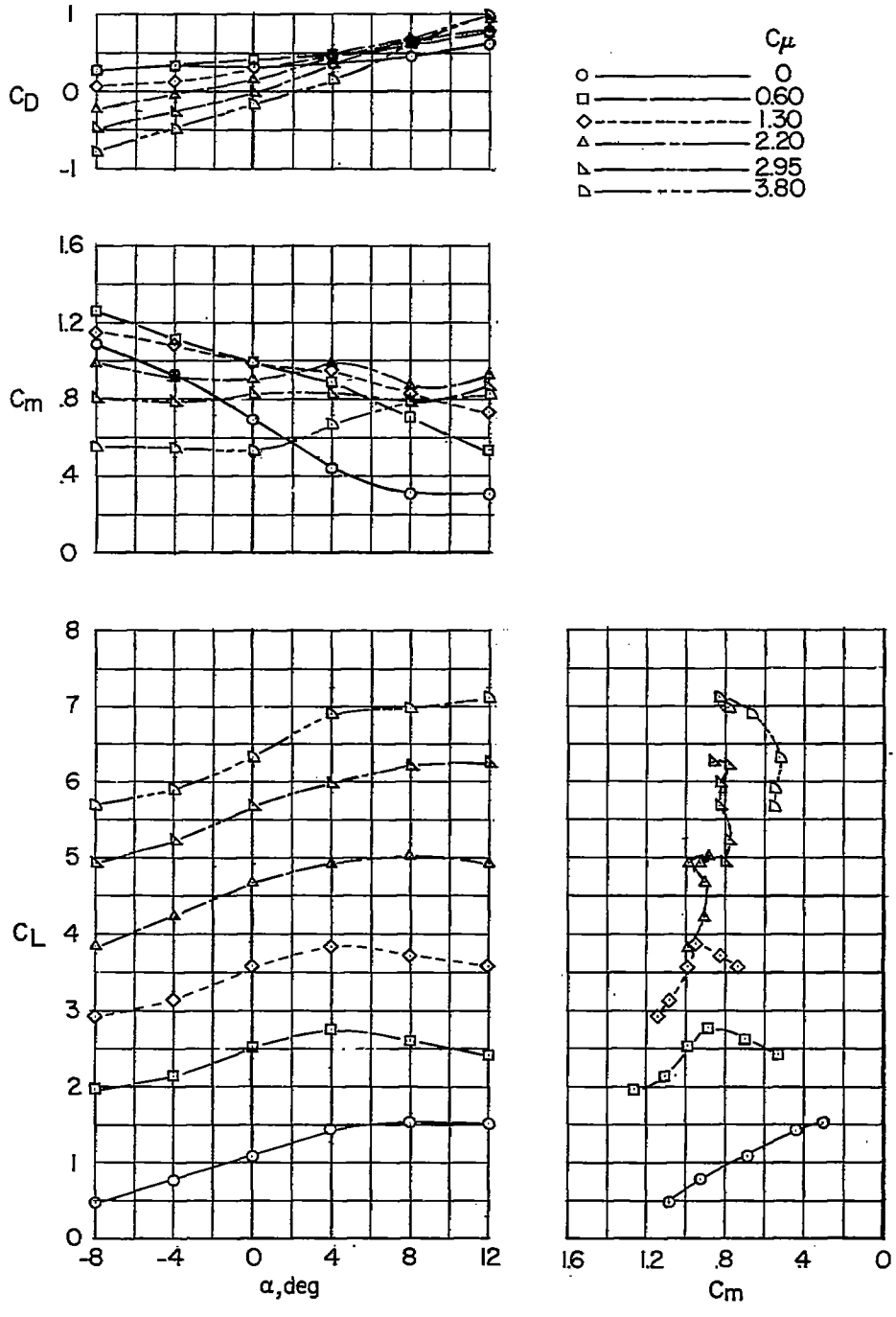

(b) $i_t = 5°$.

Figure 15.- Continued.

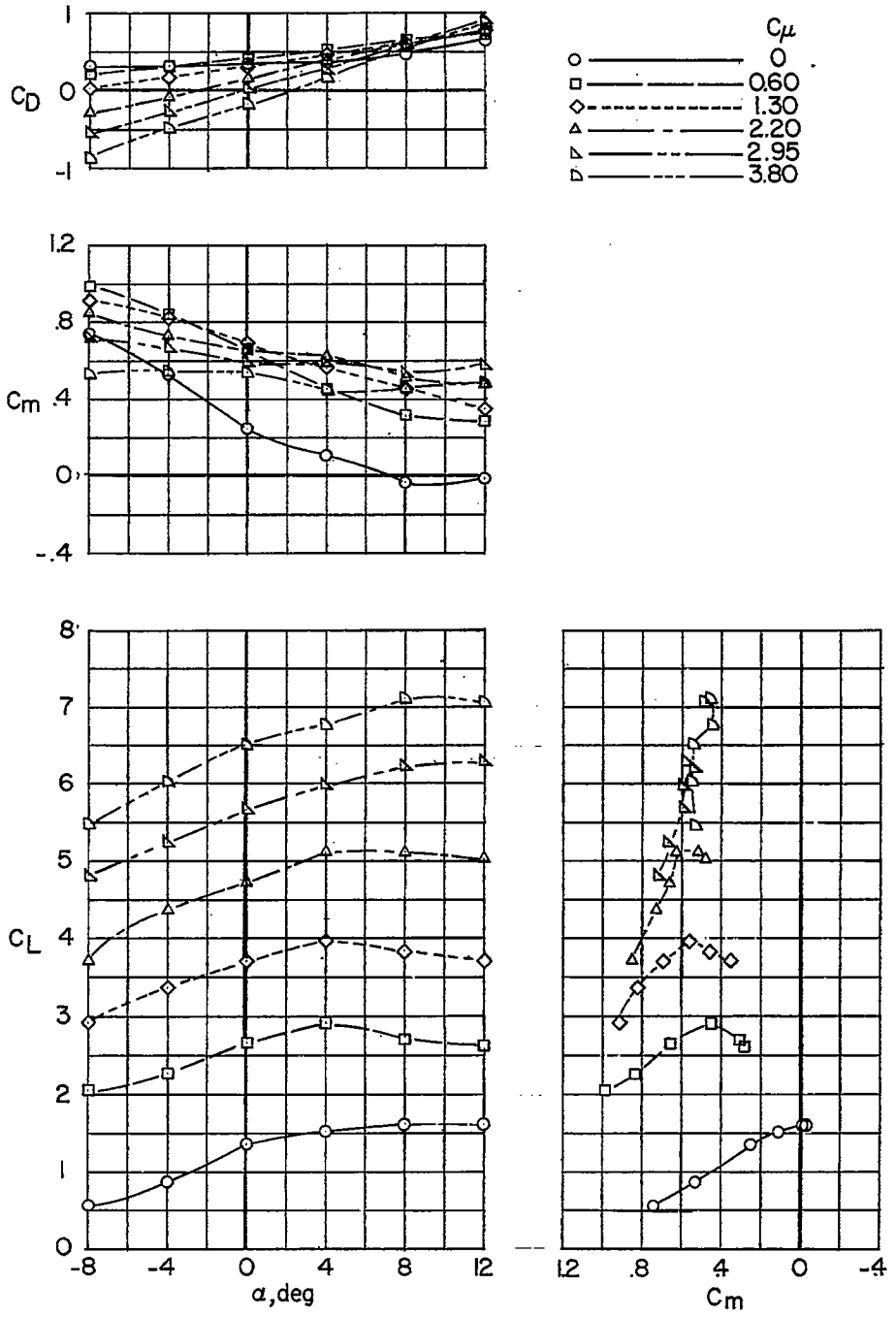

(c) $i_t = 10°$.

Figure 15.- Continued.

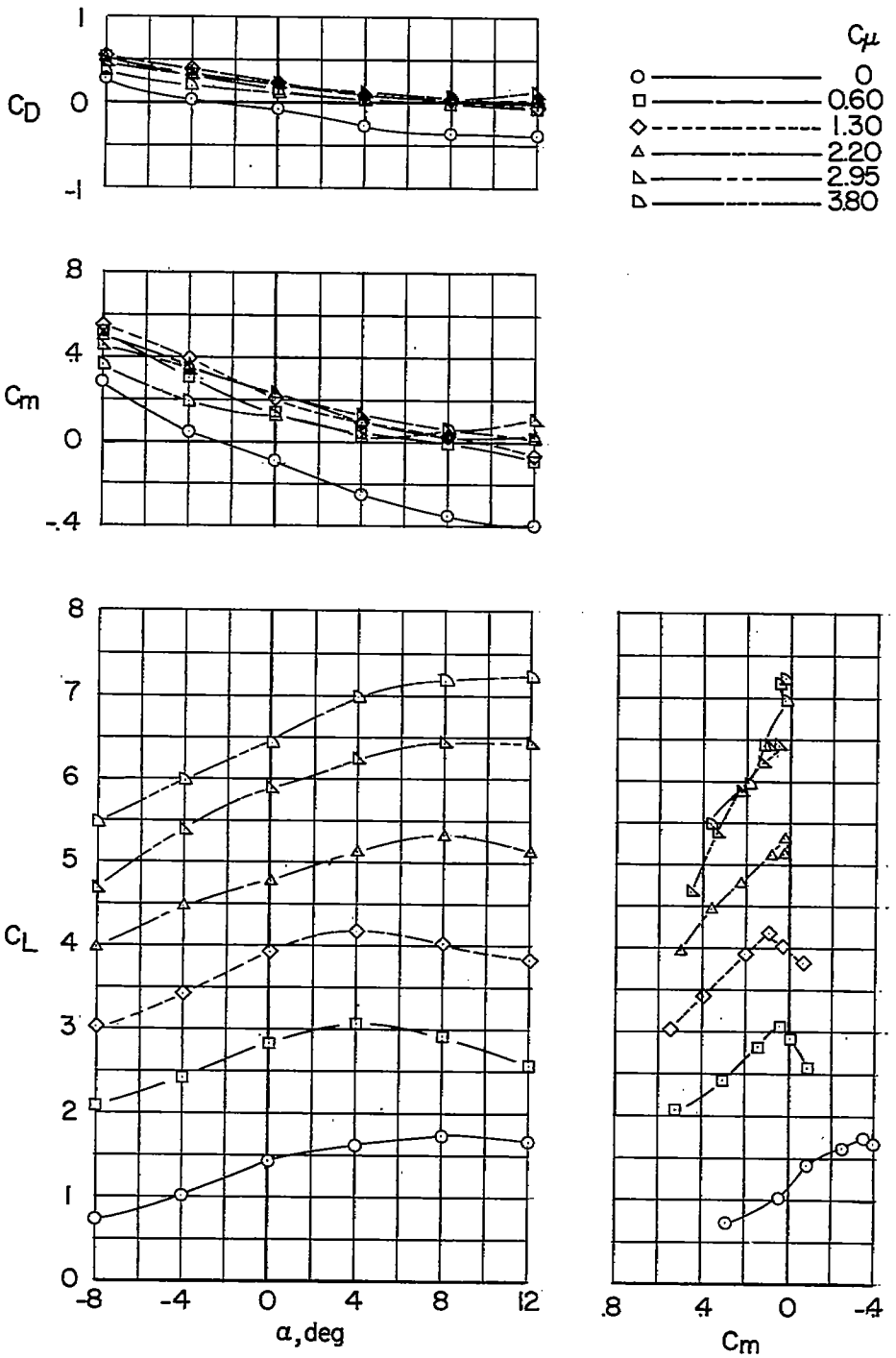

(d) $i_t = 15°$.

Figure 15.- Continued.

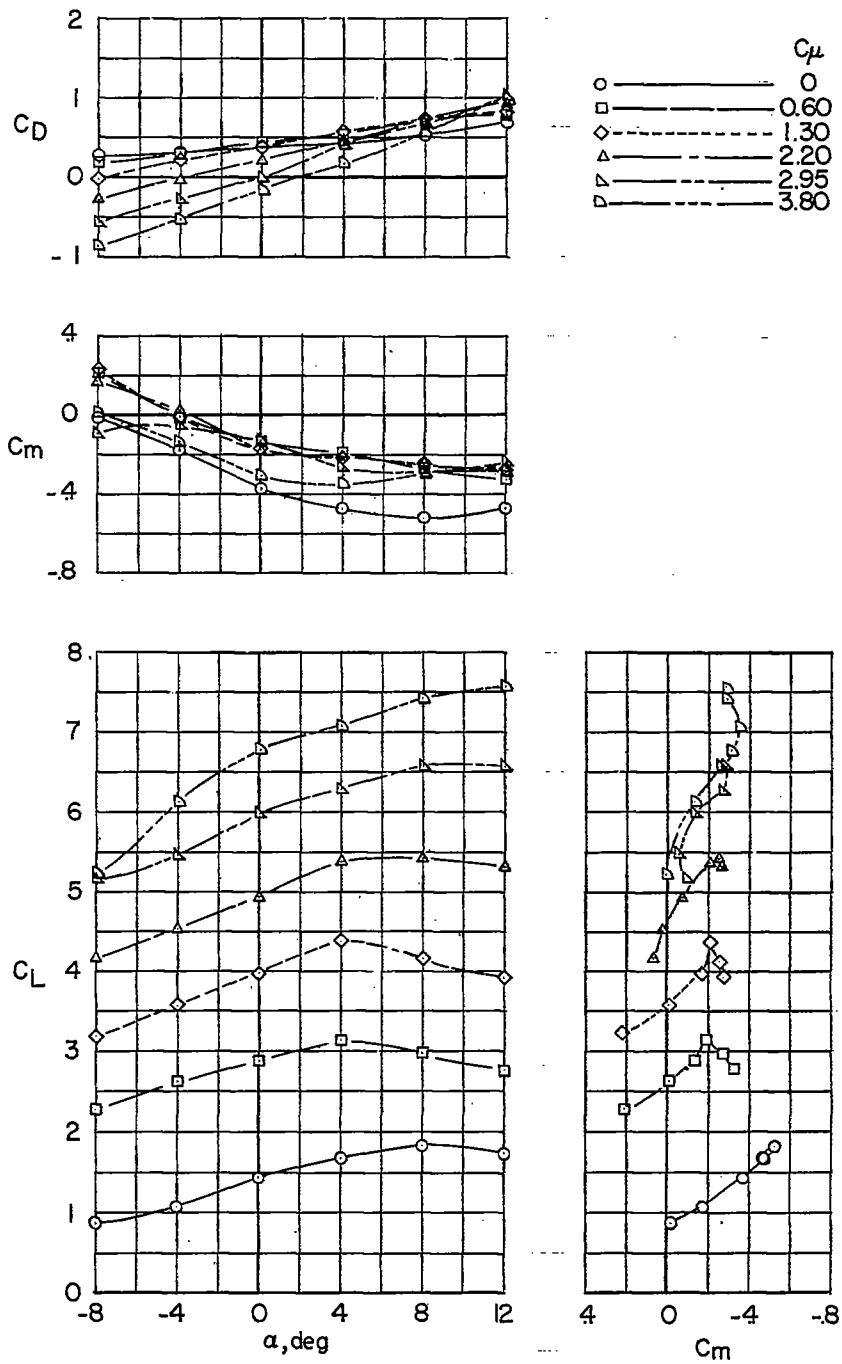

(e) $i_t = 20°$.

Figure 15.- Concluded.

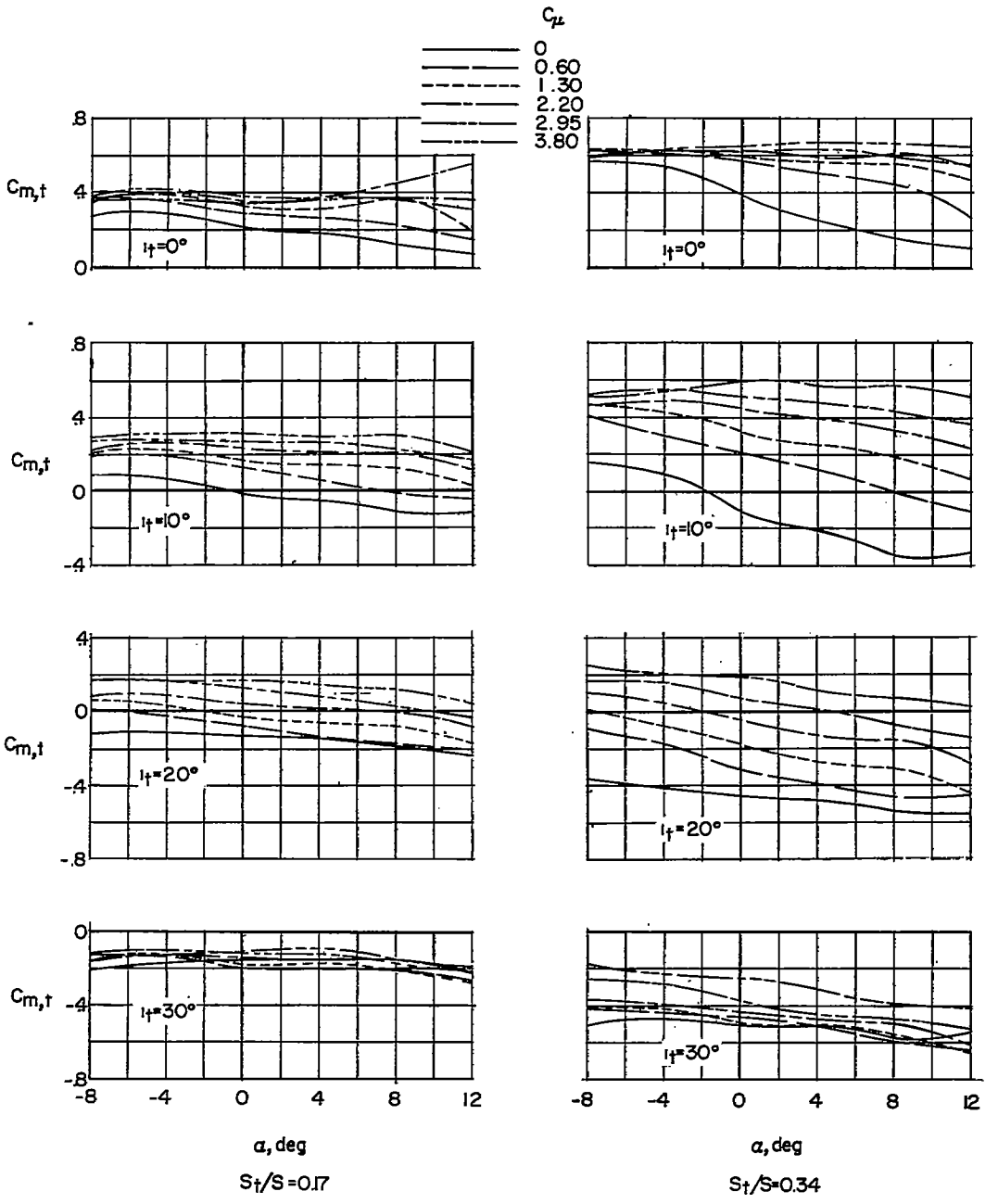

(a) Low tail position.

Figure 16.- Pitching-moment increments produced by various horizontal-tail configurations (data from figs. 3 to 6). Low-wing configuration.

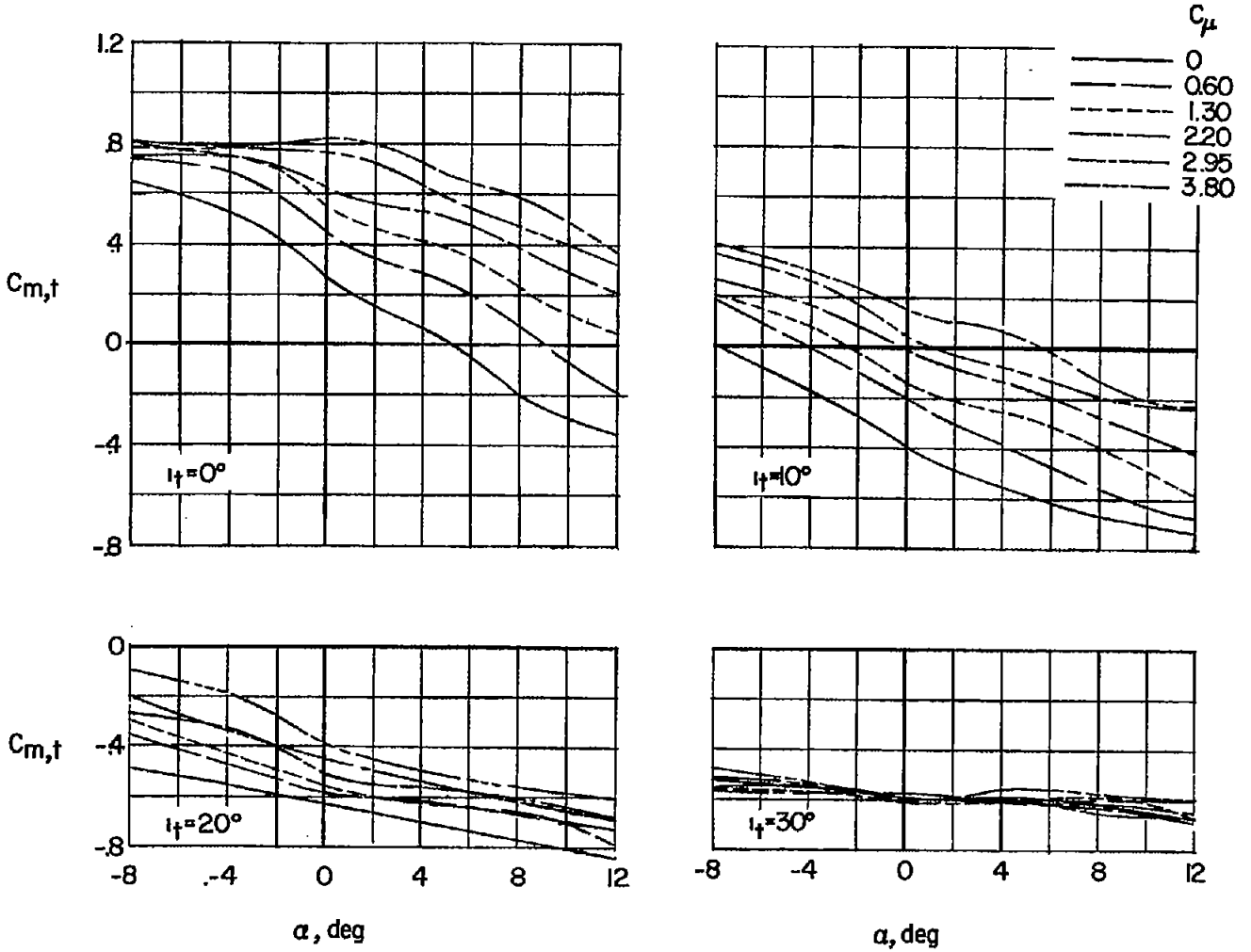

(b) High tail position. $S_t/S = 0.34$.

Figure 16.- Concluded.

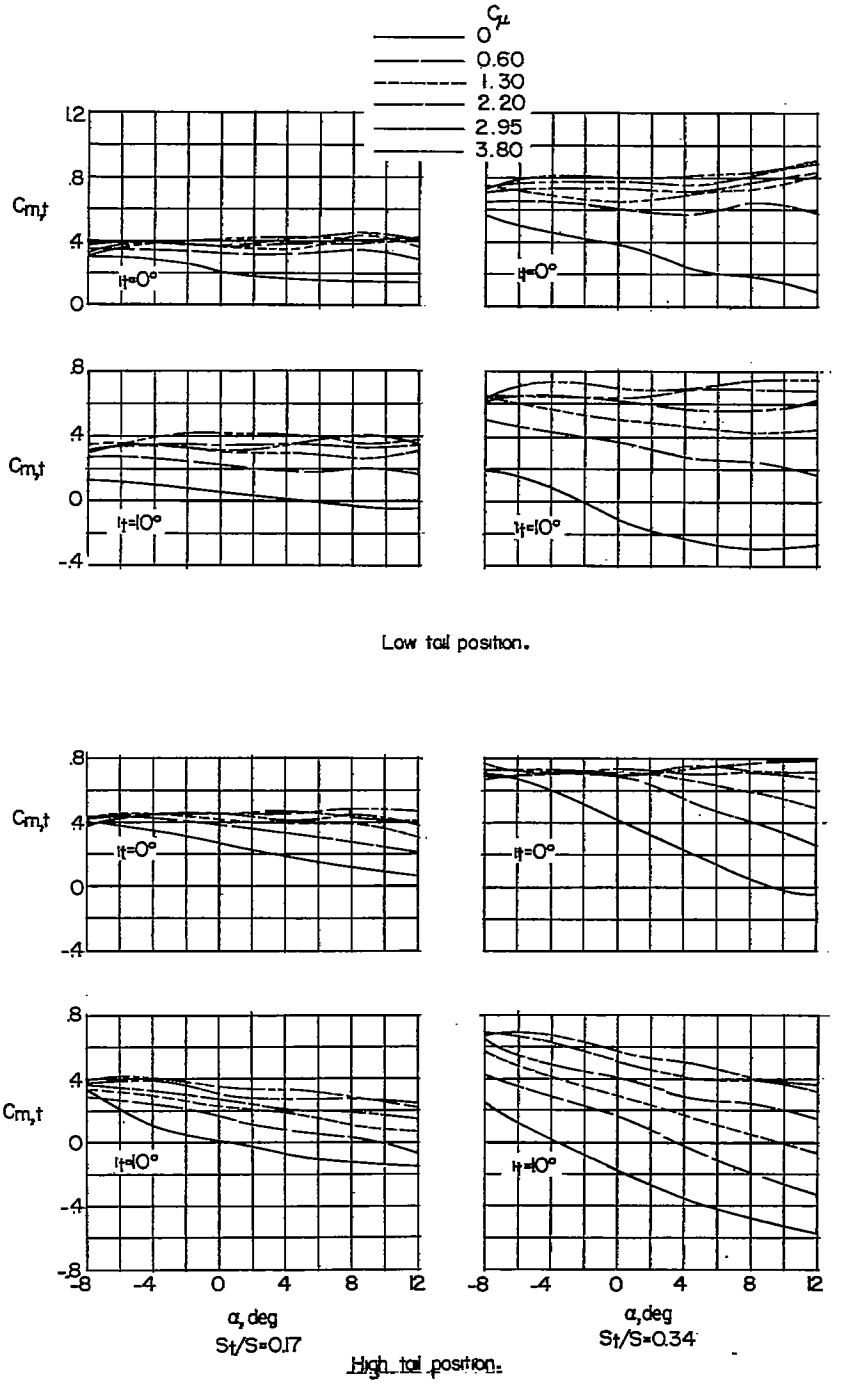

Figure 17.- Pitching-moment increments produced by various horizontal-tail configurations (data from figs. 7 to 10). High-wing configuration.

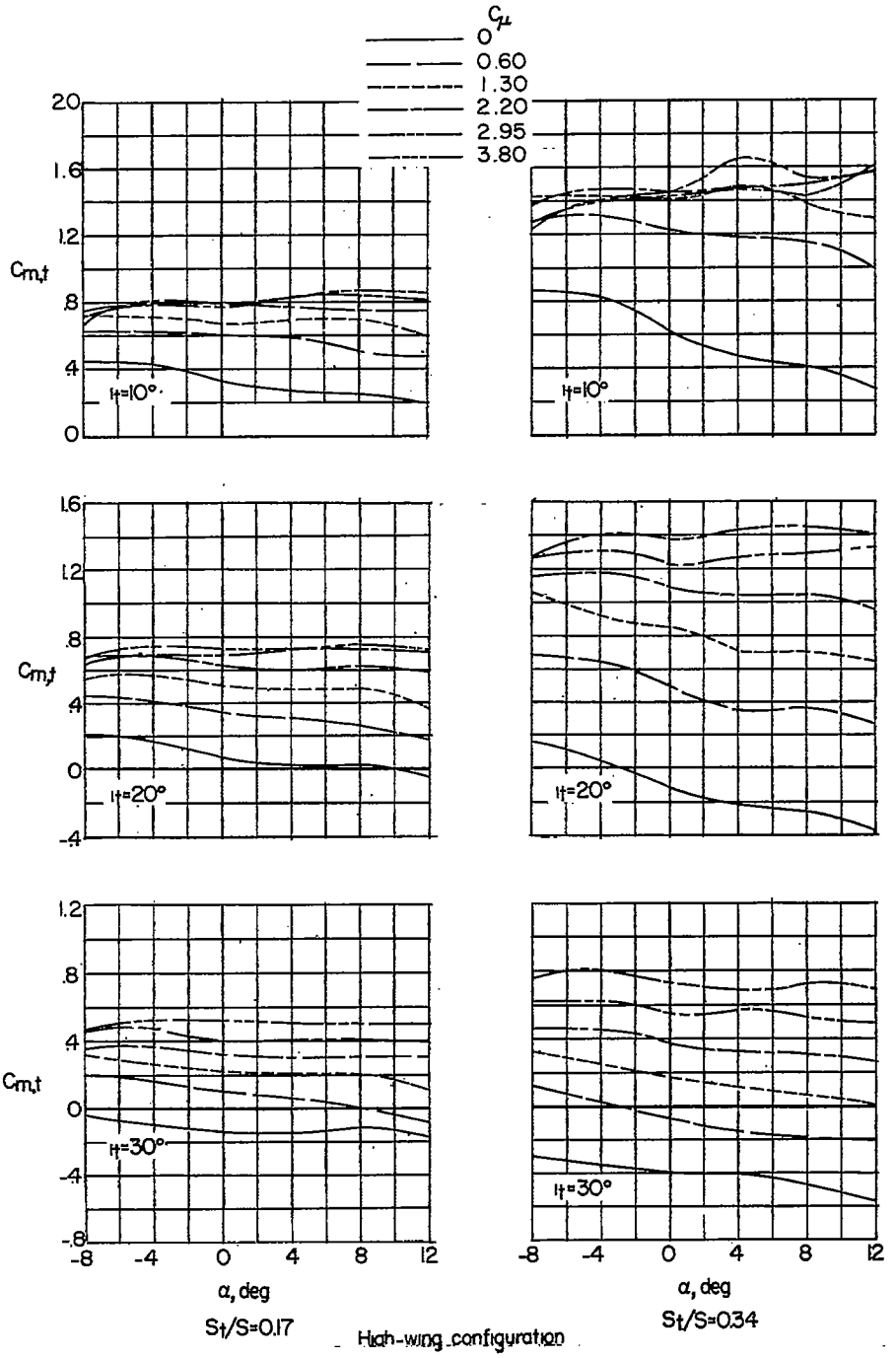

Figure 18.- Pitching-moment increments produced by various horizontal-tail configurations (data from figs. 12 and 13). Leading- and trailing-edge flaps on horizontal tail; low tail position.

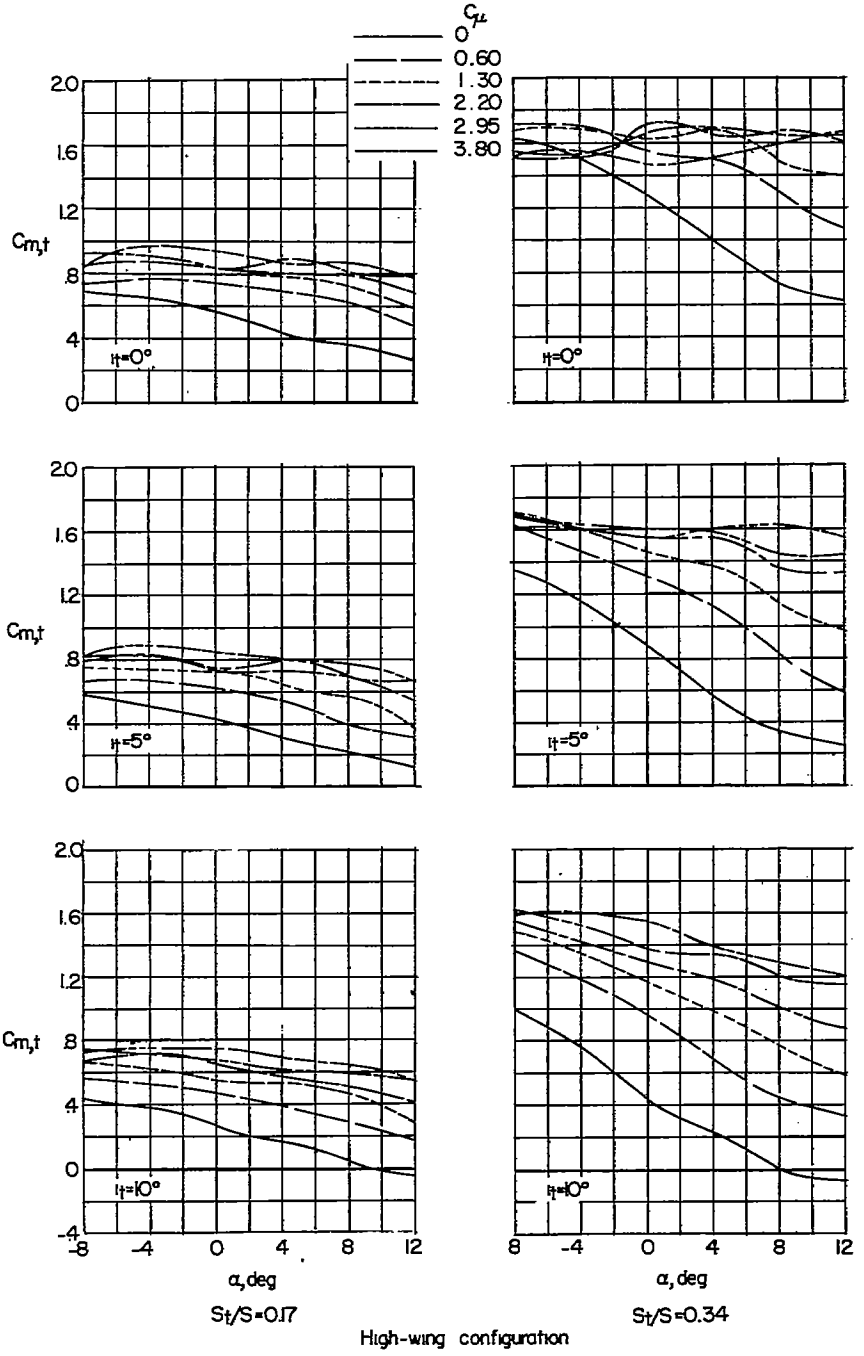

Figure 19.- Pitching-moment increments produced by various horizontal-tail configurations (data from figs. 14 and 15). Leading- and trailing-edge flaps on horizontal tail; high tail position.

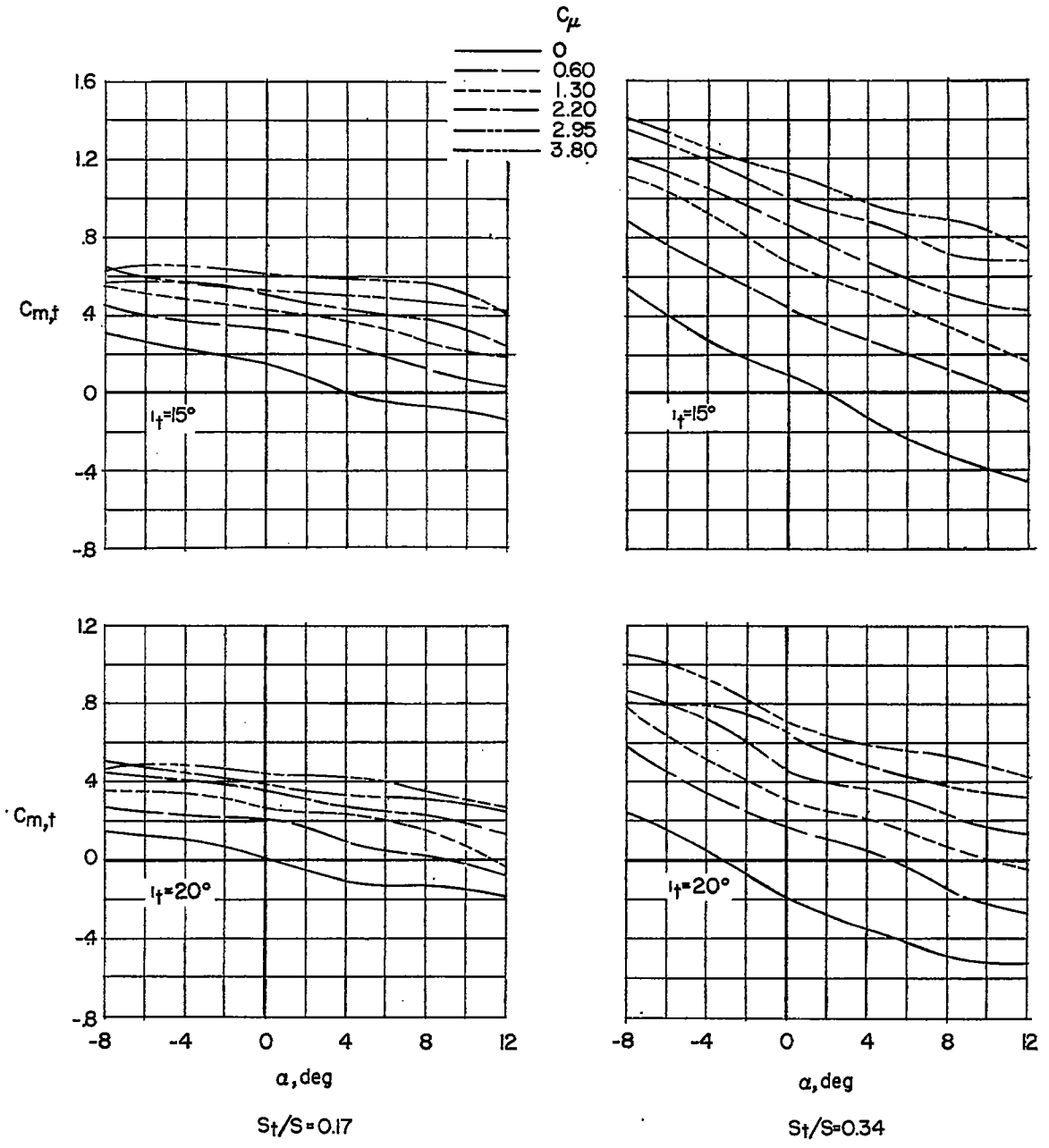

High-wing configuration

Figure 19.- Concluded.

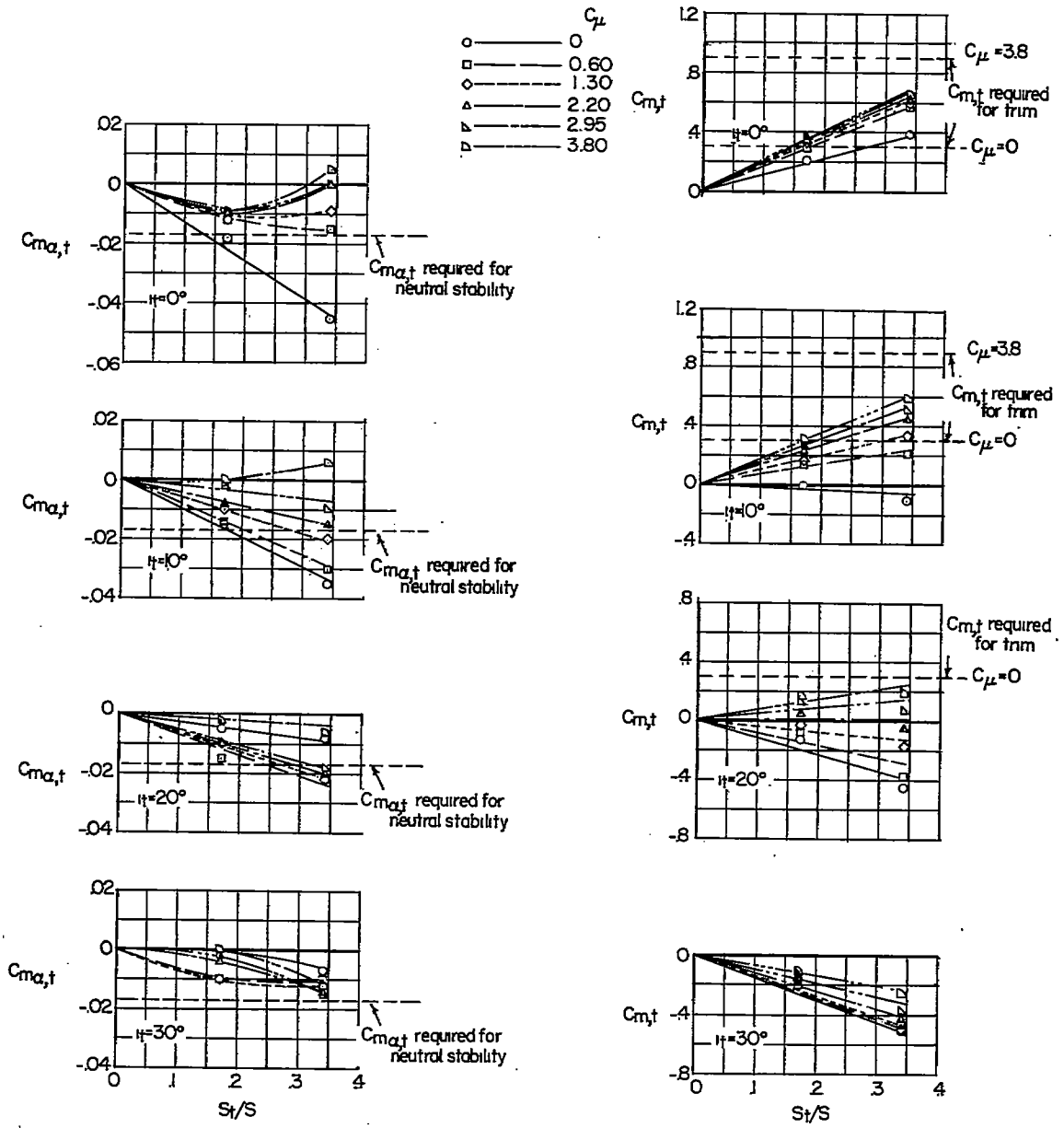

(a) Low tail position.

Figure 20.- Variation of longitudinal stability and trim parameters with horizontal-tail area (data from figs. 3 to 6). Low-wing configuration; $\alpha = 0^\circ$.

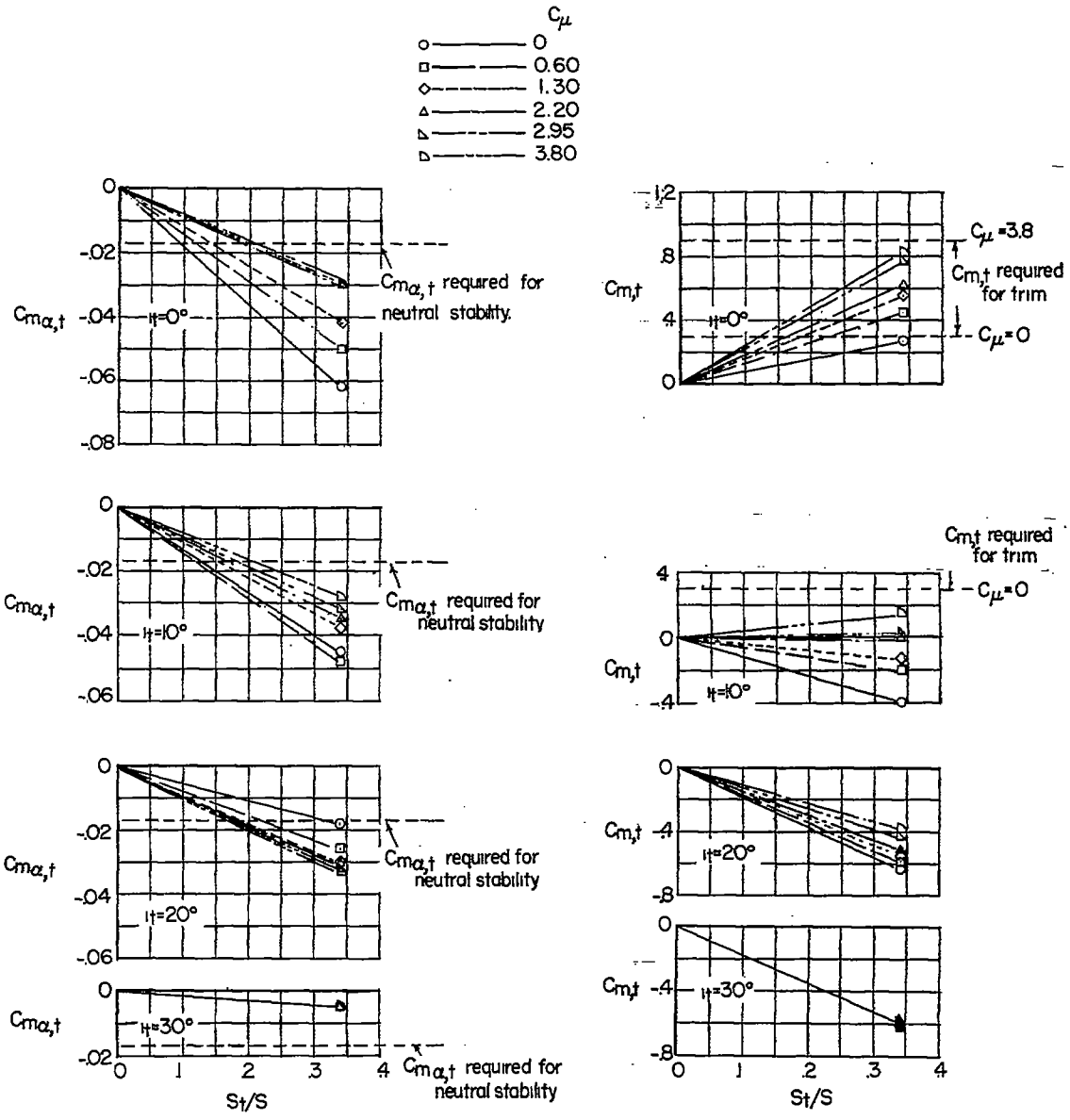

(b) High tail position.

Figure 20.- Concluded.

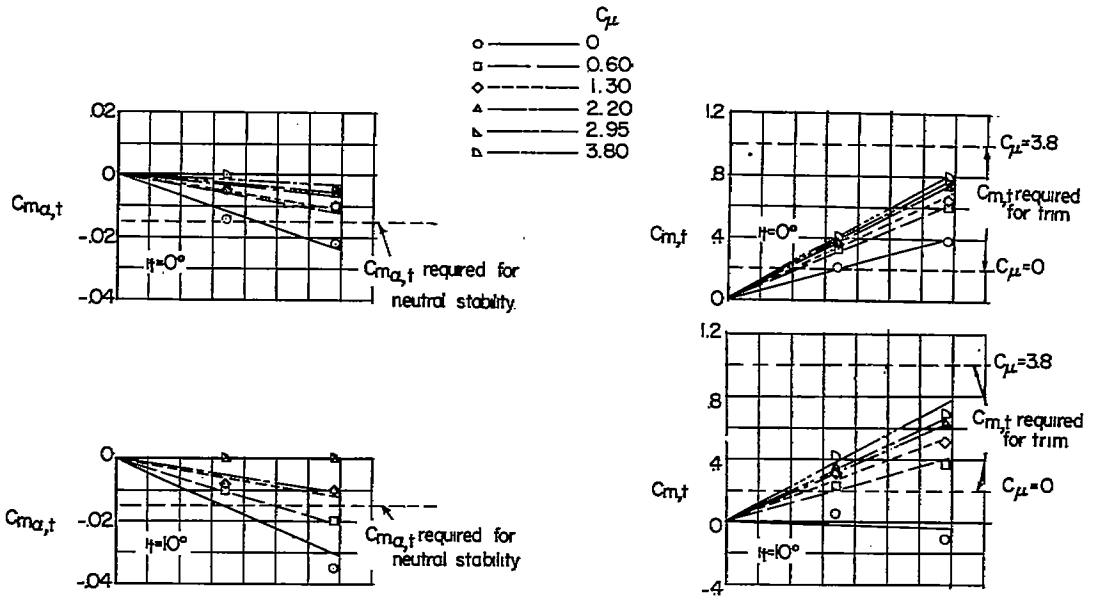

(a) Low tail position.

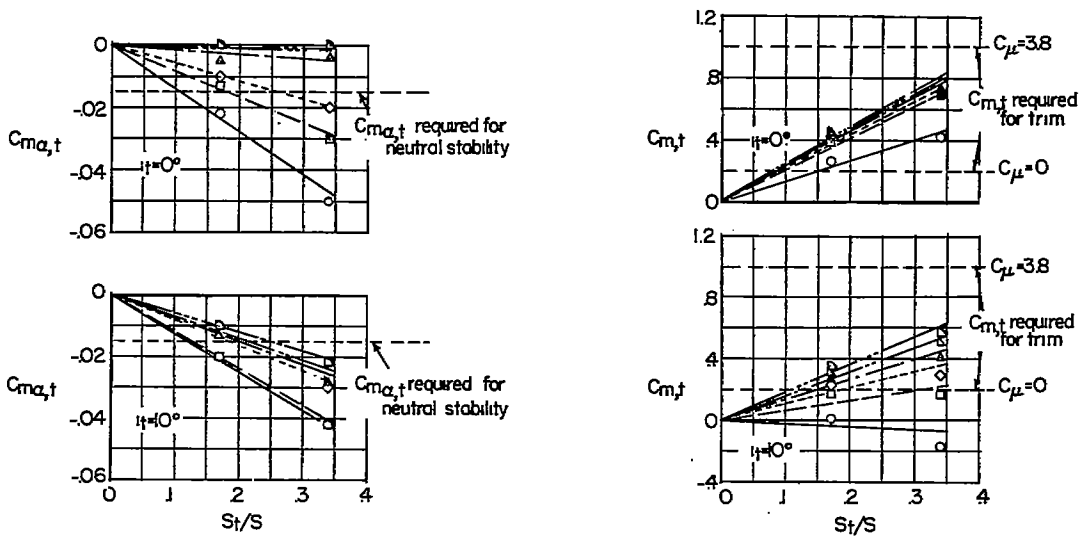

(b) High tail position.

Figure 21.- Variation of longitudinal stability and trim parameters with horizontal-tail area (data from figs. 7 to 10). High-wing configuration; $\alpha = 0^\circ$.

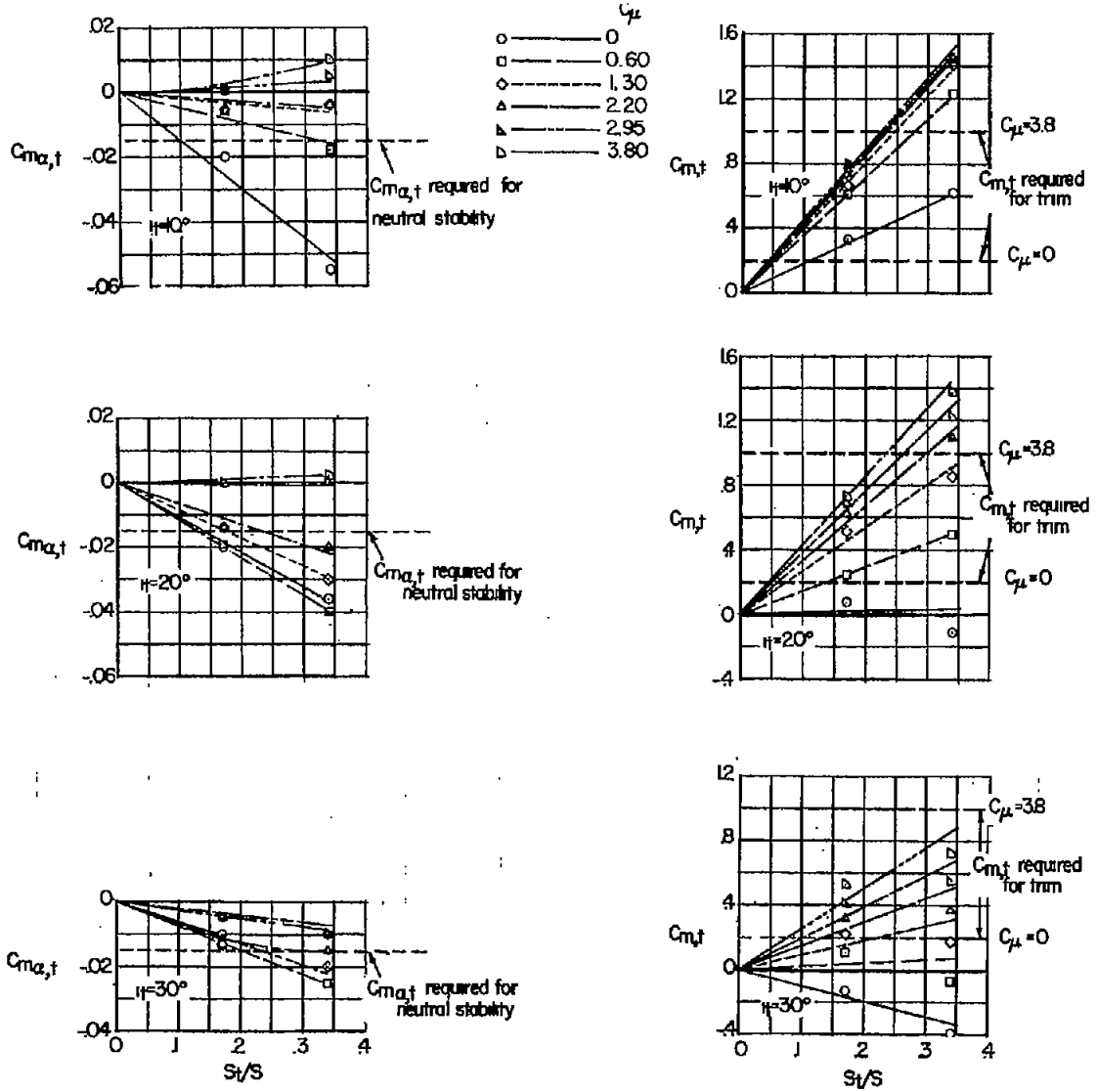

(a) Low tail position.

Figure 22.- Variations of longitudinal stability and trim parameters with horizontal-tail area (data from figs. 12 and 15). High-wing configuration; leading- and trailing-edge flaps on horizontal tail; $\alpha = 0°$.

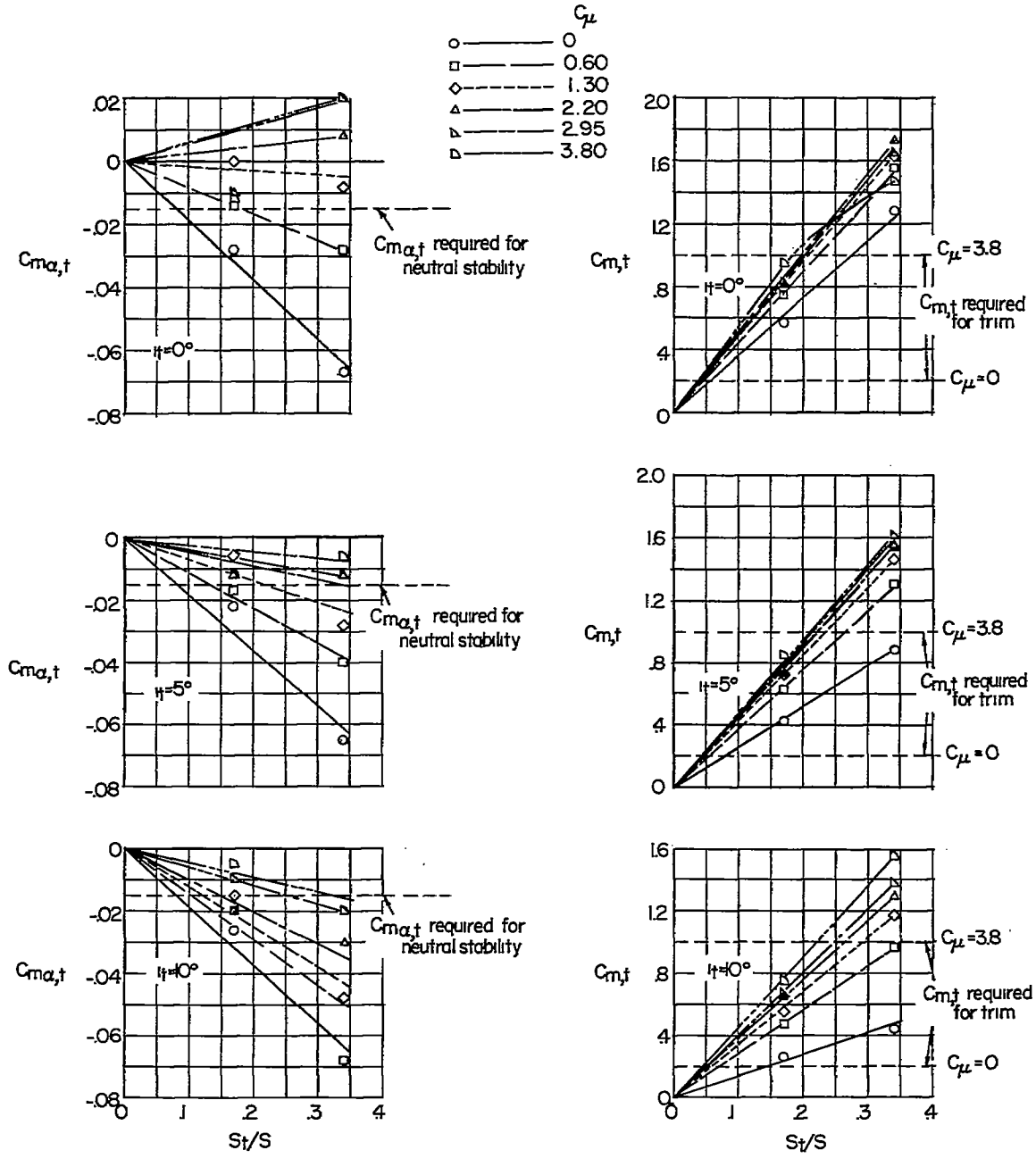

(b) High tail position.

Figure 22.- Continued.

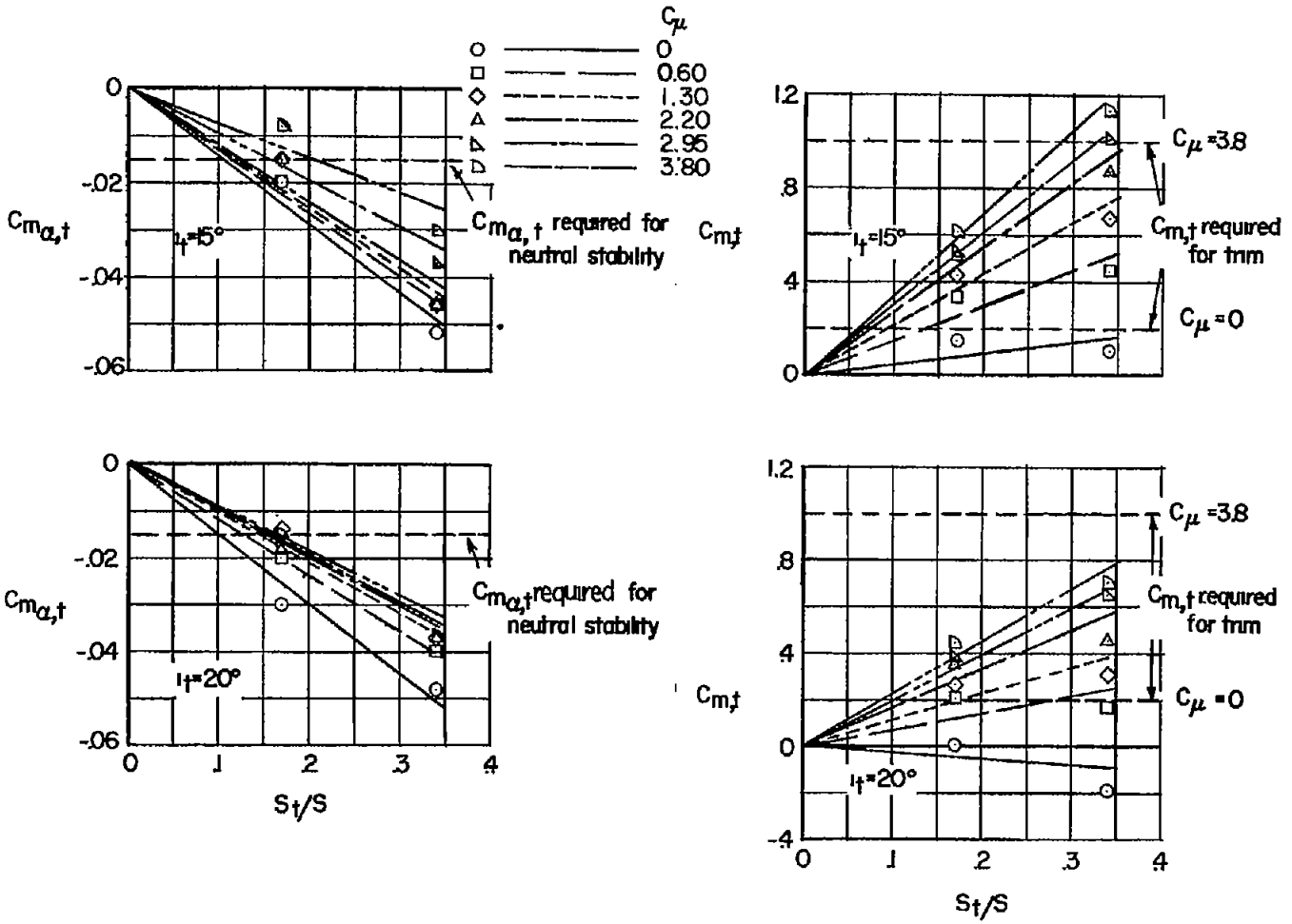

(b) High tail position. Concluded.

Figure 22.- Concluded.

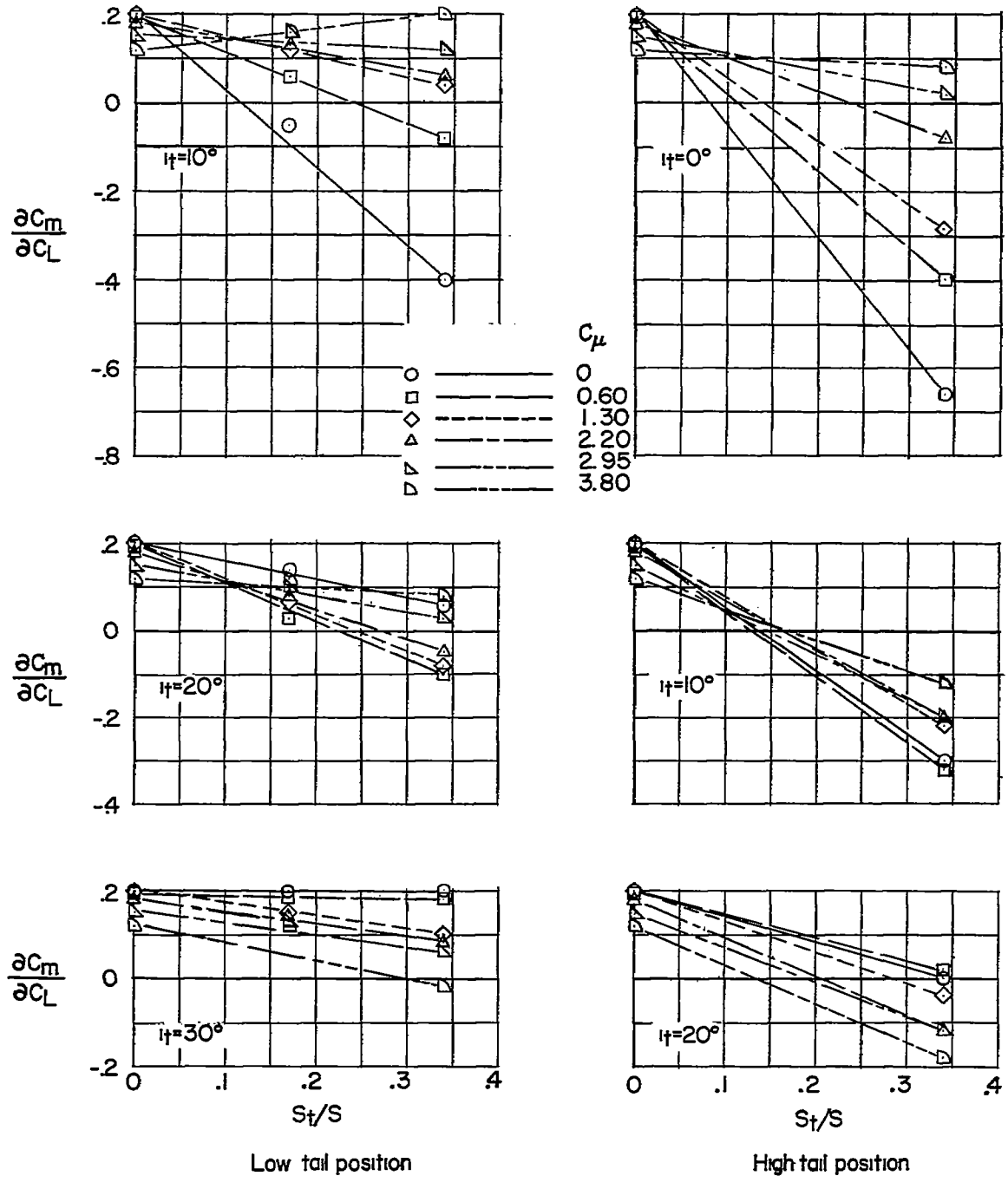

Figure 23.- Variation of longitudinal stability parameter with horizontal-tail area (data from figs. 3 to 6). Low-wing configuration; $\alpha = 0^\circ$.

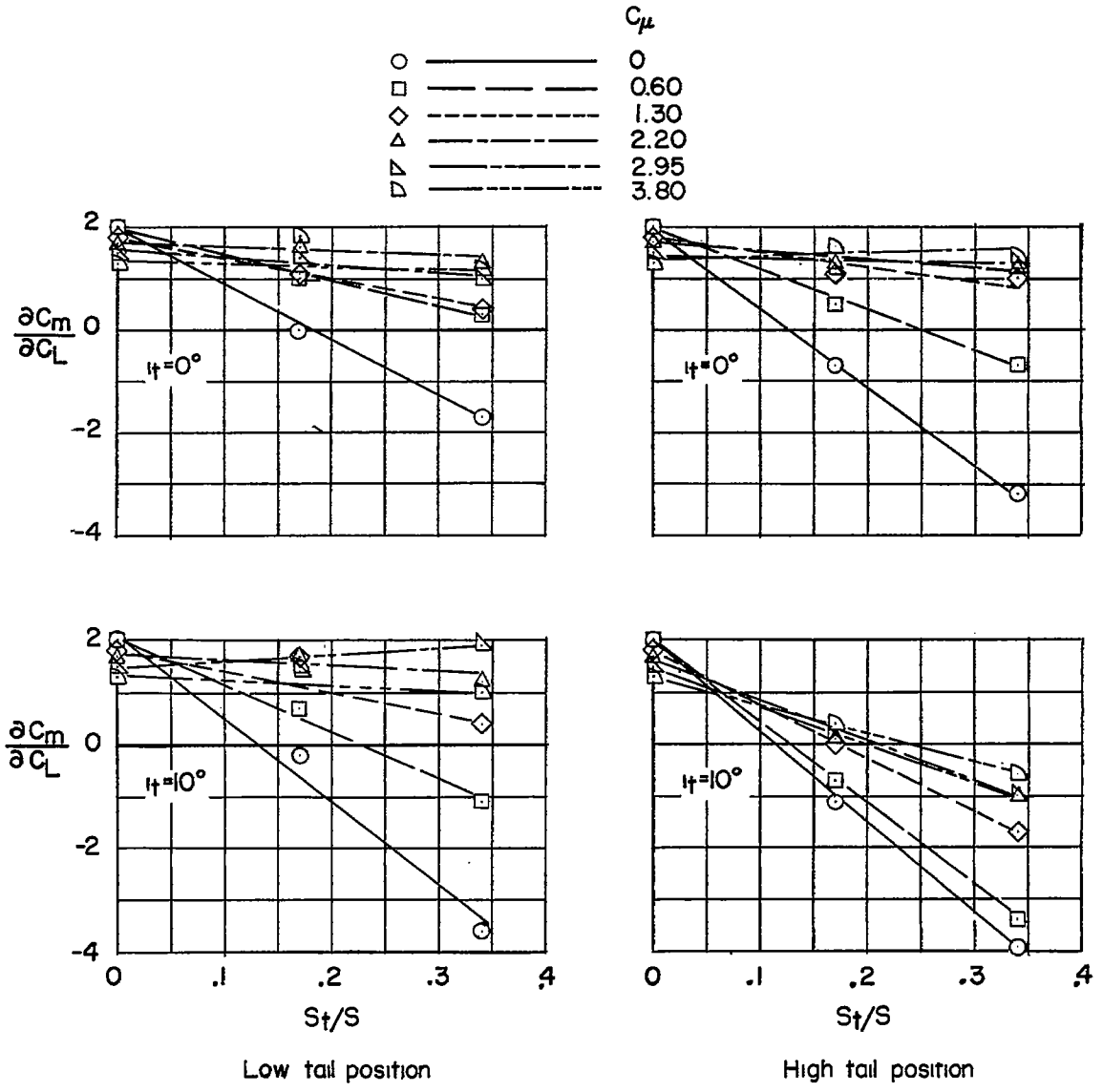

Figure 24.- Variation of longitudinal stability parameter with horizontal-tail area (data from figs. 7 to 10). High-wing configuration; $\alpha = 0^\circ$.

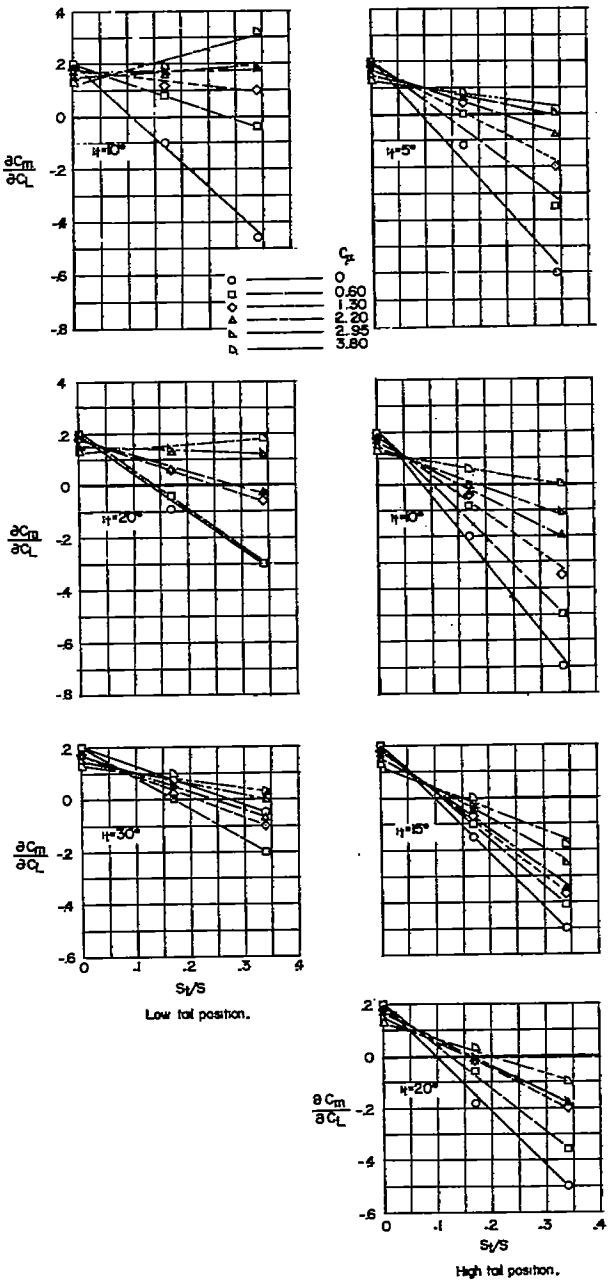

Figure 25.- Variation of longitudinal stability parameter with horizontal-tail area (data from figs. 12 to 15). High-wing configuration; leading- and trailing-edge flaps on horizontal tail; $\alpha = 0^{\circ}$.

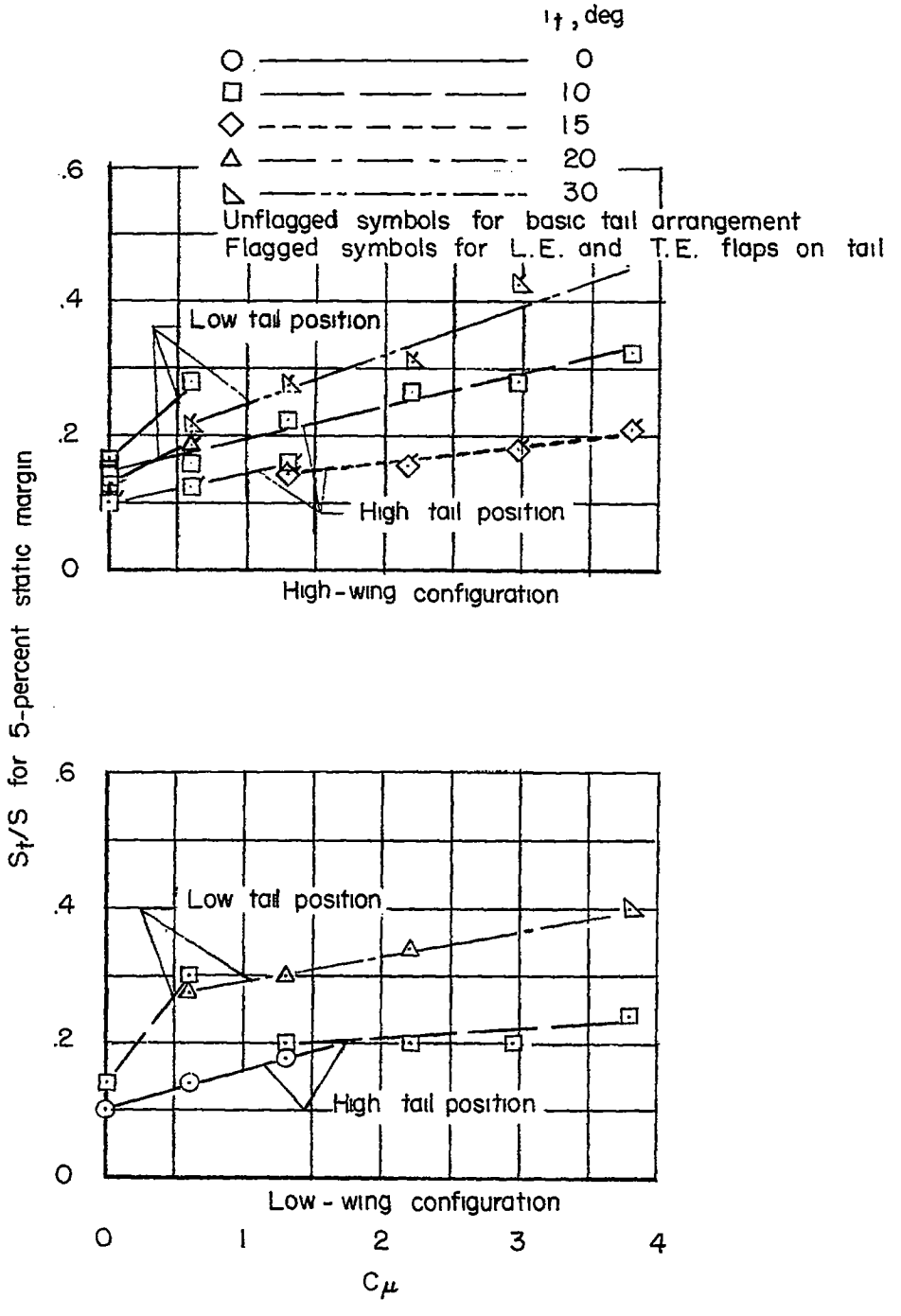

Figure 26.- Variation of horizontal-tail area required for 5-percent static margin with momentum coefficient. $\alpha = 0^\circ$.

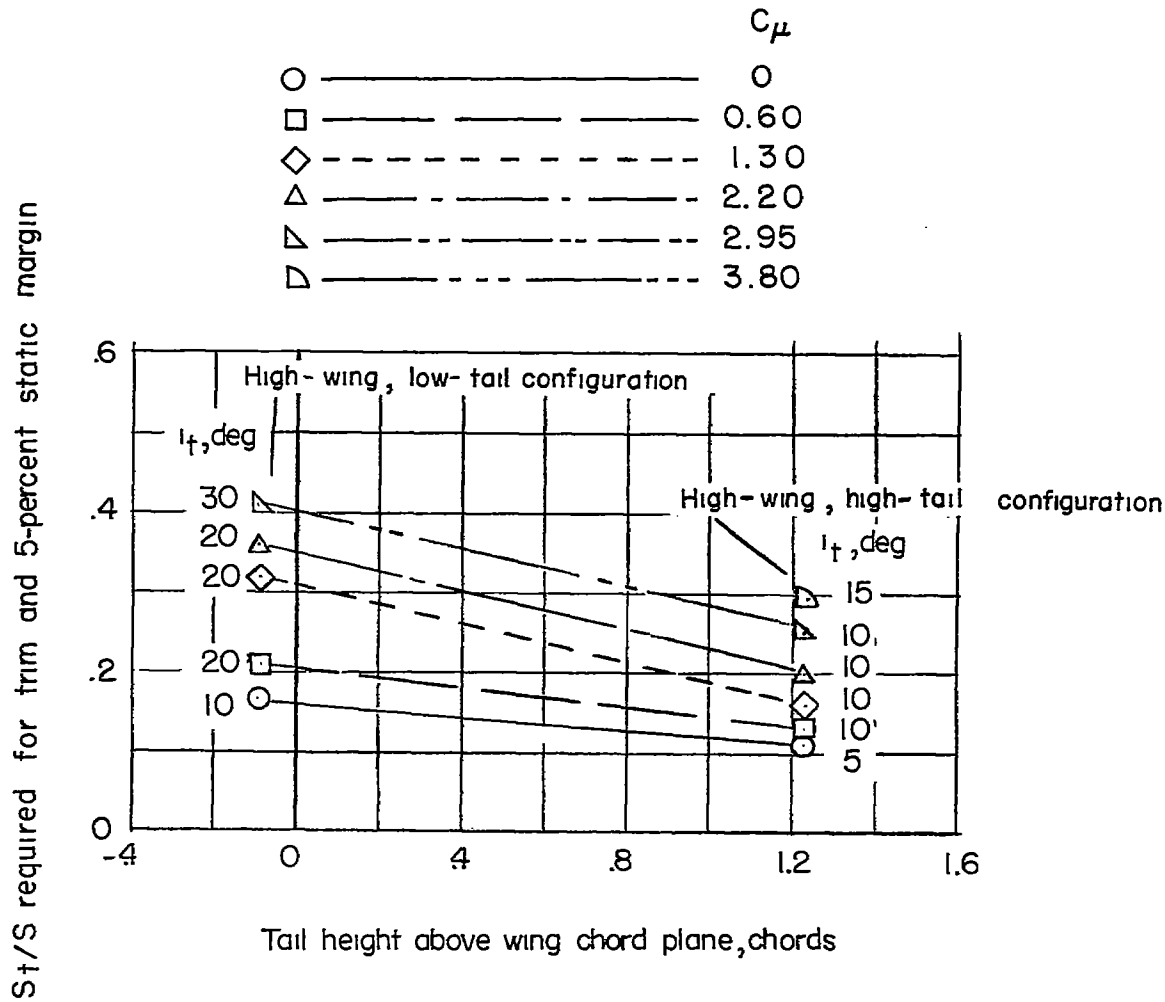

Figure 27.- Variation with horizontal-tail height of horizontal-tail area required for trim and 5-percent static margin. Leading- and trailing-edge flaps on horizontal tail; $\alpha = 0^\circ$.

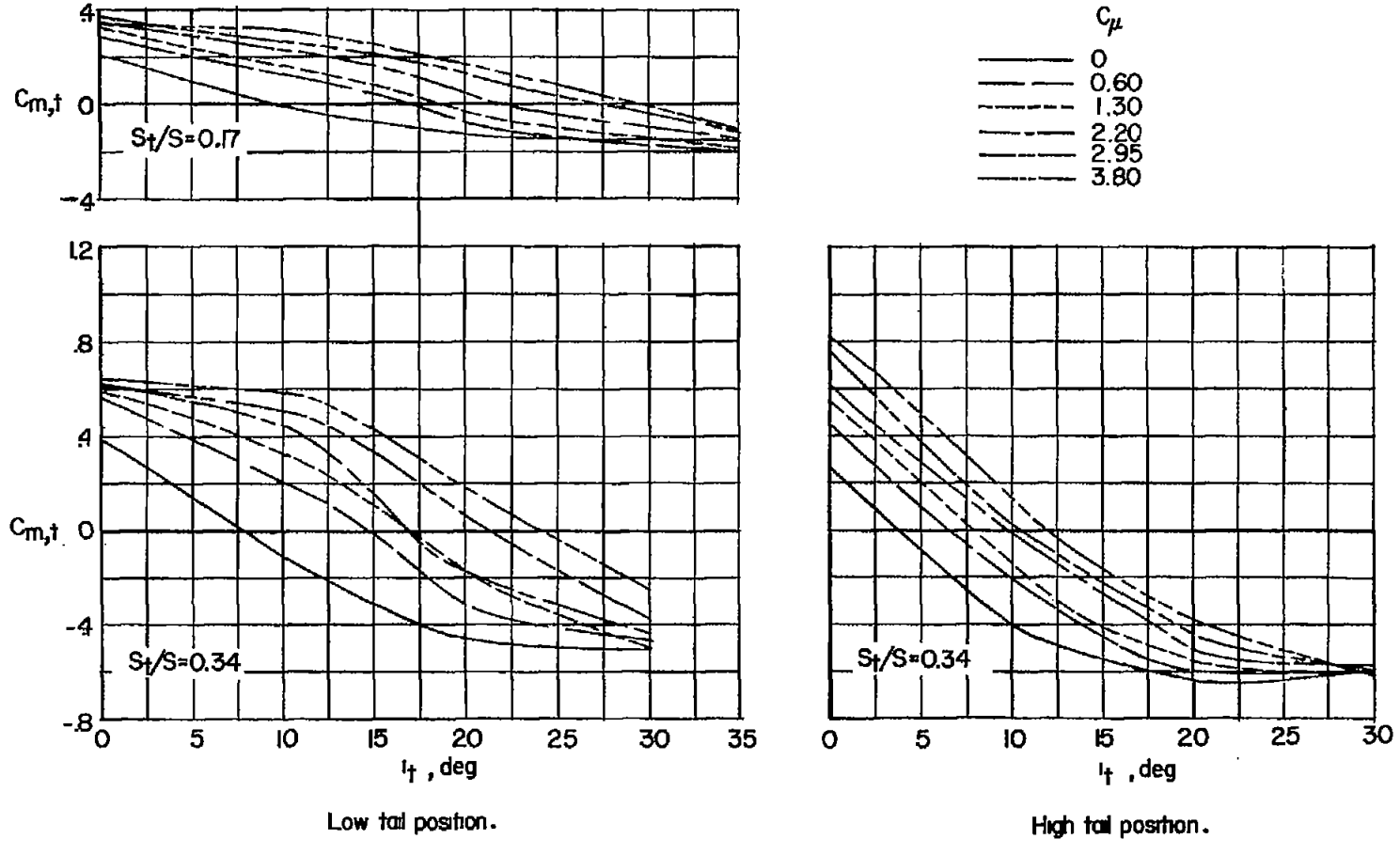

Figure 28.- Pitching-moment increments produced by various horizontal-tail configurations (data from figs. 3 to 6). Low-wing configuration; $\alpha = 0^\circ$.

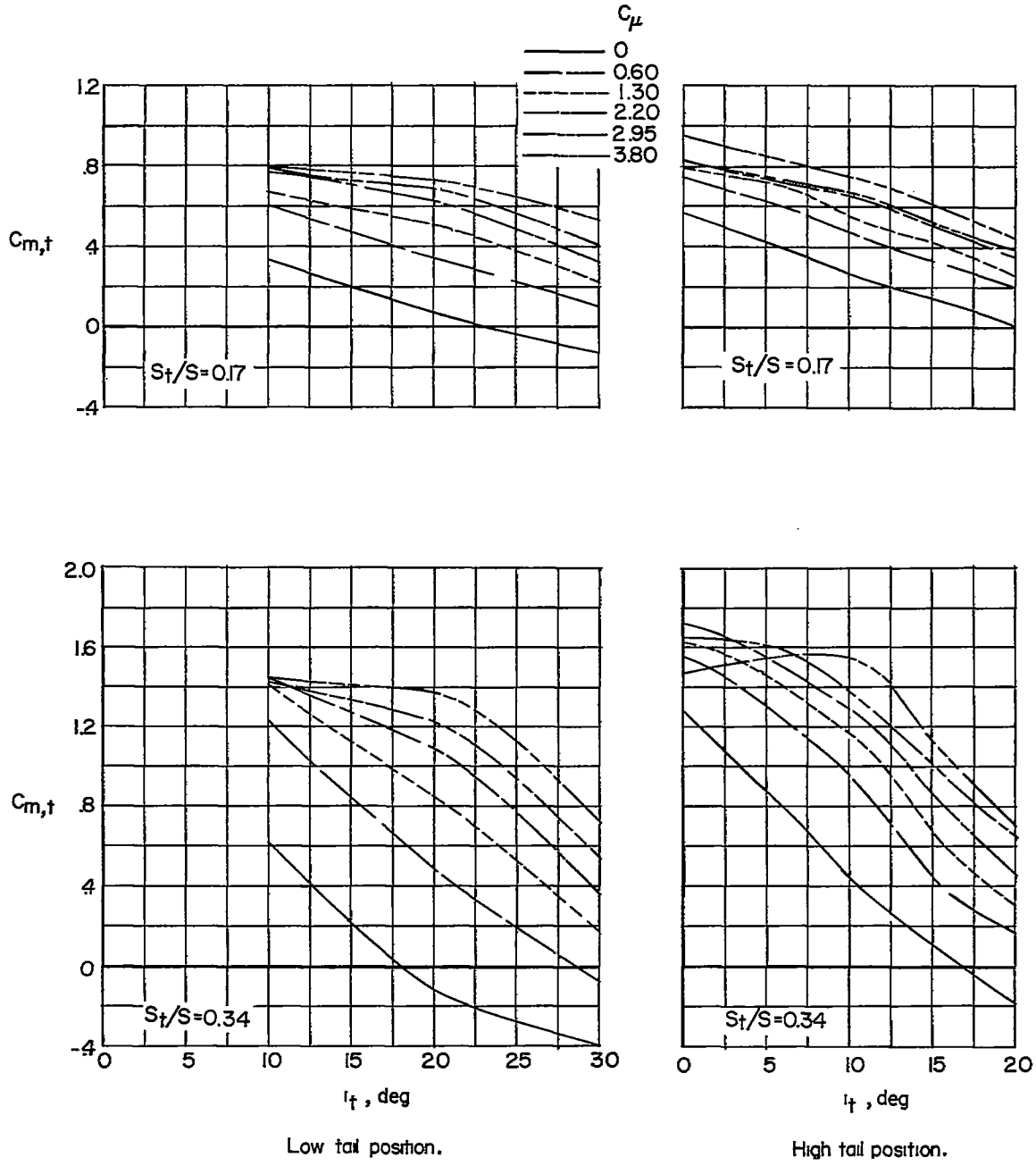

Figure 29.- Pitching-moment increments produced by various horizontal-tail configurations (data from figs. 12 to 15). High-wing configuration; leading- and trailing-edge flaps on horizontal tail; $\alpha = 0^\circ$.

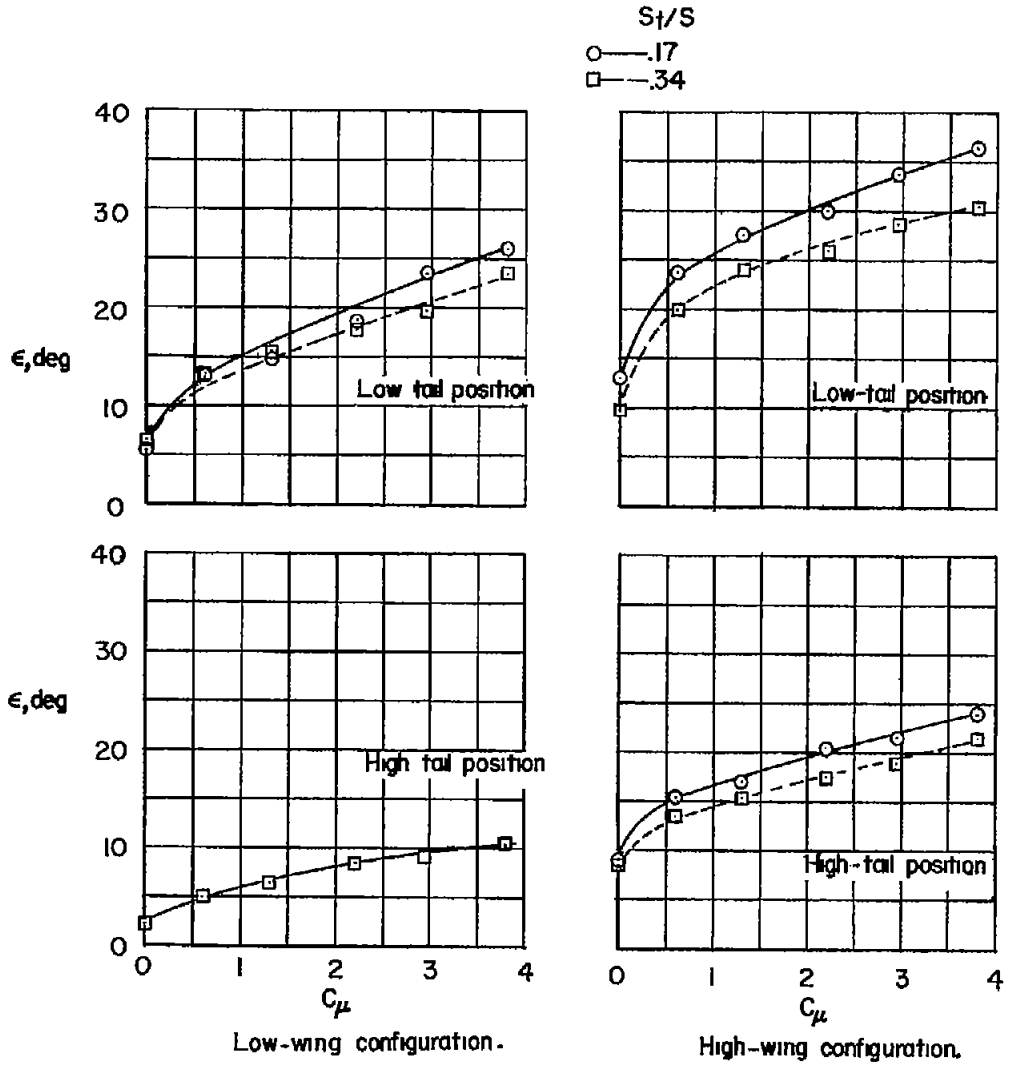

Figure 30.- Variation of downwash angle with momentum coefficient for various model configurations.

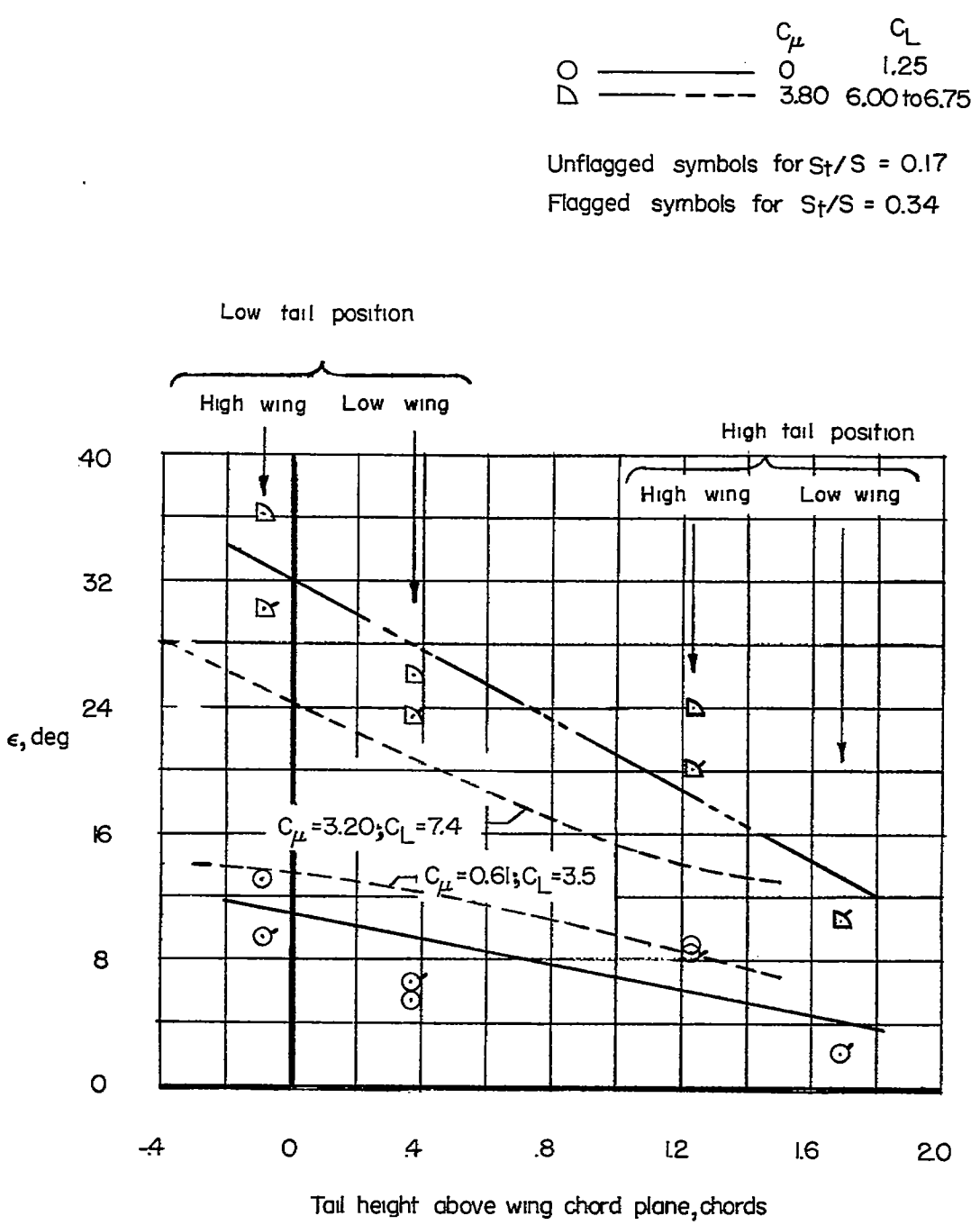

Figure 31.- Variation of downwash angle with horizontal-tail height for various model configurations. Dashed curves are data from figure 13(a) of reference 4.

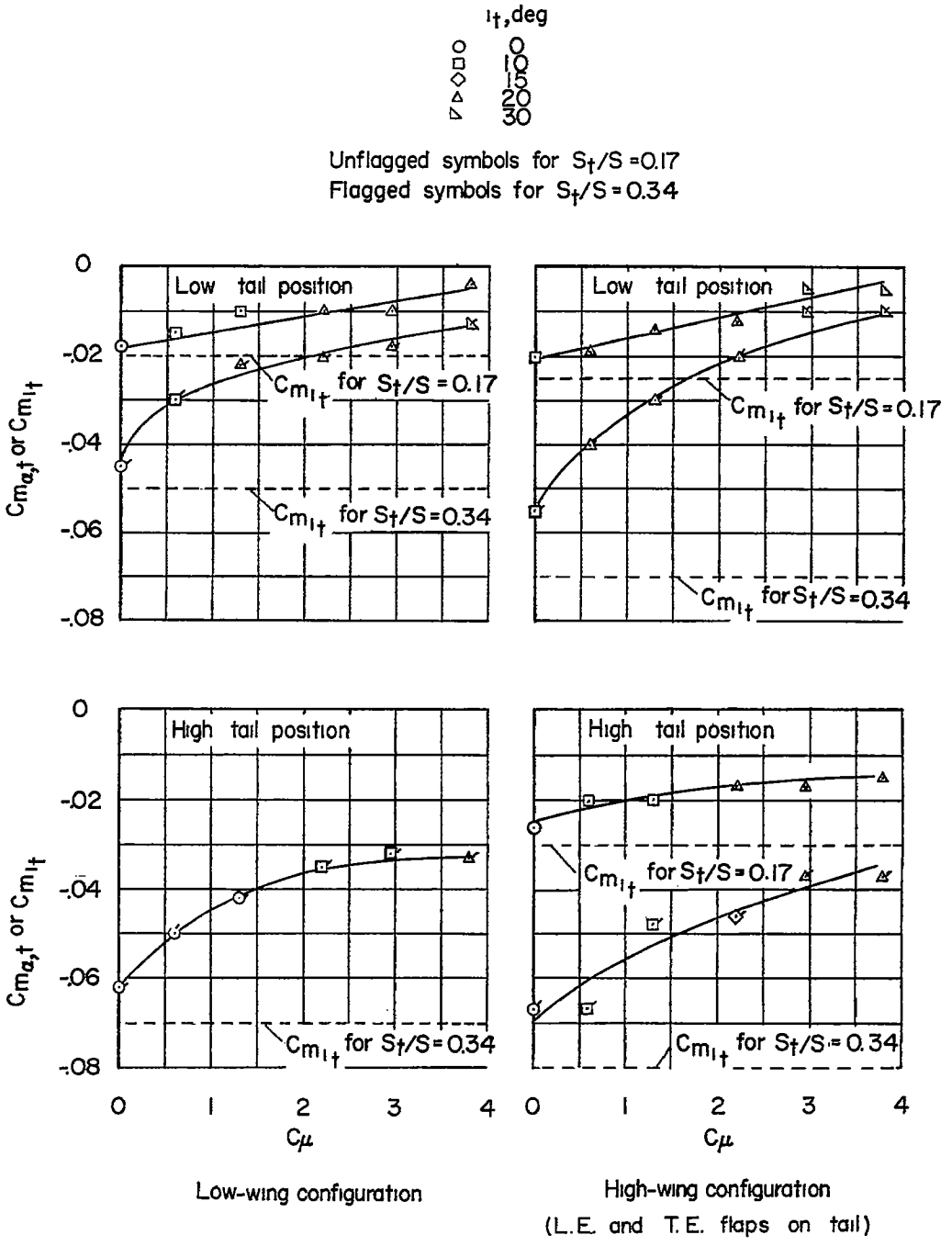

Figure 32.- Variation of $C_{m_{\alpha,t}}$ and $C_{m_{i_t}}$ with momentum coefficient for various model configurations.

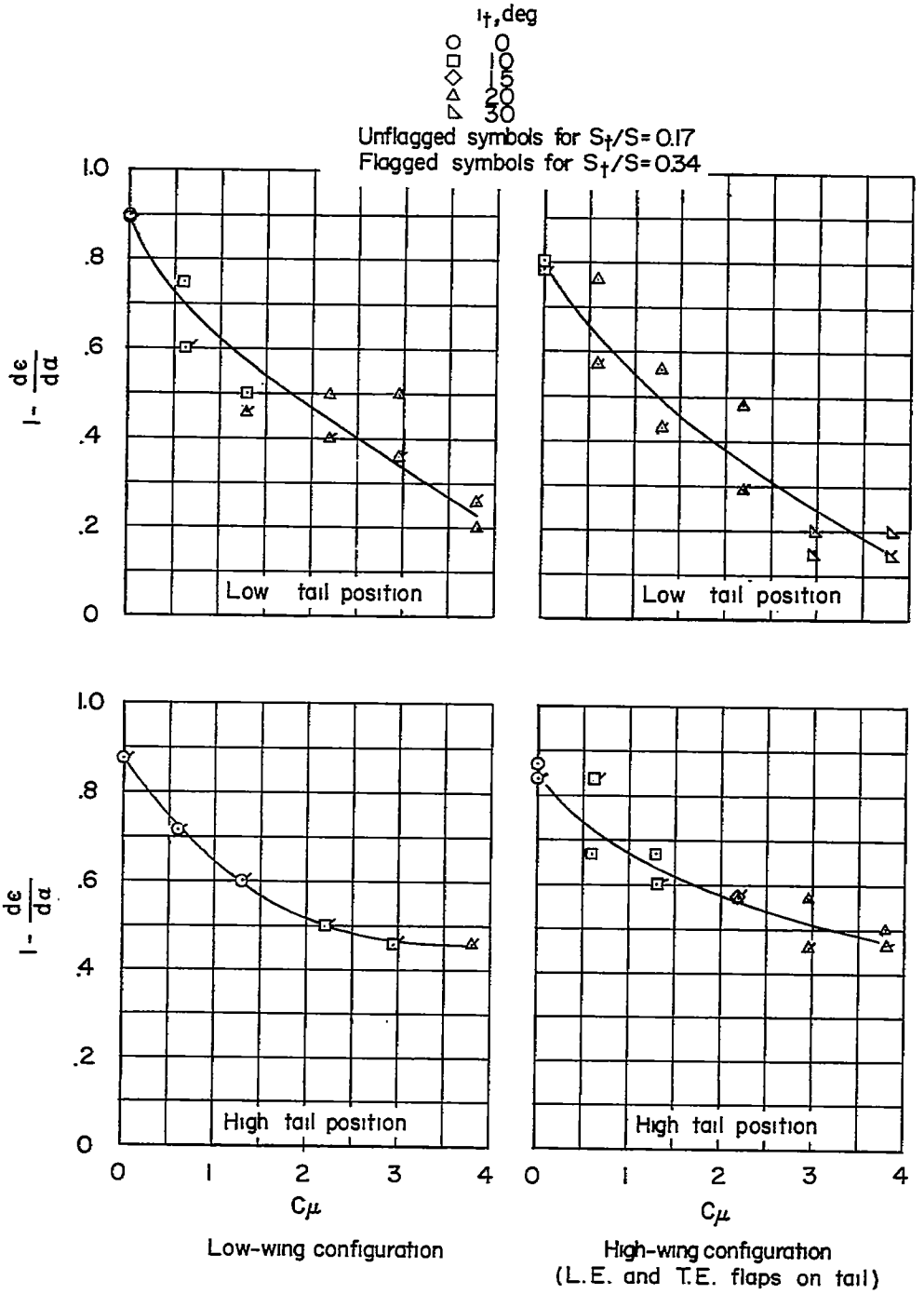

Figure 33.- Variation of downwash factor with momentum coefficient for various model configurations.

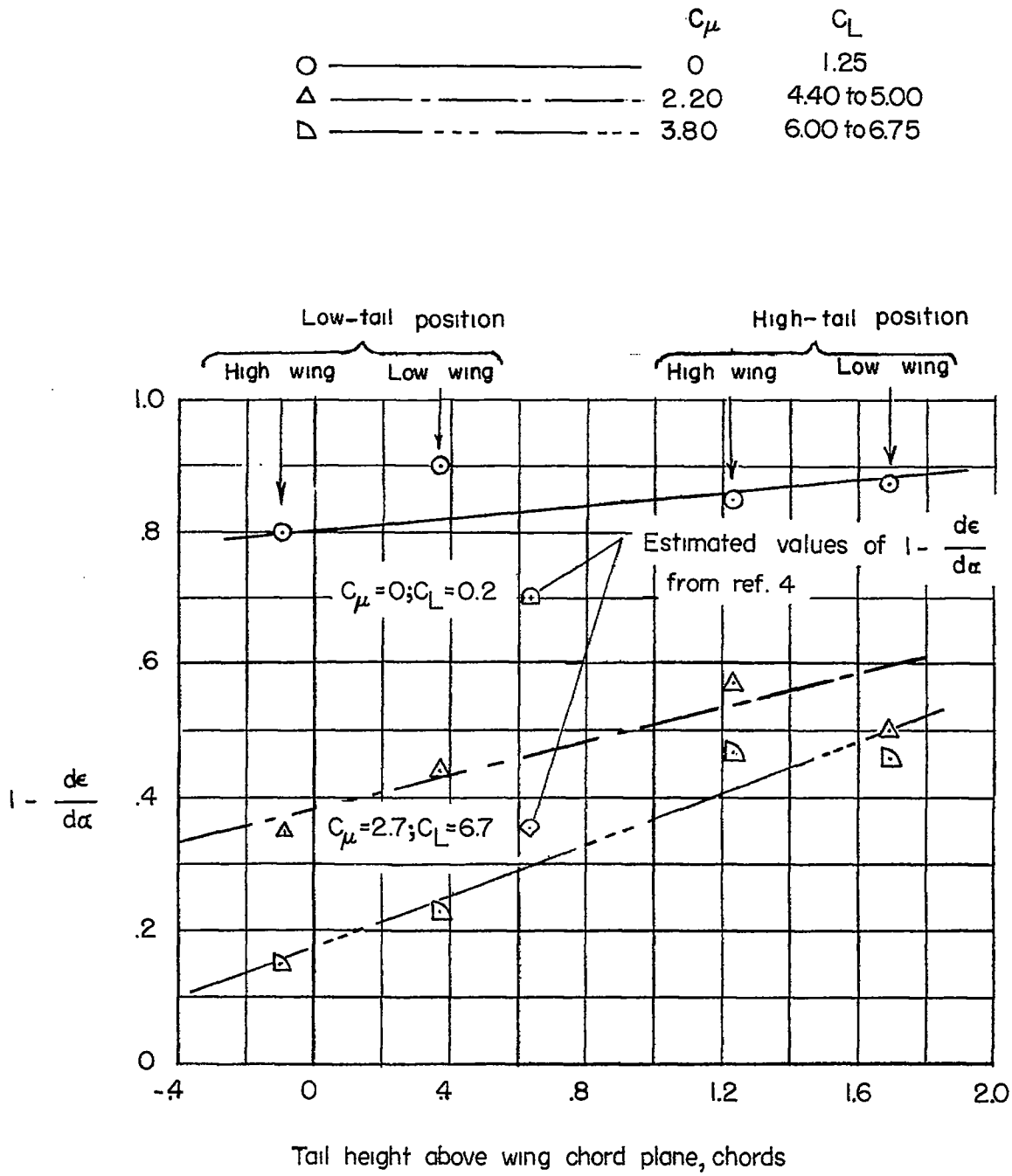

Figure 34.- Variation of downwash factor with horizontal-tail height for various model configurations.

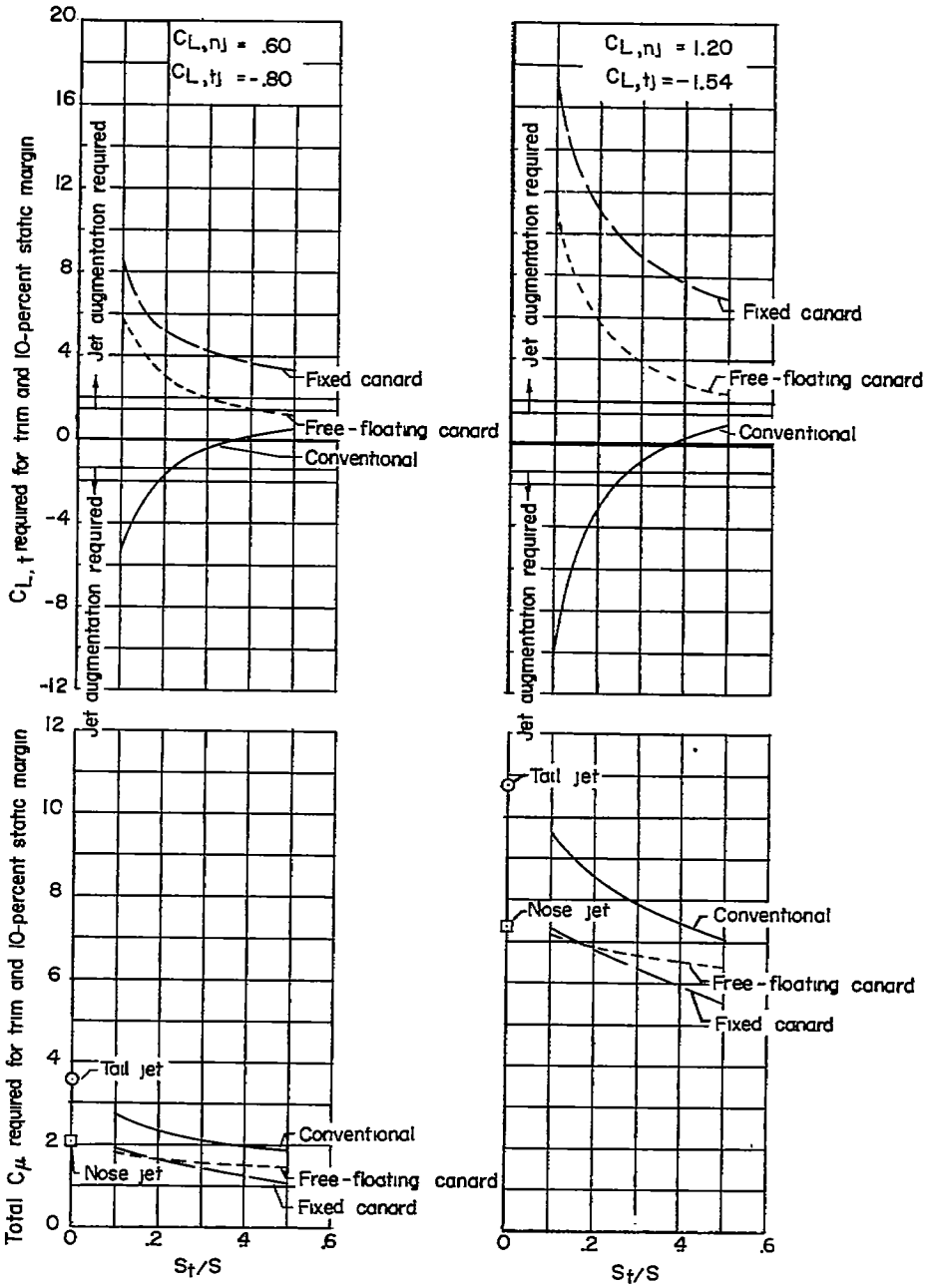

(a) $C_{L,trim}$ = 5. (b) $C_{L,trim}$ = 10.

Figure 35.- Variation of tail lift coefficient and total momentum coefficient required for trim and 10-percent static margin with tail area for various model configurations.